KfK 4332
Oktober 1989

UFOMOD
Atmospheric Dispersion and Deposition

H.-J. Panitz, C. Matzerath, J. Päsler-Sauer
Institut für Neutronenphysik und Reaktortechnik
Projekt LWR-Sicherheit

Kernforschungszentrum Karlsruhe

KERNFORSCHUNGSZENTRUM KARLSRUHE
Institut für Neutronenphysik und Reaktortechnik
Projektgruppe LWR-Sicherheit

KfK 4332

UFOMOD
Atmospheric Dispersion and Deposition

H.-J. Panitz [1]
C. Matzerath [2]
J. Päsler-Sauer

[1] present affiliation:
Institut für Meteorologie und Klimaforschung
[2] present affiliation:
Abteilung für Angewandte Systemanalyse

This work has been performed with support of the
Commission of the European Communities
Radiation Protection Programme
Contract No. BI6/F/128/D

Kernforschungszentrum Karlsruhe GmbH, Karlsruhe

Kernforschungszentrum Karlsruhe GmbH
Postfach 3640, 7500 Karlsruhe 1

ISSN 0303-4003

Abstract

The report gives an introduction into the modelling of atmospheric dispersion and deposition wich has been implemented in the new program system UFOMOD for assessing the consequences after nuclear accidents. According to the new structure of UFOMOD, different trajectory models with ranges of validity near to the site and at far distances will be applied. Emphasis will be laid on the description of the segmented plume model MUSEMET and its affilated submodels, being the removal of activity from the cloud by dry and wet deposition, and special effects like plume rise and the behaviour of plumes released into building wakes. In addition, the evaluation of γ-dose correction factors to take account of the finite extent of the radioactive plume in the near range (up to about 20 km) will be described. Only brief introductions will be given into the principles of the other models available: the puff model RIMPUFF, the long-range puff model MESOS, and the special straight-line Gaussian model ISOLA which will be used if low-level long-duration releases are condidered. To define starting times of weather sequences and the probabilities of occurrence of these sequences, it is convenient to perform stratified sampling. Therefore, the preprocessing program package METSAM has been developed to perform for generic ACAs a random sampling of weather sequences out off a population of classified weather conditions. The sampling procedure and a detailed input/output (I/O) description will be presented in the report and an additional appendix, respectively. A general overview on the I/O structure of MUSEMET as well as a brief user guide to run the KfK version of the MESOS code are also given in the appendix.

UFOMOD: Atmosphärische Ausbreitung und Ablagerung

Zusammenfassung

Der Bericht beschreibt die Modellierung der atmosphärischen Ausbreitung und Ablagerung im neuen Programmsystem UFOMOD zur Abschätzung der Konsequenzen nach Unfällen in kerntechnischen Anlagen. Die neue Struktur des UFOMOD erlaubt es, verschiedende Trajektorienmodelle, die unterschiedliche Entfernungsbereiche abdecken, anzuwenden. Schwerpunktmäßig werden im Bericht das gaußartige Trajektorienmodell MUSEMET und seine zugehörigen Teilmodelle beschrieben. Diese umfassen insbesondere die Abmagerung der Fahne durch trockene und nasse Ablagerung der Aktivität auf dem Erdboden sowie die speziellen Effekte Fahnenaufstieg und Verwirbelung der Fahne im Lee von Gebäuden. In die anderen atmosphärischen Ausbreitungsmodelle, die derzeit für das UFOMOD zur Verfügung stehen - dies sind die Puffmodelle RIMPUFF, MESOS und das geradlinige Gaußmodell ISOLA -, werden nur kurze Einführungen gegeben. Die Startzeiten von Wetterabläufen und die zugehörigen Wahrscheinlichkeiten werden allgemein mit Hilfe statistischer Auswahlverfahren ermittelt. Für generische Unfallfolgenabschätzungen wurde das Programmpaket METSAM entwickelt, das die Wetterabläufe aus einer Gesamtheit von klassifizierten Wetterbedingungen mittels zufälliger Auswahl bestimmt. Dieses Auswahlverfahren und die Ein- und Ausgabe des Programmpaketes werden beschrieben. Ein allgemeiner Überblick über die Eingabe/Ausgabe Struktur von MUSEMET und eine kurze Benutzeranleitung, um die KfK-Version des MESOS Modells anwenden zu können, befinden sich in einem Anhang.

Table of Contents

List of Illustrations

List of Tables

1. INTRODUCTION

Any **Accident Consequence Assessment (ACA)** of possible releases of radionuclides from a nuclear installation must be based on predictions of the distribution of the radioactive material throughout the environment. Accidental releases into the atmosphere are the most severe ones in terms of the radiological consequences. Therefore, modelling the atmospheric dispersion and deposition is of essential importance in an ACA. Once the material is released, the airborne particles and gases form a plume which is transported in the downwind direction and which expands horizontally and vertically due to diffusion conducted by turbulent eddies in the atmosphere (Figure 1).

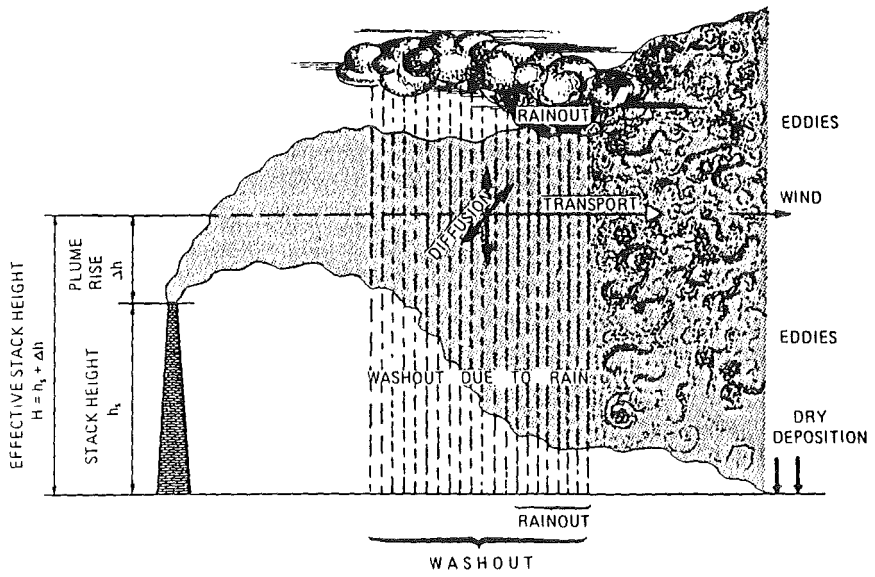

Figure 1. Behaviour of radionuclides released to the atmosphere (from [1])

During the dispersion the radioactive material may be removed from the plume by several mechanisms. Gravitational settling and contact with the ground, vegetation and structure in urban areas are referred to as dry deposition. Wet deposition may result from precipitation formation processes within the cloud, leading to removal by rainout, or from interaction between falling rain drops and the dispersing material, referred to as washout. Radioactive decay reduces the activity in the plume, and the built-up of daughter products may change the nuclide composition during dispersion. Depending on the release characteristics special features may have influence on the dispersion and deposition, for example the effect of plume rise due to the buoyancy or momentum of the released activity and the behaviour of plumes released into building wakes. Both phenomena affect the concentration distributions and, hence, the consequences arising in the vicinity of a nuclear installation.

To simulate the very complex processes whereby material is dispersed in and deposited from the atmosphere and to calculate the resulting distributions of activity concentrations

in the air and on the ground, a large number of models of different physical complexity has been developed. Due to its simplicity the straight-line Gaussian model [2] is the one most commonly used in practical applications of atmospheric dispersion modelling. Also in most of the computer programs developed for ACAs in the last ten years, e.g. CRAC [3], CRAC2 [4], MACCS [5], MARC [6] and UFOMOD [7], this model has been implemented to describe the atmospheric dispersion and deposition. The model is derived from a simplified theoretical treatment of dispersion which assumes that the atmospheric flow- and turbulence fields are homogeneous and stationary [8]. Especially, the model does not allow for changes of wind direction during the release and during the subsequent dispersion of the released material through the atmosphere, processes everybody can see in the nature observing a smoke plume coming out off a chimney. Therefore, to increase the applicability and acceptance of ACAs, much effort has been invested during the development of the new ACA program system UFOMOD [9] to substitute the straight-line Gaussian plume model by more realistic atmospheric dispersion models.

Recently, a benchmark study has been carried out at the Institut für Neutronenphysik und Reaktortechnik (INR) of the Kernforschungszentrum Karlsruhe (KfK)

- to quantify the characteristic physical features of various dispersion models [10], comprising the straight-line Gaussian plume model and Gaussian-type trajectory plume and puff models, Eulerian grid-point models, and a Lagrangian random walk model,
- to identify those models which can be applied in ACA codes under the demands of reasonable computer time and availability of meteorological input data [11],
- to quantify the implications of different concepts of dispersion modelling by comparing the results of an ACA after the application of a straight-line Gaussian plume model and improved dispersion models which take into account the changes of wind directions [11].

The study demonstrated that with respect to the demands

- high flexibility,
- user friendliness,
- acceptable computing time
- availability of meteorological input data

at present only Gaussian-like trajectory models are applicable in ACAs. Although these models use the Gaussian formalism to calculate concentration fields, the ability to consider changes of wind direction during the release and the dispersion led to more realistic consequence assessments compared to the straight-line Gaussian model.

The conclusion from the benchmark was to apply trajectory models in ACAs. In general, the range of validity of these models is limited to the region near to the site, since im most cases the meteorological data are available only from the site or a meteorological station representative for it. A Gaussian dispersion over more than some 10 kilometres based on these data is hard to defend, especially in topographically structured areas, and even over flat land, this type of dispersion has never been proven at longer distances. Therefore, long-range dispersion models are needed to describe the transport of radioactive material over large areas up to thousands of kilometres. This led to a completely

novel concept of atmospheric dispersion modelling in the new program system UFOMOD (Figure 2).

UFOMOD	
Near range model ($\leq$ 50km)	Far range model ($\geq$ 50km)
Atmospheric dispersion	
MUSEMET (KFA) RIMPUFF (RISO)	MESOS (ICST) Wind fields in the region 10°W - 50°E, 36°N - 62°N
synoptic data recorded and reported continuously at 1h intervals	synoptic data of 1982 and 1983 reported from more than 800 measuring stations at 3h intervals

Figure 2. UFOMOD: Modelling of atmospheric dispersion: (from [9])

Due to the facts, that

- site-specific characteristics are only relevant in the near range and vanish at farther distances,
- the quality and quantity of consequences in the near range (fast protective measures, early health effects) are different from the far range (long-term countermeasures, stochastic health effects),
- the near range can be modelled much more in detail than the far range, and
- many applications of ACA refer to only one of both distance ranges

different ranges of validity are distinguished and assigned to respective trajectory models:

- the near range ($\leq$ 50 km), where modified versions of the atmospheric dispersion models MUSEMET [12] and RIMPUFF [13] are used,
- the far range ($>$ 50 km), where the computer code MESOS is applied [14], [15].

The application of different atmospheric dispersion models, which calculate air and ground concentrations independent of each other in different distance ranges with different grid sizes and for different purposes, led to the division of the UFOMOD program into several parts, which are more or less independent (Figure 3).

Three subsystems have been built each conceived to assess accident consequences occurring in different time periods or distance ranges. Two subsystems cover the near

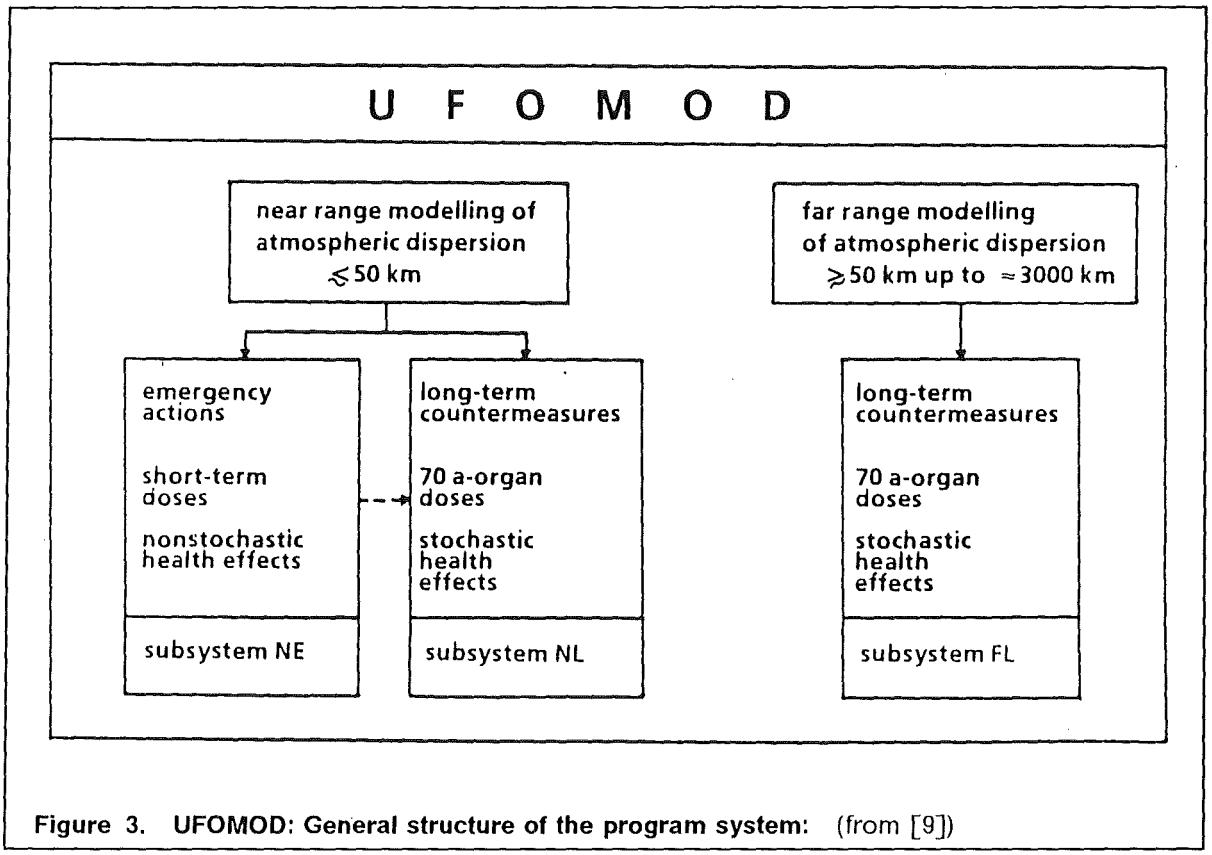

Figure 3. UFOMOD: General structure of the program system: (from [9])

range up to about 50 km and each contains models and data to assess only one type of consequences, namely

- the extent and duration of early protective measures, short-time integrated organ doses and non-stochastic health effects (version UFOMOD/NE , N for "near", E for "early");
- the extent and duration of long-term countermeasures, long-time integrated organ doses and stochastic health effects (version UFOMOD/NL for "near", L "late").

When protective measures and non-stochastic health effects are estimated in the near range, these results have to be transferred from UFOMOD/NE to version UFOMOD/NL to assess the correct long-term doses and stochastic health effects near to the site (indicated by an arrow in Figure 3).

The third subsystem covers the range from about 50 km up to about 3000 km, and it is designed mainly to estimate long-term countermeasures (e.g. food-bans and theit withdrawal), long-term doses of individuals and of the population, and the resulting stochastic health effects (version UFOMOD/FL, F for "far", L for "late").

In the present near range versions the segmented plume model MUSEMET (KFA, Jülich, F.R.G., [12]) is the standard atmospheric dispersion model, and it is implemented as a subroutine in the whole program system. RIMPUFF (RISO National Laboratory, Denmark, [13]) is a stand-alone code and requires an additional interface program to transfer the calculated concentration distributions into the actual UFOMOD system. Both models are

Gaussian-like trajectory models. Two principle differences exist between them. The first is illustrated in Figure 4.

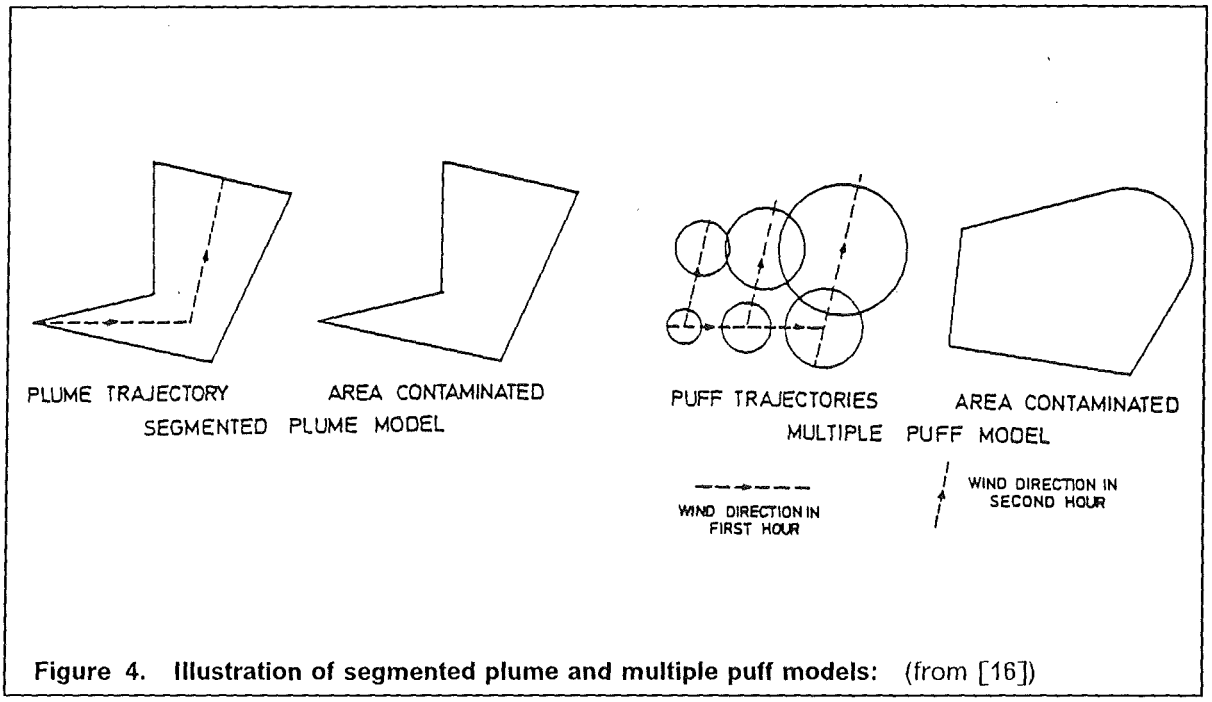

Figure 4. Illustration of segmented plume and multiple puff models: (from [16])

The segmented plume model MUSEMET transports the radioactive material along one precalculated trajectory. In the puff model RIMPUFF all puffs released experience a change of wind direction instantaneously so that each puff will follow its own trajectory. The second difference concerns the meteorological input data. MUSEMET uses wind, precipitation, and stability data measured at one meteorological station representative for the source location. During one time-step (e.g. 1 hour) homogeneous meteorological conditions are assumed. In contrast to that, in RIMPUFF the data of several stations can be considered and spatially varying wind-, precipitation,- and stability fields are generated. Therefore, it is also possible to apply RIMPUFF over structured terrain if the density of meteorological stations is sufficiently high, so that topographically induced flow conditions are taken into account implicitly.

The only long-range dispersion model available at the time of designing the new program system UFOMOD [9] was the computer code MESOS which has been developed at the Imperial College of Science and Technology, London, UK, [14]. It combines the requirement of short computing time with the ability to disperse radioactive material along precalculated wind fields derived from meteorological data measured at synoptic stations distributed nearly over the whole area of Europe (36°N - 62°N, 10°W - 50°E). Because of the density of these stations, a grid size results which does not allow to apply MESOS in the near range (< 50 km).

Differing from the new concept of using trajectory models in UFOMOD a special simplified atmospheric dispersion model has been implemented to estimate the spatial concentration distribution for long-duration (weeks or months) source terms with a rather low release rate of radioactive material. For that purpose, the straight-line Gaussian model

ISOLA (KfK, F.R.G., [17]) which bases on a statistical evaluation of the four parameters wind speed, wind direction, precipitation and stability class, has been modified for the use in UFOMOD. ISOLA will only be used in the framework of assessing the long-term protective actions and stochastic health effects because early fatalities will not occur in connection with low release rates.

All models mentioned above have already been applied and partly validated in several scientific studies. MUSEMET has been used successfully in a risk study to calculate the potential exposure after accidents in the framework of nuclear waste management [18]. With RIMPUFF satisfactory simulations of the Oeresund mesoscale dispersion experiments have been performed [19], [20]. Its applicability over structured terrain has been demonstrated by Mikkelsen et al., [21], who developed a puff-splitting technique, which in conjunction with a fast, diagnostic flow-model simulates bifuracted and shear-induced dispersion over complex terrain. But this pentapuff version of RIMPUFF has not yet been implemented in UFOMOD. Therefore, in the RIMPUFF version currently available in UFOMOD, topographical effects can only be considered implicitly on the basis of a dense meteorological observation network. The MESOS code has been used for example to analyse successfully the atmospheric dispersal of the Chernobyl release across Europe [22]. The ISOLA computer code is used to calculate the annual radiation doses in the environment of the Karlsruhe Nuclear Research Center (KfK), caused by release of α- and β-active substances into the atmosphere. Recently, the model was used to compare measured and calculated tritium concentrations in rain and snow water [23]. It was shown that the measurements of annual surface loadings due to tritium emmissions at the KfK agree well with the corresponding calculated results.

Based on the source term characteristics and the meteorological conditions, the atmospheric dispersion models in UFOMOD calculate normalized time-integrated concentrations patterns in the air near to the ground and on the ground surface. Thereby, the models distinguish between different dry and wet deposition characteristics which depend on the physical and chemical form of the isotopes released. The spatial concentration fields are transferred to subsequent modules of UFOMOD to calculate distribution functions of air concentrations, contaminated areas, organ doses and health effects together with areas and numbers of persons affected by countermeasures which are taken to reduce the exposure and thus the health implications in the population.

The following chapter describes the fundamentals of the atmospheric dispersion models which are available in the new UFOMOD sytem, including the parameterization of horizontal and vertical diffusion and the mechanisms for removal of activity from the cloud, being dry and wet deposition processes, and radioactive decay. Chapter 3 deals with the concepts of buoyant plume rise, building wake effects, and lift-off which determines whether a buoyant plume is trapped in the turbulent building wake or not. Correction factors for gamma radiation from the cloud are also calculated for the near range model. Their evaluation is considered in chapter 4. Emphasis will be laid on the description of the MUSEMET model and the submodels affilated to MUSEMET. Only rather short introductions will be given into RIMPUFF, MESOS, and ISOLA. MESOS ,which is the standard model for the version UFOMOD/FL, has already been described extensively in the literature [14], [15]. A preliminary users's guide of RIMPUFF is available as an internal, unpublished KfK-Report [24]. Publications of ISOLA and RIMPUFF, including also descriptinos of the necessary input data and their structure, are in preparation [25], [26].

In chapter 5 the meteorological sampling scheme METSAM is introduced. METSAM selects representative samples of weather sequences from a meteorological record which is typical for the source location and its surroundings, so that the spectrum of consequences which depend upon the prevailing meteorological conditions can be assessed as comprehensively as possible. Finally, an appendix defines the structure of input data sets necessary for MUSEMET, MESOS, and the METSAM program package.

The new program system UFOMOD refers to the SI units Bequerel (Bq) and Sievert (Sv) for activity and doses, respectively. Therefore, these units will also be used throughout this report.

2. MODEL FUNDAMENTALS

2.1 *The Diffusion-Advection-Equation and its Gaussian solution*

The basic differential equation for atmospheric dispersion problems is the Diffusion-Advection-Equation, which results from the gradient-transfer approach to turbulent diffusion [2], [27]

$$\frac{\partial C}{\partial t} = -\vec{v} \cdot \nabla C + \frac{\partial}{\partial x}\left(K_x \frac{\partial C}{\partial x}\right) + \frac{\partial}{\partial y}\left(K_y \frac{\partial C}{\partial y}\right) + \frac{\partial}{\partial z}\left(K_z \frac{\partial C}{\partial z}\right) \qquad (2.1)$$

with:

$C = C(\vec{r}, t)$	mean air concentration of radioactive material (Bq/m³)
$\vec{v} = \vec{v}(\vec{r}, t)$	mean three-dimensional vector of wind velocity (m/s)
K_x , K_y, K_z	x,y and z components of the eddy diffusivity (m²/s)

It is assumed that after the release into the atmosphere there exists no further source nor sink of the dispersing material. Eq. (2.1) expresses the conservation of the suspended material in an incompressible fluid. The left hand side represents the local temporal change of mean concentration at a location $\vec{r}$ at time t, which is accomplished by advection (first term on the right hand side) and by turbulent diffusion resulting from the turbulent fluctuations of the flow (second to fourth terms on the right hand side). The gradient transfer approach bases on the assumption that the turbulent flux F_i of the material is proportional to the mean concentration gradient, i. e.

$$F_i = -K_i \frac{\partial C}{\partial x_i}, \quad i = x, y, z \quad (\text{Bq m}^{-2}\,\text{s}^{-1}) \; .$$

F_j is the rate of turbulent transfer of the pollutant per unit area across a fixed surface down the mean concentration gradient.

For stationary conditions ($\frac{\partial C}{\partial t} = 0$) Eq. (2.1) can be simplified to

$$u \frac{\partial C}{\partial x} = K_y \frac{\partial^2 C}{\partial y^2} + K_z \frac{\partial^2 C}{\partial z^2} \qquad (2.2)$$

if some further assumptions are made:

1. the turbulent diffusion is of Fickian type, but anisotropic, i.e.

$$K_i = \text{const.}, \quad i = x,y,z$$
$$K_x \neq K_y \neq K_z \; ;$$

2. the mean wind field is considered as constant and it is directed along the x-axis, i.e.

$$\vec{v} = (u,0,0) = \textbf{const.} \; ;$$

3. the turbulent diffusion along the x-axis can be neglected compared to the advection by the mean wind u, i.e. $K_x = 0$.

The most common model which satifies Eq. (2.2) together with appropriate boundary conditions is obtained from the assumption of a bi-Gaussian distribution of concentration (see e.g. [8]):

$$C(x,y,z) = \frac{Q_0}{2\pi\sigma_y\sigma_z u} \exp\left(-\frac{y^2}{2\sigma_y^2}\right)\left\{\exp\left(-\frac{(z-H)^2}{2\sigma_z^2}\right) + \exp\left(-\frac{(z+H)^2}{2\sigma_z^2}\right)\right\} \quad (2.3)$$

where

$$\sigma_j^2 = 2K_j t\,, \quad j = y,z \quad (2.4)$$

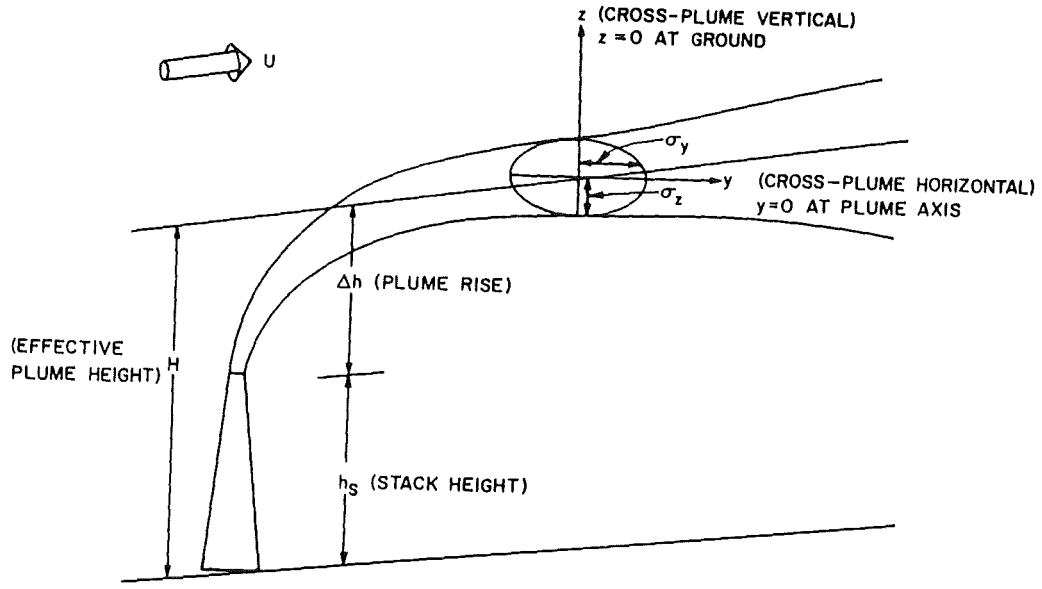

Figure 5. Schematic drawing of straight-line Gaussian plume model: (from [29])

Eq. (2.3) describes the spatial distribution of the time-integrated air concentration (T.I.C.) C on the leeside of a point source. It results from a short-term, quasi-continuous accidental release of a total amount Q_0 (in Bq) of radioactive material at an effective height H (in m) above ground in an uniform transport wind u (in m/s). For radioactive releases the T.I.C. is expressed in Bq s m^{-3}. X, y, and z are the rectangular coordinates of a cartesian frame of reference with its origin ($x = y = z = 0$) on the ground below the source; the x-axis is in the mean downwind direction, coinciding with the direction of the plume axis; y is the horizontal crosswind (lateral) distance from the plume axis and z ist the height above ground. Figure 5 is a schematic drawing which attempts to explain these definitions. The last exponential term on the right hand side of Eq. (2.3) accounts for reflection of the plume at the ground surface by assuming an image source of equal strength at $z = -H$ under the surface.

The straight-line Gaussian plume model is strictly applicable in only a limited range of atmospheric and environmental conditions, because for its derivation it is assumed that the terrain over which the material is dispersing is uniform and that atmospheric conditions are constant. The restricting assumptions of stationary and homogeneous turbulent diffusion are partly compensated by using diffusion parameters, σ_y and σ_z, which are determined experimentally. Mathematically, these parameteres are the lateral and vertical standard deviations of the assumed Gaussian concentration distribution. Physically, they describe the lateral and vertical extension of the plume at downwind distance x. Commonly it is assumed that they are power functions of travel distance (see Eq. (2.4) with $t = \frac{x}{u}$, u = const.):

$$\sigma_y = p_y x^{q_y} \tag{2.5}$$

$$\sigma_z = p_z x^{q_z} \tag{2.6}$$

The diffusion coefficients p_y, q_y, p_z, and q_z are determined by tracer experiments for different meteorological conditions, different release heights, and different conditions of the underlying surface (see for example [30], [31], [32], [33]).

Generally, with respect to Gaussian dispersion modelling, atmospheric turbulence is classified by empirical turbulence-typing schemes. The most widely used scheme is the one developed by Pasquill and Gifford ([34], Table 1), which assigns the grade of atmospheric stratification to six diffusion categories.

Pasquill-Gifford Notation	Stability Description
A	very unstable
B	moderately unstable
C	slightly unstable
D	neutral
E	moderately stable
F	very stable

Table 1. Pasquill-Gifford stability categories

Class A corresponds to very unstable conditions and is associated with small mechanical but large thermal components of turbulence. Class D represents the neutral atmospheric conditions and turbulence is only due to the mechanical component. Class F corresponds to thermally very stable conditions and the mechanical turbulence tends to be damped by buoyant forces.

The transport wind at the effective release height H is calculated from the power-law profile [35].

$$u = u_0 \left(\frac{H}{z_{ref}} \right)^p , \tag{2.7}$$

where u_0 is the measured velocity at the reference height z_{ref}, generally, 10 m above ground. The exponent p depends on diffusion category and surface roughness [35]. Val-

ues of p valid for a very rough surface (roughness length $z_0 \geq 1m$) are shown in Table 2,[36].

Diffusion Category	p
A	0.07
B	0.13
C	0.21
D	0.34
E	0.44
F	0.44

Table 2. Windprofile exponent

The power law Eq. (2.7) is an easy-to-use solution of the problem of wind speed variation with height but it should not be used at heights above 200m. Generally, it is assumed that $u(z) = u(z = 200) = u_{200}$ for $z \geq 200m$.

2.2 *The volume source model MUSEMET*

Extensions of the conventional straight-line Gaussian plume model for the computation of the dispersion of suspended material have been developed with regard to changing weather conditions, especially, wind direction. The model MUSEMET is based on the assumption that the weather conditions (wind direction, wind speed and diffusion category) are known and constant in consecutive time intervals (e.g. hourly intervals). The basic idea of the volume source model is to regard infinitesimal volume elements of the concentration distribution at the end of time interval k as point sources for diffusion calculations in the next time interval $(k+1)$ with new weather conditions. Figure 6 schematically describes the idea of the volume source model. The concentration distribution C_k at the end of each time interval Δt_k with constant weather conditions is composed of the concentrations from all the infinitesimal volume elements $dx_k dy_k dz_k$ that can be taken as point sources of inifinitesimal source strength dq_k for the diffusion calculation in the next time interval Δt_{k+1} with new weather conditions. These calculations are carried out according to the Gaussian model. The superimposed contributions of all point sources will then result again in a three-dimensional Gaussian distribution of activity concentration, C_{k+1} .

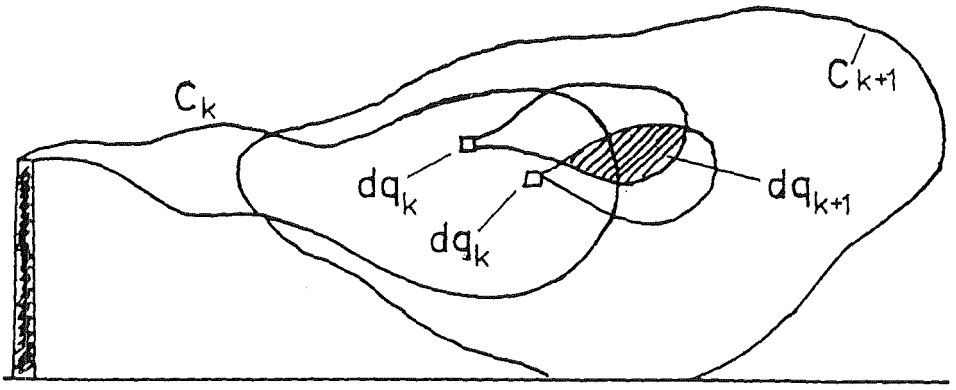

Figure 6. Schematical drawing of the volume source model: (from [37])

It has been shown in [12] that the T.I.C. in the n-th time interval can be written similar to Eq. (2.3) as

$$C_n(x,y,z) = \frac{Q_0}{2\pi\sigma_{y,eff}\sigma_{z,eff}u_n} \exp\left(-\frac{\eta_n^2}{2\sigma_{y,eff}^2}\right) \left\{\exp\left(-\frac{(z-H)^2}{2\sigma_{z,eff}^2}\right) + \exp\left(-\frac{(z+H)^2}{2\sigma_{z,eff}^2}\right)\right\} \Delta f_n \tag{2.8}$$

with:

C_n	T.I.C. at the point x,y,z, in the n-th time interval (Bq s m^{-3})
Q_0	activity released (Bq)
H	effective release height (m)
u_n	constant wind speed (m/s) at height H during the n-th time interval calculated according to Eq. (2.7)
x,y,z	downwind, crosswind, and vertical coordinates of a mathematical cartesian system with its origin below the source on the ground (see Figure 6)

For taking into account the changes of wind direction, the originally straight-line axis of the plume is turned into the direction of the real trajectory at the beginning of each time intervall Δt_n . This transformation is performed by successive translations and rotations relative to the fixed cartesian coordinate system (Figure 7).

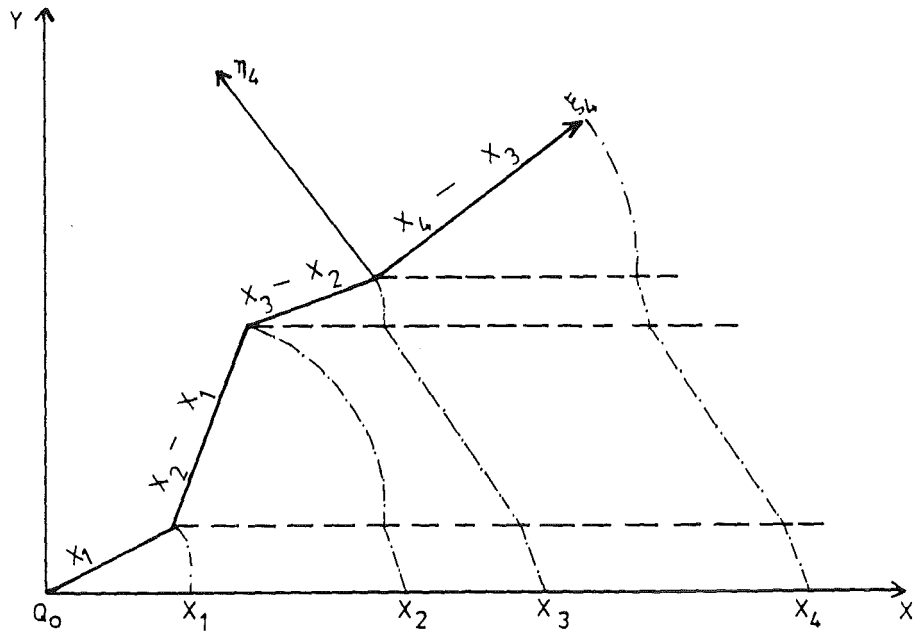

Figure 7. Determination of trajectory in MUSEMET

Thus

$$\eta_n = \frac{1}{u_n}\left\{u_{x,n}\left[y - \sum_{k=1}^{n-1} u_{y,k}(t_k - t_{k-1})\right] - u_{y,n}\left[x - \sum_{k=1}^{n-1} u_{x,k}(t_k - t_{k-1})\right]\right\}$$

with:

$u_{i,k}$ wind components in the k-th time interval relative to the fixed system, $i = x,y$

is the crosswind distance from the trajectory in the n-th time interval.

The effective dispersion paramteres $\sigma_{i,eff}$, $i = y,z$, are obtained as the sum over the variances $\sigma_{i,k}^2$ in the individual time intervals

$$\sigma_{i,eff}^2 = \sigma_{i,eff}^2(t) = \sum_{k=1}^{n-1} \sigma_{i,k}^2 + \sigma_{i,n}^2(t - t_{n-1}), \quad i = y,z$$

where, if Fickian diffusion is assumed, the dispersion parameter $\sigma_{i,k}$ in the k-th time interval $\Delta t_k = t_k - t_{k-1}$ can be written as

$$\sigma_{i,k}^2 = \sigma_{i,k}^2(t_k - t_{k-1}) = \sigma_{i,k}^2(t_k) - \sigma_{i,k}^2(t_{k-1})$$

and for the effective dispersion parameters it follows

$$\sigma^2_{i,eff} = \sigma^2_{i,eff}(t) = \sum_{k=1}^{n-1} \left(\sigma^2_{i,k}(t_k) - \sigma^2_{i,k}(t_{k-1})\right) + \sigma^2_{i,n}(t) - \sigma^2_{i,n}(t_{n-1}) , \quad i = y,z .$$

If power law functions

$$\sigma^2_{i,k} = p^2_{i,k}\, x_k^{2q_{i,k}} , \quad i = y,z$$

are assumed, we get

$$\sigma^2_{i,eff} = \sigma^2_{i,eff}(t) = \sum_{k=1}^{n-1} \left(p^2_{i,k}\left[x_k^{2q_{i,k}} - x_{k-1}^{2q_{i,k}}\right]\right) + p^2_{i,n}\left(x^{2q_{z,n}} - x_{n-1}^{2q_{z,n}}\right) , \; i = y, z \qquad (2.9)$$

$$t_{n-1} \le t < t_n \; , \; x_{n-1} \le x < x_n$$

with

$$x_k = \sum_{m=1}^{k} u_m(t_m - t_{m-1}) \; ; \; (k = 1, 2, \ldots, n-1) \; ; \; x_0 = 0 \; ; \; x_n = x_{n-1} + u_n \Delta t_n .$$

At a given time instant $t = t_s$ of the n-th time interval $t_{n-1} \le t < t_n$, the front of the plume reaches the position $x = x_s = x_{n-1} + u_n(t_s - t_{n-1})$ on the x-axis. Eq. (2.8) with the corresponding values $\sigma_{i,eff}(x_s)$, (i = y, z) of the diffusion parameters yield the concentration distribution in the whole (y,z)-half-plane over the ground i.e. in the plane $x = x_s$ that is attached to the plume's front at time $t = t_s$ [12].

The factor Δf_n in Eq. (2.8) represents a correction with respect to the calculation of the T.I.C.. Instead of carrying out the time integration from $-\infty$ to $+\infty$ passing a receptor point, as it is common practice when using the straight-line Gaussian model, integration now is performed only for the duration of the respective time interval, resulting in a difference of error functions [38].

$$\Delta f_n = \frac{1}{2}\left\{ \mathrm{erf}\left(\frac{u_n(t_n - t_{n-1}) - \xi_n}{\sqrt{2}\,\sigma_{y,eff}} \right) - \mathrm{erf}\left(\frac{-\xi_n}{\sqrt{2}\,\sigma_{y,eff}} \right) \right\} \qquad (2.10)$$

$$\mathrm{erf}(x) = \frac{2}{\sqrt{\pi}} \int_0^x \exp(-s^2) ds \quad \text{error function}$$

with

ξ_n downwind coordinate of the receptor point related to the trajectory in the n-th time interval.

$$\xi_n = \frac{1}{u_n} \left\{ u_{x,n}\left[x - \sum_{k=1}^{n-1} u_{x,k}(t_k - t_{k-1}) \right] - u_{y,n}\left[y - \sum_{k=1}^{n-1} u_{y,k}(t_k - t_{k-1}) \right] \right\} .$$

Thus, Δf_n describes that part of the plume which passes by the receptor point during the n-th time interval.

In the derivation of Eq. (2.10) it has been assumed that the turbulent downwind diffusion, σ_x, is equal to the lateral diffusion, σ_y. Test calculations in [11] revealed that the assumption $\sigma_x = \sigma_y$ might lead to a predominance of the turbulent downwind diffusion compared to the advection by the mean wind. This is in contradiction to one of the basic assumptions of the Gaussian model types. Under certain circumstances unrealistic high concentration values could be observed near to the source in the downwind, and even in the upwind direction, especially, if dispersion parameters were used which led to rather broad plumes, for example if they were derived over rough terrain so that the mechanical component of turbulence is rather strong or if they comprise low-frequency meandering of the horizontal wind during stable atmospheric conditions [32]. To overcome this problem, Geiß [39]proposed not to change the assumption $\sigma_x = \sigma_y$ but to relate σ_x to short-term (e.g. 10-minute averaged) standard deviations, σ_θ of the horizontal wind direction. Therefore, σ_x has been parameterized as

$$\sigma_x = \frac{2}{3} x \tan \sigma_\theta \tag{2.11}$$

The effective downwind diffusion parameter is then given as

$$\sigma_{x,eff} = \sigma_{x,eff}(t) = \sum_{k=1}^{n-1} \sigma_{x,k} + \sigma_{x,n}(t - t_{n-1})$$

with:

$$\sigma_{x,k}(t_k - t_{k-1}) = \sigma_{x,k}(t_k) - \sigma_{x,k}(t_{k-1}) = \frac{2}{3} \Delta x_k \tan \sigma_{\theta,k}$$
$$\Delta x_k = x_k - x_{k-1}, \quad (k = 1, 2, \ldots, n-1)$$

Typical values of σ_θ (Table 3) are available from measurements at the nuclear research centres in Jülich and Karlsruhe at heights of 50m and 100m, respectively [40], [41].

Diffusion category	Standard deviations σ_θ of horizontal wind direction (degree)	
	50m height	100m height
A	23.8	20.5
B	18.9	13.9
C	15.3	10.1
D	12.6	6.9
E	10.2	4.0
F	8.6	2.0

Table 3. Standard deviations of horizontal wind direction (degree)

But it should be noticed that the linear increase of σ_x with source distance x (or travel time t) is only valid if the travel time of the plume is smaller than the Lagrangian turbulence time scale [35]. With increasing travel time the rate of diffusion decreases to

$$\sigma_x = \sigma_y \sim \sqrt{t} \sim \sqrt{x}$$

which also comes out from the assumption of Fickian diffusion for the Gaussian model (see Eq. (2.4)). Thus, for larger travel times Eq. (2.11) might also lead to an unrealistic overestimation of the turbulent downwind diffusion and the corresponding σ_x-values might even become higher than the σ_y parameters determined from dispersion experiments. In such cases the experimental σ_y values are again used for σ_x.

Figure 8, which shows the normalized time-integrated air concentrations near to the ground under the axis of a straight-line Gaussian plume resulting from a unit release at 100m height under stable atmospheric conditions, illustrates the problem of σ_x -parameterization.

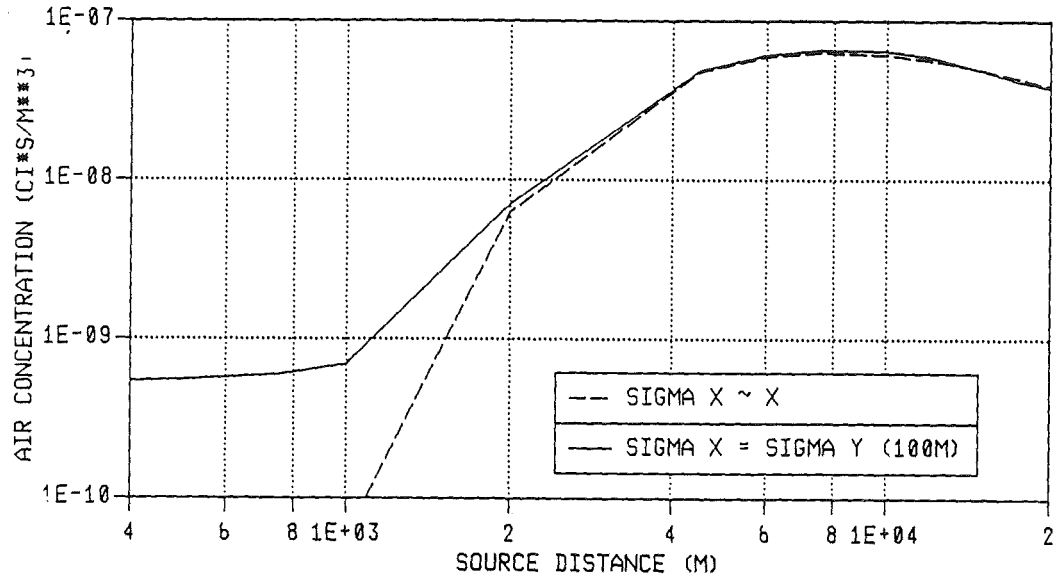

Figure 8. Illustration of "backward diffusion" in MUSEMET: release height: H = 100m stability category: F

Concentration values are unrealistically high near to the source under the assumption of $\sigma_x = \sigma_y$ with σ_y according to Eq. (2.9). The long-dashed line shows as an example the result of the σ_x -parameterization described above. It is evident that the concentration distribution now becomes more realistic.

2.3 *The puff diffusion model RIMPUFF*

The puff model RIMPUFF has been developed to describe the dispersion of time-dependent atmospheric releases taking into account non-stationary and non-homogeneous atmospheric conditions [13]. A puff is defined as a short-time release of a few seconds up to a few minutes. Thus, a continuous release can be simulated by a series of individual puffs each containing the same release rate. Figure 9a depicts an typical instanta-

neous plume together with the instantaneous concentration and the long-term average plume concentration. The puff model prediction is shown in Figure 9b.

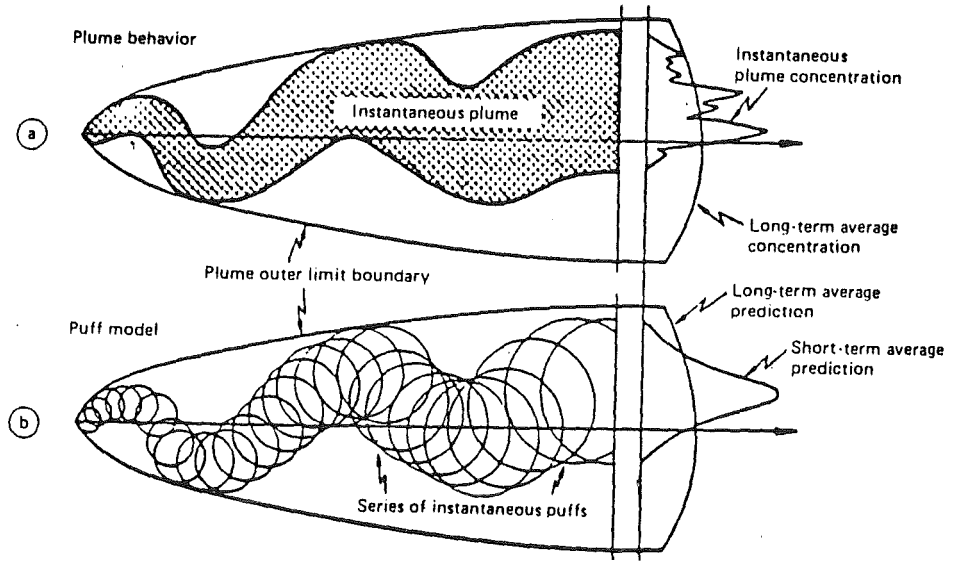

Figure 9. Schematic drawing of diffusion of a plume: simulation by a finite number of puffs,in case of changing wind direction (from [13])

The puffs are advected downwind by a wind field which is updated after certain time intervals, e.g. hourly intervals. It is assumed that the short-term average concentration is Gaussian-shaped and that it represents a reasonable approximation to ensemble-averaged instantaneous plume concentration profile. The long-term average concentration of the puff model is expected to be identical to the long-term concentration of Figure 9a.

Each puff contributes to the spatial concentration distribution which corresponds to the three-dimensional Gaussian solution of Eq. (2.1) for an instantaneous point emission [8]:

$$C_i(x,y,z) = \frac{Q_i}{(2\pi)^{3/2}\sigma_x\sigma_y\sigma_z} \exp\left(-\frac{1}{2}\left[\frac{(x-ut)^2}{\sigma_x^2} + \frac{(x-vt)^2}{\sigma_y^2} \right] \right) \left\{ \exp\left(-\frac{(z-H)^2}{2\sigma_z^2} \right) + \exp\left(-\frac{(z+H)^2}{2\sigma_z^2} \right) \right\} \quad (2.12)$$

with:

C_i	contribution of puff i to concentration at point x,y,z at time t (Bq/m³)
Q_i	total amount of released quantity carried by the i-th puff (Bq)
σ_x	longitudinal diffusion parameter (m); generally, $\sigma_x = \sigma_y$ is assumed
x,y,z	rectangular coordinates of a three-dimensional grid containing the whole area over which material is dispersing
u,v	time- and space dependent components of wind vector in the x and y direction, respectively (m/s)

Then the total concentration at each point is calculated by summing the contributions from all puffs in the grid at each time step. Once a puff is released, it is advected over a rectangular advection grid by the mean wind vector at its center-of-mass position at each time step [13]. The inhomogeneous wind field is estimated from a network of available observations by the method of objective wind analysis. A $1/r^2$-weighting function, where r is the distance from the grid point to the measurement station, is used for the interpolation [42]. Of course, the wind field can be determined by measurements at a single point at or nearby the source location as it is done in the plume model MUSEMET, restricting the validity of the model to homogeneous meteorological situations. At each grid point the vertical wind profile is calculated according to Eq. (2.7).

As the individual puffs advect with the wind, they grow in size in accordance with the local diffusion category. Fundamentally, the expansion of a single puff is related to the relative diffusion process which is most conveniently described as function of local turbulence intensities and downwind distances [43], [44]. Alternatively, in the absence of turbulence intensity data, the expansion of the puff can be described by suitable plume diffusion parameters. Eq. (2.5 - 2.6)). The sigma values after a given advection step Δx and for a given local stability are obtained by differentiation of Eq. (2.5 - 2.6) and, subsequently, integration

$$\sigma_j(x + \Delta x) = \left(\sigma(x)^{1/q_j} + p_j^{1/q_j} \cdot \Delta x\right)^{q_j}, \quad j = x,y,z \qquad (2.13)$$

2.4 *The MESOS model*

For the application in the far range (> 50km), where the site-specific characteristics (meteorological and topographical conditions) become less important, the MESOS model [14] is available. It is a trajectory-puff model which simulates the transport, dispersion, and deposition of airborne material up to distances of thousands of kilometres, thereby taking into account the changing local meteorological conditions obtained from a data base of standard meteorological observations from synoptic stations and ships every 3 hours across Europe. In MESOS a 3 hour release is simulated by explicitly tracing the histories and developments of puffs released at the beginning and at the end of the 3 hourly period. Further it is assumed that a continuous release over 3 hours is treated by a continuous sequence of intermediate puffs following intermediate trajectories. Their position, dispersion, and depletion will be calculated by interpolation between the tracked puffs leading to a contamination of the whole area along and between the calculated trajectories. The procedure is illustrated in Figure 10.

The model consists of three parts:

1. In a purely Lagrangian part the trajectories and the vertical dispersion of successive puffs are calculated in discrete time steps according to the local meteorological conditions (the Puff Development Module, PDM)
2. In the Eulerian part PEM (Population Exposure Module) the results of the PDM, the so-called puff histories, are used to calculate the exposure in a specified network of grid points.

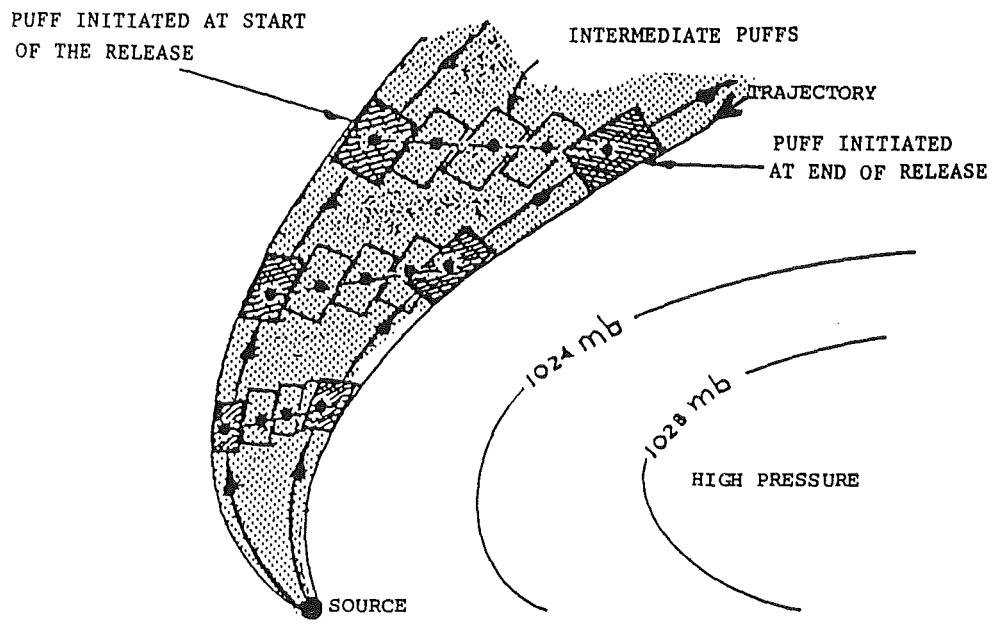

Figure 10. Lateral dispersion in MESOS

3. The third module EXPGRID, which will not be considered in further detail in this report, relates the polar concentration grid around the source to the geographical frame of reference which expresses the coordinates of the points of reference in degrees longitude and latitude (see also Sect. 2.10). The puff histories calculated in the PDM refer to geographical coordinates. Therefore, the coordinate transformation is necessary before the concentrations are calculated in the PEM.

1) Puff Development Module (PDM)

Once a puff is released it is advected through a series of time steps of 10min intervals for the first 3 hours and thereafter at 1 hour intervals using the average wind over the vertical extent of the puff. The mean wind is based on the the geostrophic wind which is backed and reduced within the mixing layer. The wind profile, u(z), within this layer is approximated by a power law

$$u(z) = u_g\left(\frac{z}{h_{mix}}\right)^p \quad \text{for } z < h_{mix} \tag{2.14}$$

such that the geostrophic wind speed, u_g, is attained at the top of the mixing layer. Above h_{mix} the wind is assumed geostrophic. The exponent p is determined as a function of h_{mix} in such a way that the conditions

$$u(10) = 0.5u_g \quad \text{over land}$$
$$u(10) = 0.85u_g \quad \text{over the sea}$$

are fulfilled for the 10m wind.

The direction of the mean wind is backed by an angle

$$a(z) = \frac{2(u_g - u(z))}{u_g} a_{10} \tag{2.15}$$

so that $a(z)$ tends to zero as $u \rightarrow u_g$ and to a_{10} as $u \rightarrow u(10)$.

The vertical development of a puff is calculated using σ_z parameters which corresponds to the prevailing stability class. The stability category is assessed differently according to whether the underlying surface is land or sea. Overland the Pasquill-Gifford category is derived according to a method described in [45] on the basis of windspeed, cloud cover, and, during the day, insolation calculated from solar elevation. If the vertical puff column fills the whole of the current mixing layer, the subsequent vertical evolution of the puff purely depends on the daily variation of the depth of the mixing layer (Figure 11).

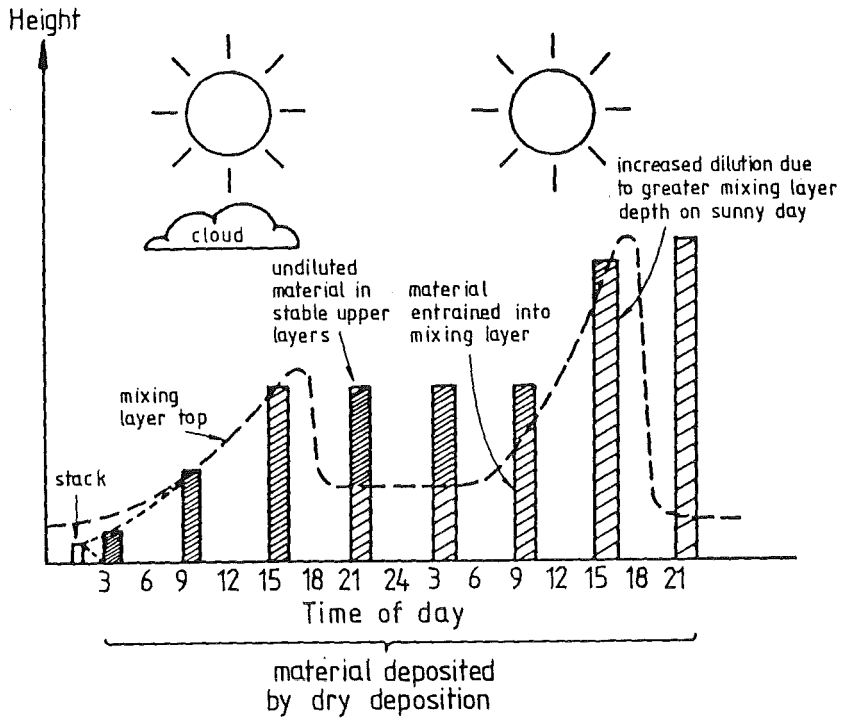

Figure 11. Simplified illustration of vertical dispersion in MESOS: (from [14])

If the layer increases then the radioactive material is diluted over the increased depth. If the layer shrinks parts of the activity becomes isolated in the stable layer above the inversion and it cannot be deposited on the ground by dry deposition until the top of the mixing layer rises again. Then the activity are re-entrained what might cause high con-

centrations near to the ground at greater distances. The growth of the convective layer during the day-time is calculated by assessing the heating of the layer due to insolation. To account for the effect of mechanical mixing a minimum depth proportional to the windspeed is taken into account as an inital value of h_{mix},

$$h_{mix}^{mech} = c\, u_g$$

and it is taken as the depth of the mixing layer if the additional heat input is too low to rise the top of the layer by convection. The whole method is adapted from [46] and evaluated in detail in [15]. For neutral and stable conditions the mixing layer height is proportional to the windspeed where the constant of proportionality decreases with increasing stability.

$$h_{mix} = c\, u_g$$

The height h_{mix} is set to a minimum value if the windspeed is to low (Table 4).

Diffusion category	constant of proportionality, c	height of mixing layer, h_{mix} (m)
D	90	$h_{mix} = 90\ u_g$
E	50	$h_{mix} = \max(50\ u_g, 200)$
F	25	$h_{mix} = \max(25\ u_g, 200)$

Table 4. Mixing layer heights for neutral and stable conditions overland: (adapted from [15])

It is more difficult to derive accurately the stability category and height of mixing layer over the sea. Surface roughness is relatively low so that mechanical turbulence will be less effective. Therefore, it is assumed that with moderate or strong wind conditions ($u_g \geq 12$m/s) the stratification is neutral but with a smaller h_{mix}, taking into account the smoother surface (see Table 5, category D). With lower wind speeds the predictions of stability and mixing layer depends on the difference between the air temperature just above the sea surface, T_s, and the temperature at 300m height, T_{300} , which may be taken from the temperature profile for a puff as it leaves the land (Table 5)

Diffusion category	Temperature difference $T_{300} - T_s$, (K)	height of mixing layer, h_{mix} (m)
D	< 3	$h_{mix} = 50\ u_g$
E	3 ... 6	200
F	> 6	200

Table 5. Mixing layer heights over the sea for low windspeed conditions

The air surface temperature, T_s, depends on the sea surface temperature (SST). For the North Sea the SST is taken as a sinusoidal function of the day of the year. The Mediterranian temperature lies 7.5K above the SST of the North Sea. Conditions of enhanced evaporation and latent heat fluxes causing a growth of the mixing layer over the sea have

not been considered in MESOS because there is too much uncertainty in the description of these processes [15].

2) Population Exposure Module (PEM)

As already mentioned it is assumed that a continuous release during a 3 hourly interval is simulated by a sequence of intermediate puffs which spread out between the two trajectories being calculated for those puffs which have been started at time t_0 and $t_0 + \Delta t$ ($\Delta t = 3h$) (Figure 10). These two trajectories define the plume boundaries and it is assumed that the area under plume is exposed completely by the passing activity in the plume. The lateral expansion of the plume is dominated by the divergence of successive trajectories caused by the synoptic wind conditions, while the small scale lateral turbulent diffusion of an individual puff, which is caused by relativley small-scale eddies in the atmosphere, only leads to a broadening of the plume beyond the trajectories forming the boundaries. Therefore, the horizontal diffusion parameter, σ_y (in m), is simply assumed to be proportional to the travel time, t (in sec), of a puff according to Doury's system [47].

$$\sigma_y = 0.5\,t \tag{2.16}$$

Having defined a plume, it is possible to assess the time integrated atmospheric concentrations and the dry and wet deposition at receptor points passed by the plume using the calculated histories of the boundary puffs. The assessment is performed for each tracked puff at the beginning and end of travel-time steps of 10min intervals for the first 3 hours and thereafter of 1 hour intervals.

The time integrated air concentration from one single puff is given by

$$C_p = \frac{Q}{u B_p h_p} \tag{2.17}$$

with

C_p	time integrated puff concentration in the air near the ground (Bq s m^{-3})
Q	airborne radioactive material (Bq) (Bq s m^{-3})
u	transport velocity (m/s)
B_p	puff width (m)
h_p	puff heigth (m)

Since it is assumed that C_p is the same as the air concentration under the axis of a Gaussian plume with dispersion parameters σ_y and σ_z, the puff width and height are given by

$$B_p = 0.5\,t\sqrt{2\pi} = \sigma_y\sqrt{2\pi}$$

and

$$h_p = \sigma_z\sqrt{\frac{\pi}{2}}\ ,$$

respectively, using Eq. (2.16) for σ_y.

The contribution of intermediate puffs to the envorinmental impact is interpolated. Only those intermediate puffs are considered which pass the respective receptor point within half a puff width, $B_p/2$.

Principal modifications:

Three principal modifications have been made to MESOS at KfK:

1. The number of "persecution days" of each puff in the PDM was enlarged from 5 to 15 days. Now 90 percent of puffs can be tracked unitl leaving the MESOS region.
2. The module EXPGRID got a new option to modify the polar concentration grid. In the original version of MESOS the number of azimuthal grid points increased from 16 for the inner radii to 64 for the outer radii. In the modified version of MESOS it possible to use a constant number of 64 azimuthal grid points in all distances. The new option was necessary to adapt MESOS to the UFOMOD requirements.
3. The PEM has been modified in such a way that now differential concentration patterns (values for each 3 hourly time interval) are available. They represent the concentration distributions resulting from release phases which last 3 hours. In addition, the arrival time of trajectories at each grid point will now be determined (see also Sect. 2.11).

2.5 *The ISOLA model*

Recent studies on the source terms showed that accidental releases might occur which extend over time periods from about four days up to several months. They can be characterized, as illustrated in Figure 12, as long-term, quasi-continuous accidental releases with a low release rate and which might be interrupted by a short-term peak release.

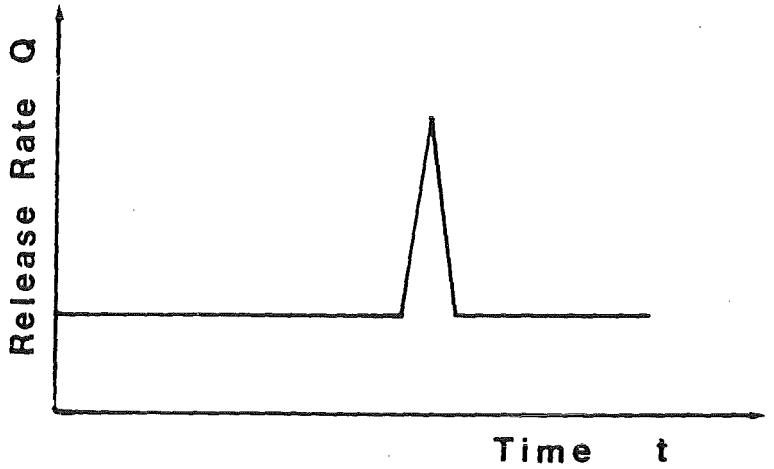

Figure 12. Illustration of long-term, quasi-continuous low-rate release

Although Gaussian-like trajectory models are potentially able to simulate the atmospheric dispersion during a long-term release, the computer time required would be very large.

STATISTICS OF DISPERSION CONDITIONS
1. 1.1982 - 31.12.1982
PRECIPITATION INTENSITY: I = 0 MM/H 86.54 %
CALMS (<=0.5M/S) 9.93 %

WIND DIRECTION 210 GRAD (3.85 %)

SPEED (M/S)	DIFFUSION CATEGORY						
	A	B	C	D	E	F	SUM
0.6- 1.0	0.34	0.00	0.00	0.00	0.68	2.40	3.42
1.1- 1.5	0.00	0.34	1.03	0.34	2.05	1.37	5.14
1.6- 2.0	0.00	0.34	0.34	1.03	0.68	1.71	4.11
2.1- 4.0	2.05	0.34	3.77	16.78	3.77	0.00	26.71
4.1- 8.0	0.34	0.00	3.08	49.66	0.00	0.00	53.08
8.1-15.0	0.00	0.00	0.34	7.19	0.00	0.00	7.53
15.1-30.0	0.00	0.00	0.00	0.00	0.00	0.00	0.00
SUM	2.74	1.03	8.56	75.00	7.19	5.48	100.00

WIND DIRECTION 220 GRAD (5.62 %)

SPEED (M/S)	DIFFUSION CATEGORY						
	A	B	C	D	E	F	SUM
0.6- 1.0	0.00	0.00	0.00	0.23	0.23	1.41	1.88
1.1- 1.5	0.00	0.47	0.23	0.94	2.58	2.82	7.04
1.6- 2.0	0.23	0.47	0.70	1.17	3.29	3.76	9.62
2.1- 4.0	0.47	0.94	2.82	19.95	3.99	0.00	28.17
4.1- 8.0	0.00	0.94	2.58	45.77	0.00	0.00	49.30
8.1-15.0	0.00	0.00	0.47	3.52	0.00	0.00	3.99
15.1-30.0	0.00	0.00	0.00	0.00	0.00	0.00	0.00
SUM	0.70	2.82	6.81	71.60	10.09	7.98	100.00

WIND DIRECTION 230 GRAD (5.34 %)

SPEED (M/S)	DIFFUSION CATEGORY						
	A	B	C	D	E	F	SUM
0.6- 1.0	0.00	0.25	0.00	0.00	1.23	1.73	3.21
1.1- 1.5	0.49	0.25	0.99	0.49	2.72	2.22	7.16
1.6- 2.0	0.25	0.00	0.74	0.99	2.22	1.48	5.68
2.1- 4.0	1.23	1.98	5.68	20.25	3.21	0.00	32.35
4.1- 8.0	0.00	0.74	5.19	39.75	0.00	0.00	45.68
8.1-15.0	0.00	0.00	0.99	4.94	0.00	0.00	5.93
15.1-30.0	0.00	0.00	0.00	0.00	0.00	0.00	0.00
SUM	1.98	3.21	13.58	66.42	9.38	5.43	100.00

STATISTICS SUMMED OVER ALL WIND DIRECTIONS
1. 1.1982 - 31.12.1982

SPEED (M/S)	DIFFUSION CATEGORY						
	A	B	C	D	E	F	SUM
0.0- 0.5	0.07	0.58	0.08	0.21	2.59	6.41	9.93
0.6- 1.0	0.18	0.46	0.11	0.18	1.79	3.36	6.09
1.1- 1.5	0.44	0.58	0.90	0.71	3.07	4.01	9.71
1.6- 2.0	0.63	0.67	1.06	0.82	2.60	3.79	9.56
2.1- 4.0	1.93	3.22	7.37	13.92	5.78	0.13	32.34
4.1- 8.0	0.45	1.28	5.46	23.02	0.00	0.00	30.21
8.1-15.0	0.00	0.01	0.25	1.89	0.00	0.00	2.15
15.1-30.0	0.00	0.00	0.00	0.00	0.00	0.00	0.00
SUM	3.69	6.81	15.22	40.75	15.83	17.70	100.00

Figure 13. Example of 4-parametric statistics of meteorological data used as input for ISOLA: figures are given in %

On the other hand, if the release duration is sufficiently long, different atmospheric conditions during the release can be evaluated statistically by classifying the wind directions, the wind speeds, diffusion categories, and precipitation intensities. In those cases, a modified version of the fast-running straight-line Gaussian model ISOLA, [17], developed at the Institute for Meteorology and Climatology (IMK) at KfK, can be applied to calculate the time-integrated air concentrations and ground contamination patterns according to the meteorological conditions represented by each of the statistical classes. Afterwards all concentrations are summed up taking into account the frequency of each class. Figure 13 shows parts of a statistical evaluation of hourly meteorological data measured at an observation station in Hamburg/F.R.G. during the year 1982. The statistics represents the whole year.

The atmospheric dispersion after the possible short-term peak release, which might interrupt the long-duration source term (Figure 12), will be modelled seperately by a trajectory model. The concentration distribution of the complete release is obtained by a superposition of the ISOLA and trajectory model results. To test this concept a comparison between the trajectory model MUSEMET and ISOLA has been performed. As an example, Figure 14 shows the ground concentrations after an 144 hours release. It can be seen that the results of both models are in good agreement.

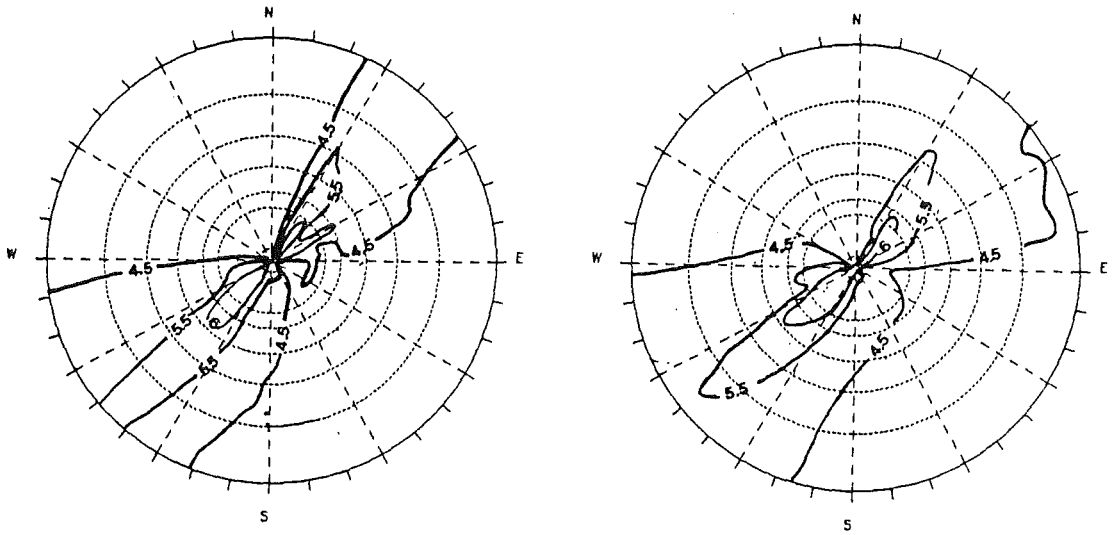

Figure 14. Ground concentrations after a long duration release (144h): isolines represent the decadic logarithms of concentrations
left: MUSEMET
right: ISOLA
outer radius r=87.5km

Thus, the statistical evaluation of rather long atmospheric sequences leads to similar results as the explicit consideration of dispersion situations by a trajectory model. The CPU-time saved applying ISOLA depends on the duration of the release. For each release ISOLA needs about 30 seconds, regardless of the release duration. In the example mentioned above the ISOLA model was about a factor of three faster than MUSEMET. This factor will of course increase with increasing release duration.

The principal properties of ISOLA can be summarized as follows:

1. consideration of four-parametric statistics of meteorological conditions;
2. highest spatial resolution for a wind direction sector: 10 °
3. calculation of time-integrated air concentrations and ground contamination patterns due to dry and wet deposition at predefined receptor point in each sector using the bi-Gaussian distribution function;
4. thereby taking into account the contribution of radioactivity from neighbour sectors;
5. depletion of the radioactive plume due to fallout, washout, and radioactive decay;
6. assumption of a "cold" source (no thermal plume rise);
7. consideration of turbulent mixing in the wake of the source.

A more detailed discussion of these properties will be given in [26].

2.6 *Dispersion parameters σ_y and σ_z*

In MUSEMET, RIMPUFF, and ISOLA the horizontal and vertical dispersion parameters σ_y and σ_z are assumed to be power functions of the source distance (Eq. (2.5 - 2.6)). The appropriate dispersion coefficients depend on the atmospheric stability, the surface roughness z_0, and the release height. In their standard versions the models distinguish between two different sets of dispersion coefficients valid for two different surface roughnesses. Those determined experimentally at the Belgian Nuclear Energy Research Centre (SCK/CEN, Mol, Belgium) are used for dispersion calculations over rather smooth terrain (0.1 m $\leq z_0 <$ 1 m) [33] (see Table 6 and Figure 15). They have been checked for hourly values at a height of 69 m above ground. Originally, the SCK/CEN turbulence typing scheme consists of seven dispersion categories. Six classes (E1 to E6) correspond to the Pasquill-Gifford categories F to A (see Table 1).

Height (m)	Stability Category	Diffusion Coefficients			
		p_y	q_y	p_z	q_z
69	A	0.946	0.796	1.321	0.711
	B	0.826	0.796	0.950	0.711
	C	0.586	0.796	0.700	0.711
	D	0.418	0.796	0.520	0.711
	E	0.297	0.796	0.382	0.711
	F	0.235	0.796	0.311	0.711

Table 6. SCK/CEN dispersion coefficients: (from: [33])

The seventh class E7 which represents neutral conditions with high speed ($u \geq 11.5$m/s) will not be considered in the UFOMOD atmospheric dispersion models. Over rough terrain ($z_0 \geq 1$) the height dependent Karlsruhe - Jülich sigma parameter system will be applied [48] (see Table 7 and Figure 16).

Height (m)	Stability Category	Diffusion Coefficients			
		p_y	q_y	p_z	q_z
50	A	1.503	0.833	0.151	1.219
	B	0.876	0.823	0.127	1.108
	C	0.659	0.807	0.165	0.996
	D	0.640	0.784	0.215	0.885
	E	0.801	0.754	0.264	0.774
	F	1.294	0.718	0.241	0.662
100	A	0.179	1.296	0.051	1.317
	B	0.324	1.025	0.070	1.151
	C	0.466	0.866	0.137	0.985
	D	0.504	0.818	0.265	0.818
	E	0.411	0.882	0.487	0.652
	F	0.253	1.057	0.717	0.486
180	A	0.671	0.903	0.025	1.500
	B	0.415	0.903	0.033	1.320
	C	0.232	0.903	0.104	0.997
	D	0.208	0.903	0.307	0.734
	E	0.245	0.903	0.546	0.557
	F	0.671	0.903	0.484	0.500

Table 7. Diffusion coefficients: Karlsruhe-Jülich-system as function of stability category and height (from: [48])

The parameterization of lateral dispersion in MESOS has already been described in Section 2.4 (Eq. (2.16)). The vertical dispersion parameters σ_z are derived from Smith's scheme for estimating the vertical dispersion of a plume from a source near ground level for a surface roughness $z_0 = 0.3$m [45] (see Figure 17)

2.7 *Height of mixing layer*

The mixing layer is the part of the atmosphere above the ground where most of the atmospheric dispersion and deposition processes take place and where the radionuclides are well mixed vertically due to thermal and mechanical turbulence. The upper boundary of this layer varies with stability. Generally, it is assumed that this boundary is formed by an inversion layer which cannot be penetrated by the plume. An exception is the MESOS model where parts of the radioactive material remain above the inversion if the mixing layer shrinks (see Sect. 2.4). The models MUSEMET and RIMPUFF do not explicitly model the daily variations of the depth of the mixing layer. Preselected values

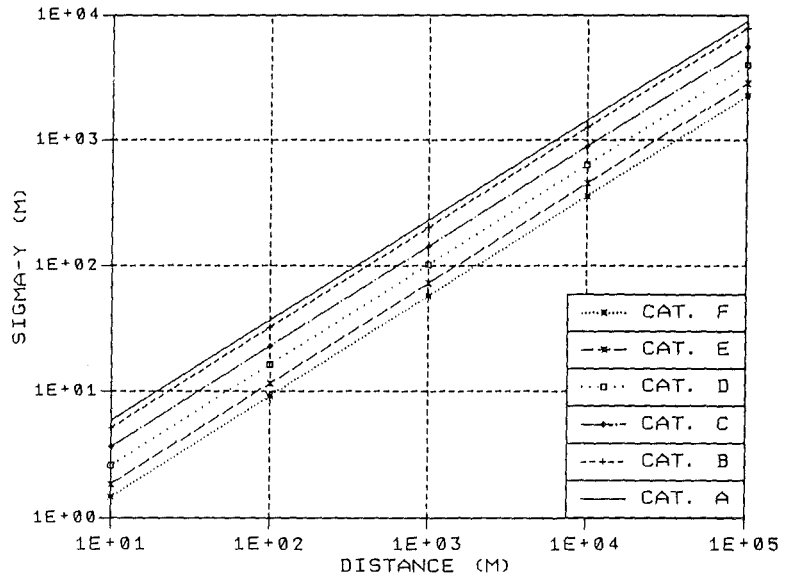

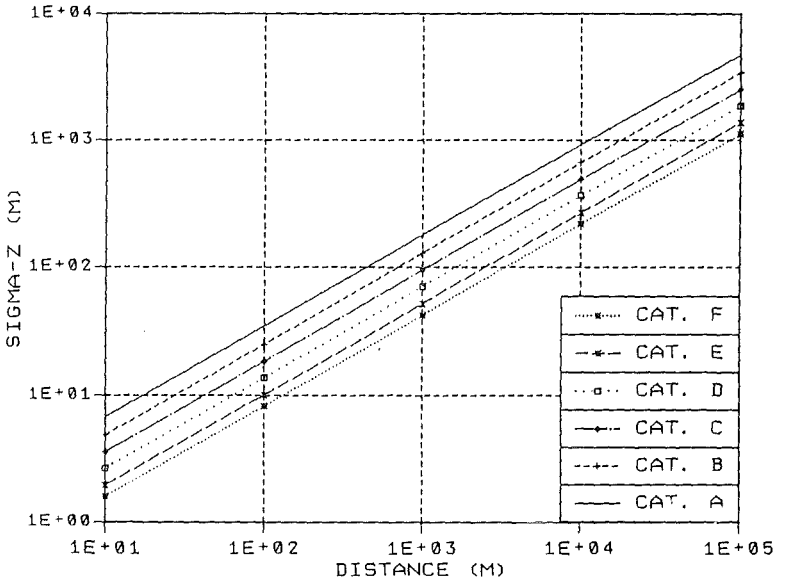

Figure 15. SCK/CEN dispersion parameters:
top: horizontal parameters, σ_y
bottom: vertical parameters, σ_z

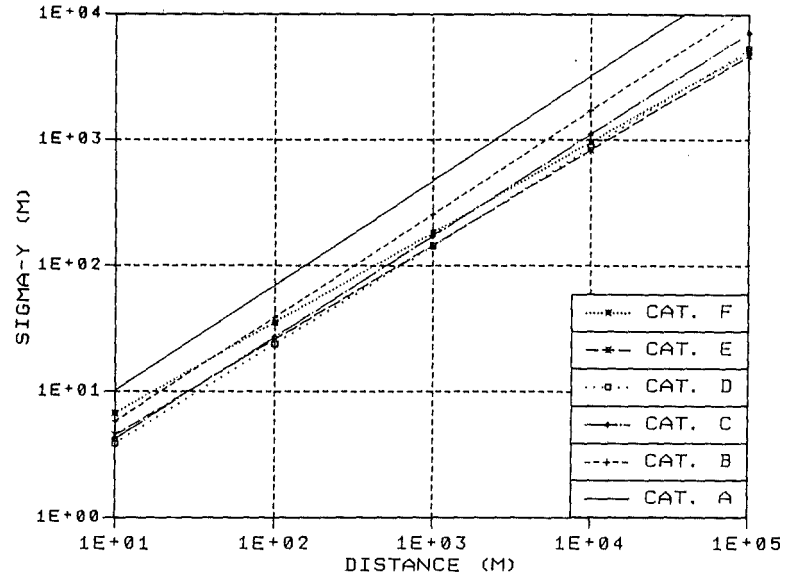

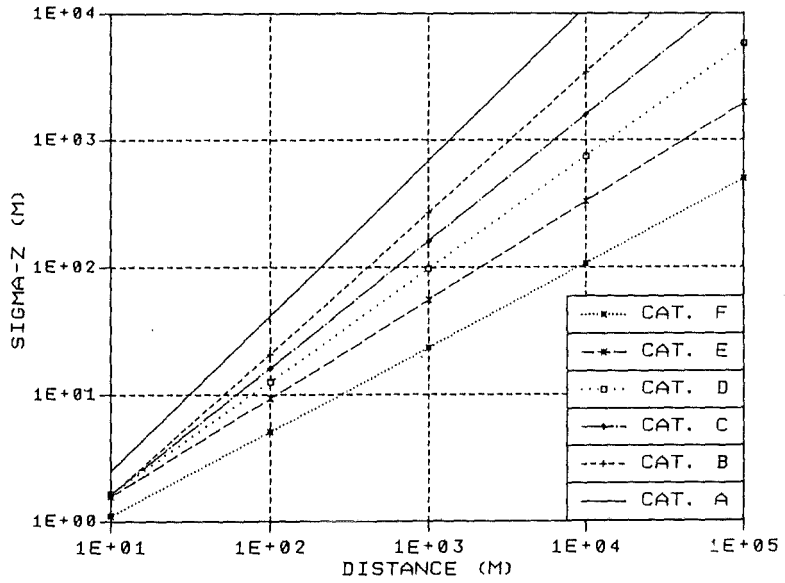

Figure 16. Example of Karlsruhe - Jülich sigma parameters for 50 m release height:
top: horizontal parameters, σ_y
bottom: vertical parameters, σ_z

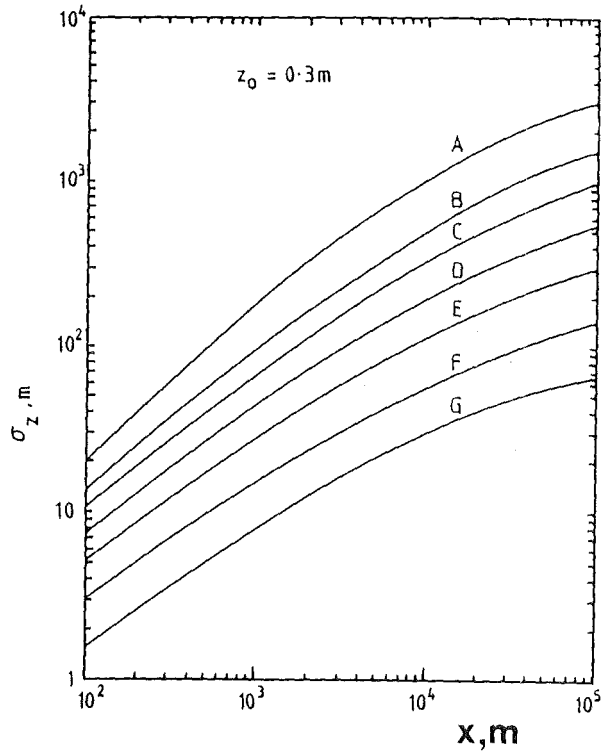

Figure 17. Vertical dispersion parameter σ_z in MESOS for z_0 = 0.3 m: (from [45])

depending on the stability class are used (Table 8). Neither the final plume rise height nor the vertical diffusion can exceed the mixing height. Multiple perfect reflection of the plume at this lid is taken into account by limiting the vertical diffusion parameter σ_z according to [49].

$$\sigma_z = \sigma_z^{max} = 0.8h_{mix}, \quad \text{if } \sigma_z \geq \sigma_z^{max} \tag{2.18}$$

Diffusion category	Height of mixing layer (m)	
	MUSEMET/ISOLA	RIMPUFF
A	1600	1600
B	1200	1200
C	800	800
D	560	600
E	320	300
F	200	200

Table 8. Height of mixing layer

Further, it is assumed that once a certain height of the mixing layer is reached during the course of the day, it cannot decrease, even if the atmospheric stratification turns to more

stable conditions. If inhomgeneous meteorological data with different stability regions and thus different mixing heights are available for RIMPUFF, the highest value for h_{mix} is chosen to apply for all stability regions. For ISOLA also the values shown in Table 8 are used. Since it is assumed that the meteorological conditions represented by each of the four-parameter statistics are constant throughout the release and the dispersion, temporal variations of the mixing layer have not to be taken into account. Only the limitation of σ_z according to Eq. (2.18) is considered.

2.8 *Modelling of deposition processes*

During the dispersion material may be removed from the plume by dry and wet deposition resulting in the contamination of the ground.

Dry deposition is due to the contact of the plume on surfaces, such as walls, leaves and ground; gravitational settling will not yet be considered. It is assumed that the resulting surface contamination C_d (in Bq/m^2) is proportional to the T.I.C. near the ground, generally, at 1m height [2]:

$$C_d = v_d C \qquad (2.19)$$

where v_d is referred to as the dry deposition velocity (in m/s). It depends on the physical and chemical form of the isotopes released: noble gases which will not be deposited, particulate material (aerosols) with a typical diameter of 1 μm, elemental and organically bound iodine. Typical values of v_d are given in Table 9.

Structure of surface	Aerosols (1 μm)	Iodine	
		elemental	organic
smooth surfaces incl. streets	2.E-4	2.E-3	5.E-4
agricultural surfaces	1.E-3	1.E-2	5.E-4
forest canopies	1.E-2	1.E-2	5.E-4
averaged values (used in UFOMOD)	3.E-3	1.E-2	5.E-4

Table 9. Typical dry deposition velocities (m/s): (derived from [50])

It can be seen that especially for aerosols v_d strongly depends on characteristics of the underlying surface. Over forests it is about 10 times higher than over agricultural surfaces. Because the average percentage of forests in the Federal Republic of Germany (F.R.G.) is about 30%, an average value of ($v_d = 3. 10^{-3}$ m/s) is used in UFOMOD to take account of the stronger depletion of a plume over forests than over agricultural areas. But in terms of accident consequences only the deposition on agricultural surfaces and on urban areas is of interest. Therefore, to calculate the ground contamination due to dry deposition according to Eq. (2.19) the dry deposition velocities have to be corrected by factors like those shown in Table 10.

Type of nuclide	v_d (m/s)	Correction Factor
noble gases	0.0	1.0
aerosols	3.E-3	3.333E-1
elemental iodine	1.E-2	1.0
organically bound iodine	5.E-4	1.0
particulate iodine	3.E-3	3.333E-1

Table 10. Dry deposition velocities and correction factors used in UFOMOD

Generally, in Gaussian-type dispersion models the loss of activity in the plume due to dry deposition is accounted for by reducing the source strength with downwind distance. This so called source depletion model [35] implicitly assumes that the depletion occurs over the whole depth of the plume rather than at the surface; therefore, the shape of the plume's vertical profile does not change. The rate of change of source strength, Q, with distance, x, is

$$\frac{\partial Q}{\partial x} = -\int_{-\infty}^{\infty} C_d(x, y)dy = -\sqrt{\frac{2}{\pi}}\,\frac{v_d Q}{u\sigma_z}\,\exp\left(-\frac{H^2}{2\sigma_z^2}\right)$$

which leads to

$$\frac{Q(x)}{Q_0} = f_d = \exp\left[-\sqrt{\frac{2}{\pi}}\,\frac{v_d}{u}\,I\right]$$

$$\text{with } I = \int_0^x \exp\left(-\frac{H^2}{2\sigma_z^2}\right)\frac{dx}{\sigma_z} \qquad (2.20)$$

In MUSEMET the depletion factor f_{d_n} during the n-th time interval is given simply by substituting u by u_n, σ_z by $\sigma_{z,eff}$, and integrating from x_{n-1} to x, with $x_{n-1} < x \leq x_n$, where x is the effective trajectory length.

Three different cases have to be considered:

1. $\sigma_{z,eff} < \sigma_{z,eff}^{max} = 0.8\, h_{mix}$

   The activity is not yet distributed uniformly over the whole depth of the mixing layer and $\sigma_{z,eff}(x)$ increases with x according to Eq. (2.6) (Figure 18a). In this case the integral I is converted into into an integral over $\sigma_{z,eff}$ by the following substitution:

$$\frac{d\sigma_{z,eff}}{dx} = \frac{d\sqrt{\sigma_{z,eff}^2}}{dx} = \frac{1}{\sigma_{z,eff}}\,\frac{q_{z,n}}{x}\,\sigma_{z,n}^2$$

$$\text{with } \sigma_{z,n}^2 = p_{z,n}^2 x^{2q_{z,n}}$$

   which leads to

$$I_1 = \int_{\sigma_{z,eff}(x_{n-1})}^{\sigma_{z,eff}(x)} \exp\left(\frac{-H^2}{2\sigma_{z,eff}^2}\right) \frac{x}{\sigma_{z,n}^2 q_{z,n}} \, d(\sigma_{z,eff}) \qquad (2.21)$$

Current values for $\sigma_{z,n}^2$ and x can be calculated from Eq. (2.9). Then Eq. (2.21) is solved numerically according to the Newton-Cotes formula with five knots [51].

2. $\sigma_{z,eff} = \sigma_{z,eff}^{max} = 0.8\, h_{mix}$

The second case characterizes the complete mixing of the activity over the whole depth of the mixing layer (Figure 18b). Thus, $\sigma_{z,eff} = \sigma_{z,eff}^{max} = \text{const.}$, and the solution of integral I is

$$I_2 = \frac{\exp\left(\frac{-H^2}{2\sigma_{z,eff}^2}\right)}{\sigma_{z,eff}} (x - x_{n-1}) \qquad (2.22)$$

3. The third case (Figure 18) is a combination of the cases 1) and 2). Uniform vertical distribution will be achieved during the n-th time interval at an effective source distance x_m. The integral I is seperated into two parts

$$I_3 = \int_{x_{n-1}}^{x_m} \exp\left(\frac{-H^2}{2\sigma_{z,eff}^2}\right) \frac{dx}{\sigma_{z,eff}} + \int_{x_m}^{x} \exp\left(\frac{-H^2}{2(\sigma_{z,eff}^{max})^2}\right) \frac{dx'}{\sigma_{z,eff}^{max}} = I_1 + I_2 \qquad (2.23)$$

I_1 is treated numerically according to Eq. (2.21) and I_2 is solved according to Eq. (2.22). The reduction factor f_{d_n} is then written as

$$f_{d_n} = \exp\left[\frac{-v_d}{u_n}\sqrt{\frac{2}{\pi}}\,(I_1 + I_2)\right] = f_{d_n}^{(1)} f_{d_n}^{(2)} \qquad (2.24)$$

A numerical solution of Eq. (2.20) is also performed in ISOLA [26].

In RIMPUFF, Eq. (2.20) is approximated by

$$f_d = 1 - \frac{\Delta x}{u}\sqrt{\frac{2}{\pi}}\,\frac{v_d}{\sigma_z}\exp\left(-\frac{H^2}{2\sigma_z^2}\right) \qquad (2.25)$$

where Δx is the advection step of a puff.

In MESOS an effective deposition velocity, $v_{d,eff}$, is introduced. The basic dry deposition velocity, v_d, is modified by a stability dependent resistance term, r, added.

$$\frac{1}{v_{d,eff}} = \frac{1}{v_d} + r \qquad (2.26)$$

In stable conditions this resistance term account for the low diffusivity in the lowest layers. This means that material near the ground will be depleted faster than it can be

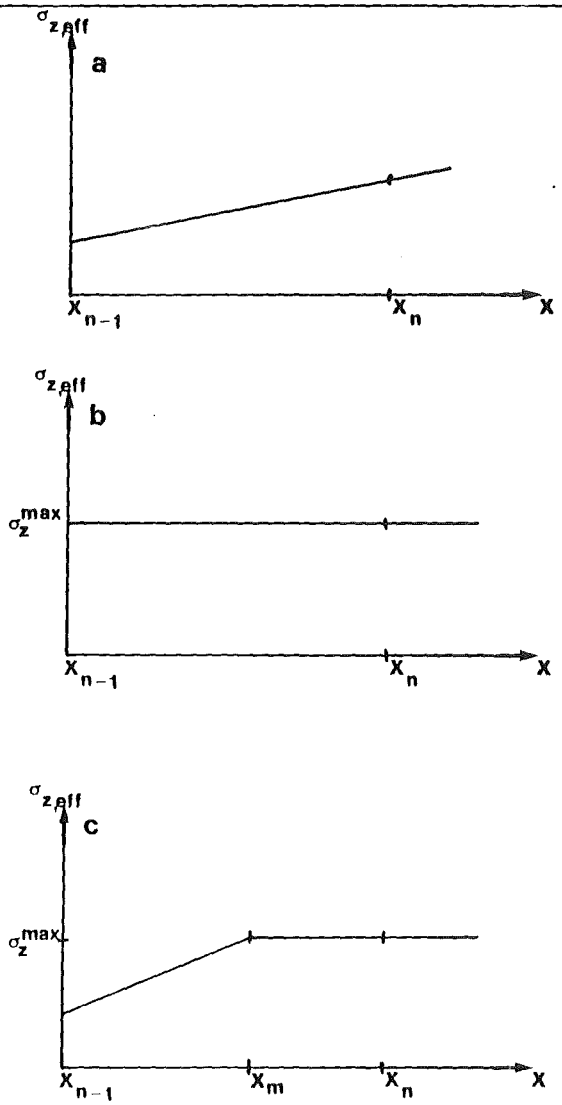

Figure 18. Illustration of cases which have to be considered in dry deposition modelling

replenished from above, and a vertical concentration profile will develop with reduced concentrations near the ground limiting the rate of deposition. The resistance term is usually small overland (Table 11), whereas for prolonged transport over the sea in stable conditions, the dry deposition may be substantially reduced. The depletion of the puffs is also modelled by the source depletion model.

Diffusion category	r, overland (s/m)	r, over sea (s/m)
A - D	0	0
E	20	300
F	40	800

Table 11. Resistance terms, r, for dry deposition in MESOS

The source depletion model does not correspond to the physical reality because the deposition only causes a reduction of material in the lowest layer near the ground. Consistently, the source depletion model overpredicts the surface air concentration and the dry deposition at downwind locations close to the source, and as a consequence, the model is biased in the opposite sense for locations far from the source. At all distances the total deposition between source and receptor is overestimated, and consequently, the material remaining airborne is underpredicted. Horst [52] provided a more realistic surface depletion model which selectively depletes the Gaussian plume in the vicinity of the deposition surface. Unfortunately, the surface depletion model is computationally too complex and hence often inappropriate in application with the Gaussian plume diffusion model. Therefore, Horst [53], [54] developed a corrected source depletion model whose computational requirements are comparable to those of the source depletion model and whose predictions are in close agreement with those of the surface depletion model. In this new approach, the change of vertical concentration distribution caused by deposition has been accounted for by a profile correction factor. Doran and Horst [55] showed that the corrected source depletion model gave the best agreement with observations, when they evaluated Gaussian plume depletion models with dual-tracer field experiments. The corrected source depletion model has not yet been implemented in the UFOMOD atmospheric dispersion and deposition models. But to model as realistic as possible without increasing the computational effort this is planned for next versions.

The mechanism contributing to wet deposition on the ground is washout. It describes the contamination of the ground by rain, snow and hail formed above and falling through the plume and thereby collecting particulates and soluble gases or vapours; rainout, which refers to the removal of airborne constituents during the formation and growth of rain drops in the plume, will not be considered. The resulting source depletion is accounted for by applying the following correction factor [2]:

$$f_w(x) = \exp\left(-\frac{\lambda}{u}x\right) \tag{2.27}$$

where λ is the washout coefficient (s^{-1}), u the wind speed (m/s) in release height H, and x the downwind distance (m). The coefficient λ describes the amount of precipitation scavenging and the rate of wet deposition on the ground. It depends on the physico-chemical porperties of the airborne material and the precipitation intensity. In MESOS, λ is determined as a function of precipitation intensity, i (in mm/h), according to the power law [35]

$$\lambda = a\, i^b \ . \tag{2.28}$$

The coefficients a and b shown in Table 12 are taken from [50]. This modelling of precipitation scavenging can optionally be chosen also in MUSEMET, RIMPUFF.

Type of nuclide	Coefficient a	Exponent b
noble gases	0.0	0.0
aerosols	8.E-5	0.8
elemental iodine	8.E-5	0.6
organically bound iodine	8.E-5	0.6
particulate iodine	8.E-5	0.8

Table 12. Coefficients and exponents of power law to determine the washout coefficient λ

Another possibility in MUSEMET, RIMPUFF, and ISOLA is to use precalculated values of λ which have been evaluated for gaseous and particulate radionuclides for three different precipitation classes [56] (Table 13). Additionally, a characteristic relative duration of rainfall, which is derived from a ten years record of rain intensity measurements at the Kernforschungszenturm Karlsruhe (Table 14), is linked to each intensity class.

Type of nuclide	Precipitation intensity class		
	$i < 1$mm/h	1mm/h $\leq i <$ 3mm/h	$i \geq$ 3mm/h
noble gases	0	0	0
aerosols	3.4E-5	1.17E-4	3.33E-4
elemental iodine	4.2E-5	1.06E-4	2.33E-4
organically bound iodine	4.2E-7	1.06E-6	2.33E-6
particulate iodine	3.4E-5	1.17E-4	3.33E-4

Table 13. Precalculated washout coefficients (1/sec)

Type of nuclide	Precipitation intensity class		
	$i < 1$mm/h	1mm/h $\leq i <$ 3mm/h	$i \geq$ 3mm/h
noble gases	0	0	0
aerosols	0.50	0.73	0.58
elemental iodine	0.47	0.73	0.62
organically bound iodine	0.75	0.78	0.67
particulate iodine	0.50	0.73	0.58

Table 14. Relative duration of rainfall for precipitation scavenging

The precipitation induced flux of activity to the ground is given by

$$C_w(x, y) = \Lambda \int_0^{z_w} C(x,y,z)dz \quad , \quad (Bq/m^2) \tag{2.29}$$

where z_w is the depth of the wetted plume.

Assuming that the coefficient Λ is independent of both space and time, Eq. (2.29) gives for rain falling through a bi-Gaussian plume

$$C_w(x, y) = \frac{\Lambda Q}{(2\pi)^{1/2}\sigma_y u} \exp\left(-\frac{y^2}{2\sigma_y^2} \right) \tag{2.30}$$

For a three-dimensional Gaussian puff as in RIMPUFF, the wet contribution to the ground contamination is given by

$$C_w(x, y) = \frac{\Lambda Q}{2\pi\sigma_y\sigma_x u} \exp\left(-\frac{y^2}{2\sigma_y^2} \right) \exp\left(-\frac{1}{2}\frac{(x-ut)^2}{\sigma_x^2} \right) \tag{2.31}$$

If the duration of the precipitation is taken into account, the right hand sides of Eq. (2.29 - 2.31) have to be multiplied with the appropriate relative duration factor listed in Table 14. To correct for the depletion due to precipitation, the argument of the exponential function in Eq. (2.27) has to be multiplied with the duration factor.

The total contamination, $C_g(x, y)$, is then given by the sum of $C_d(x, y)$ and $C_w(x, y)$.

2.9 *Meteorological input data*

All models have been devised with the requirement that they should use real meteorological data, extracted from routine observations recorded and reported from meteorological stations. Generally, for MUSEMET, RIMPUFF, and ISOLA, hourly meteorological data are used. The necessary data input consists of wind speed, wind direction, precipitation intensity, and the Pasquill-Gifford stability classes. The consequences after a nuclear accident will vary considerably with the prevailing meteorological conditions. Therefore, the length of the the complete record of meteorological input data should be at least one year to ensure that a large spectrum of different weather situations is comprised.

For ACAs, which should have been carried out with the UFOMOD/NE and UFOMOD/NL versions within the framework of the DRS-B, hourly data of the years 1982 and 1983 have been made available by the German Weather Service for several stations in the FRG. But also any other meteorological data set measured at a synoptic station, which is representative for any arbitrary nuclear site, can be used, provided that the structure of the input data is evaluated as described in the UFOMOD user guide [69].

The MESOS models needs three hourly synoptic data. They are measured at synoptic stations distributed nearly over the whole area of Europe (36°N - 62°N, 10°W - 50°E) (Figure 19) and they also cover the 1982/1983 period.

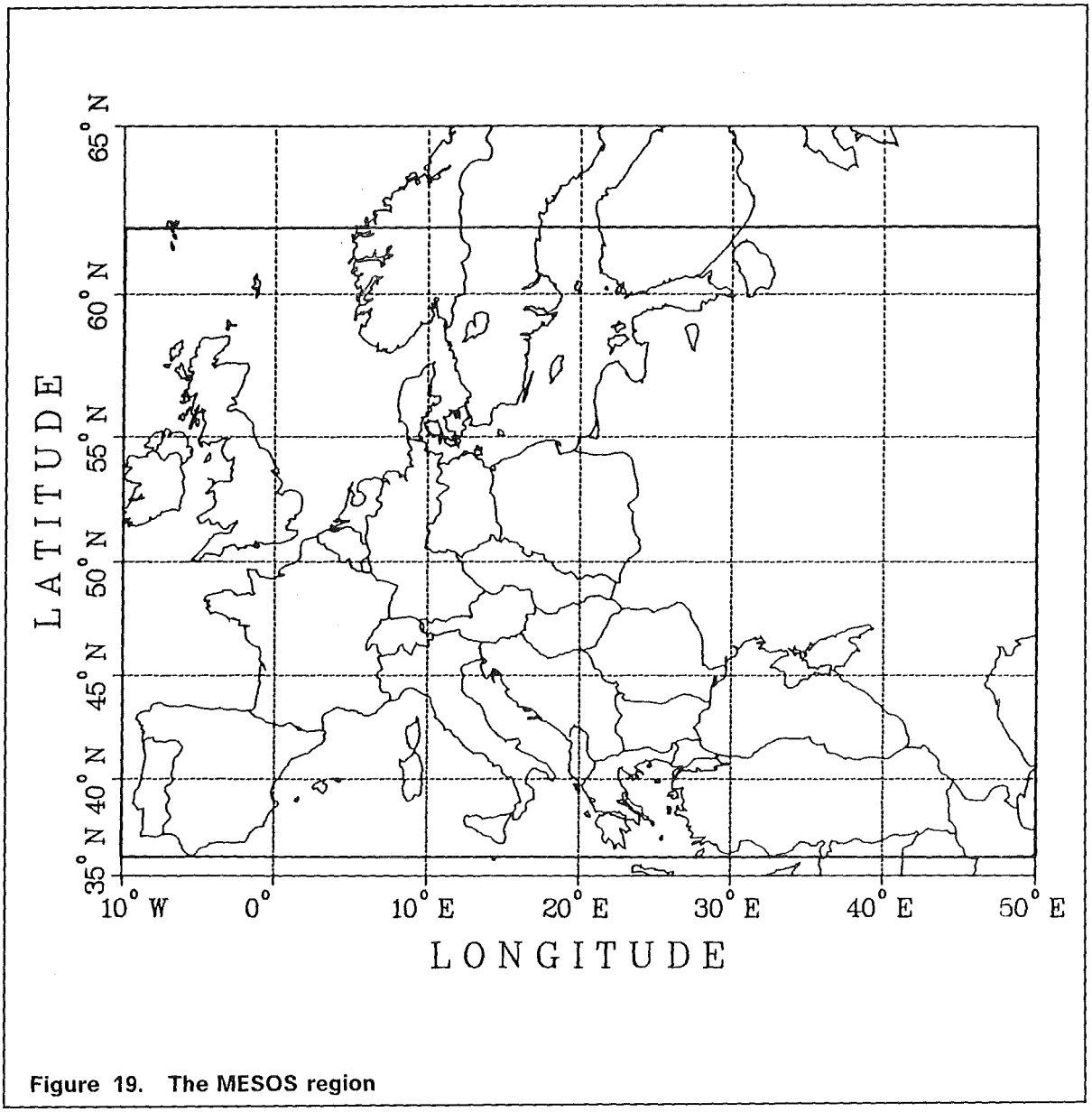

Figure 19. The MESOS region

The data consists of surface pressure, air temperature, relative humidity, cloud cover and height of cloud level, and informations on precipitation intensity. Other parameters necessary for modelling a dispersion process like wind speed, wind direction, stability class, height of mixing layer are derived from the input data by several submodels (Table 15).

MESOS database	Derived quantities
pressure and cloud cover	geostrophic wind, insolation, stability, mixing layer height
air temperature	stratification over sea
precipitation intensity	wet deposition rate
relative humidity and height of cloud level	not yet used

Table 15. Meteorological database of MESOS and derived quantities

The MESOS raw data were converted into grid point values using objective analyses methods and interpolation schemes which are described in [15]. This work has been performed at the Imperial College of Science of Technology. All parameters except surface pressure are available on a grid at intervals of 1° latitude and2 ° longitude. Pressure values exists on a 0.5° latitude / 1° longitude grid.

A somewhat special quantity is the precipitation intensity. The amount of rainfall in the locality of a synoptic station is generally available only in the form of the "present weather" code. This code contains 100 different weather specifications. The code numbers 50 to 99 are used to indicate various types of precipitation occurring at the time of observation, whilst codes 20 to 29 are reserved for precipitation in the previous hour. But since all models need precipitation intensities in mm/h, the code numbers have to be converted into figures which are typical for the different types of precipitation. The conversion methods performed in MESOS and for the MUSEMET, RIMPUFF, and ISOLA input data will be briefly outlined in the Appendix A.

2.10 *The concentration grid*

The structure of all UFOMOD versions is based on a polar coordinate grid system with the centre point at the location of the nuclear facility. The radial and azimuthal resolution of the near range versions can be preselected but the standard values of 20 radii and 72 azimuthal sectors are recommended. In the far range model, the grid size of 35 radial distance bands and 64 equidistant azimuthal intervals are obligatory on the use of the MESOS code (Figure 20).

The polar system is defined in accordance with the wind rose. The polar angle, ϕ, is counted clockwise and it is zero if it coincides with the northern direction (Figure 21).

To calculate concentrations according to the Gaussian formalism the polar coordinates of the reference points have to be transformed into the coordinates of a rectangular cartesian frame of reference. Figure 21 illustrates also the relationship between the polar concentration grid and the cartesian system as it is valid for MUSEMET and ISOLA. The (R, ϕ) - coordinates of any polar grid point are converted into cartesian coordinates by the simple transformation

$$x_p = R \cos \alpha$$
$$y_p = R \sin \alpha \qquad (2.32)$$

index	radii of the grid system (default values)	
	UFOMOD/NE/NL [km]	UFOMOD/FL [km]
1	0.250	10
2	0.400	20
3	0.625	30
4	0.875	40
5	1.150	50
6	1.550	60
7	2.10	70
8	2.70	80
9	3.70	90
10	4.90	100
11	6.55	125
12	8.75	150
12	11.5	175
14	15.5	200
15	21.0	300
16	27.0	400
17	37.0	500
18	49.0	600
19	65.5	700
20	87.5	800
21		900
22		1000
23		1100
24		1200
25		1300
26		1400
27		1500
28		1600
29		1700
30		1800
31		1900
32		2000
33		2100
34		2200
35		2300

Figure 20. UFOMOD: Radial grid of the subsystems: (from [9])

where R denotes the radial distance (in m) and a can be calculated from the definition of the modulus

$$w_1 = 450 - \phi \equiv a(\text{ mod } 360).$$
$$a = w_1 - \left[\frac{w_1}{360} \right] 360 \qquad (2.33)$$

The bracket indicates that the largest integer whose magnitude does not exceeds the magnitude of $w_1/360$ is used.

In RIMPUFF the transformation has to be performed with respect to the rectangular (x,y)-advection grid [25] (Figure 22).

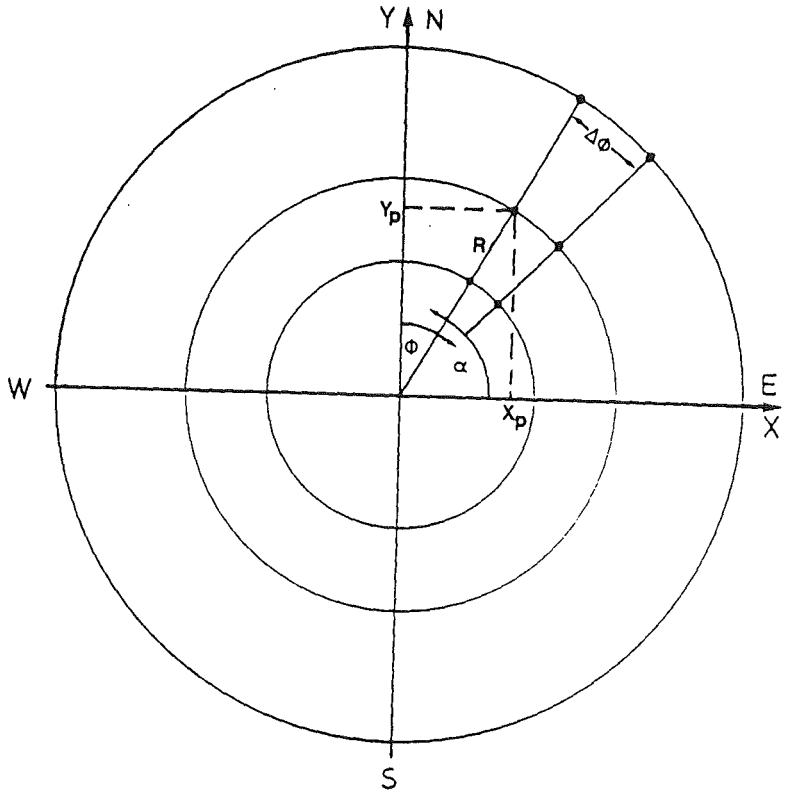

Figure 21. Illustration of concentration grid in UFOMOD

The source and the origin of the corresponding polar system are located just in the centre of the advection grid at the position (x_s, y_s) so that the transformation equations are given by

$$x_p = R \cos \alpha + x_s$$
$$y_p = R \sin \alpha + y_s \qquad (2.34)$$

with α according to Eq. (2.33).

In MESOS the transformation is more complicated. At first, the fixed coordinates of the polar system are transformed into geographical coordinates (longitude and latitude). This can be performed knowing the geographical position of the source. Then the geographical coordinates are converted into rectangular cartesian coordinates with respect to the source location, and the positive x and y axes point to the East and North, respectively. Calculating the x coordinate the convergence of longitudinal circles towards the poles is taken into account. The plume boundaries defined by the trajectories of two tracked puffs and the distance each puff travels along its trajectory during an advection time step define a completely general quadrilateral. Only those reference points lying inside this area are considered and the concentrations are calculated according to a method described in more detail in [15].

Figure 23a illustrates how concentrations are calculated in MUSEMET. Once knowing the cartesian coordinates (x_p, y_p) of the polar grid points, these are transformed into rectangular coordinates (ξ, η) with respect to a trajectory frame of reference. This transforma-

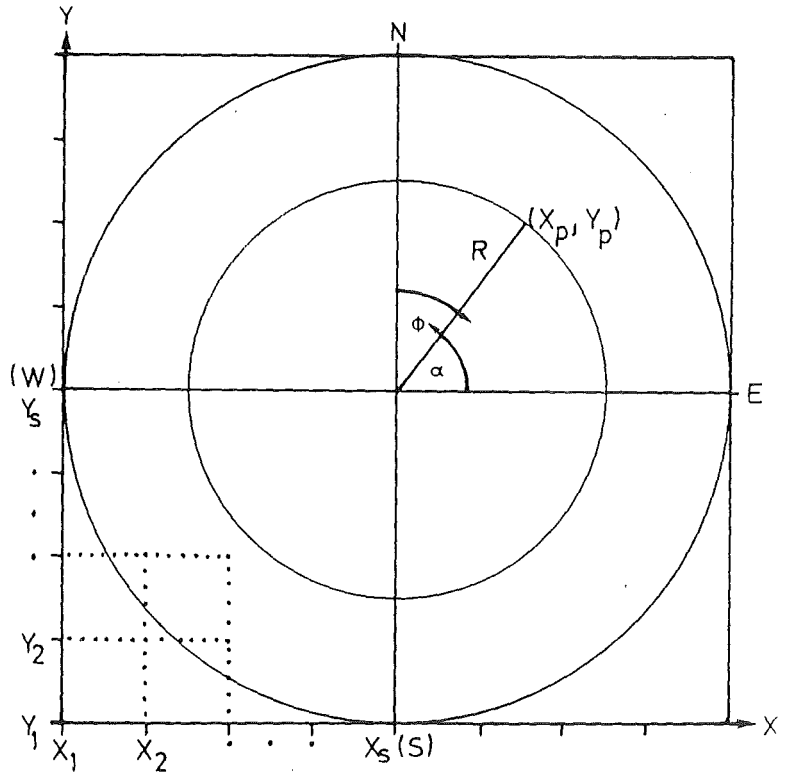

Figure 22. Illustration of concentration and advection grids in RIMPUFF

tion will be performed in each hourly time step by successive translations and rotations according to the prevailing wind conditions (see also Section 2.2, Figure 7). The origin of the trajectory system of the k-th time interval lies in the starting point of the k-th straight-line trajectory segment. The ξ-axis coincides with the trajectory segment (or the plume's axis) and is directed downwind. Knowing the (ξ_k, η_k) - coordinates of each polar reference point, the concentration contributions are calculated for all reference points with $0 \leq \xi_k \leq u_k \Delta t$.

Since MUSEMET behaves like a straight-line Gaussian model along the straight-line trajectory segments, it is inherently not able to follow the trajectory if a change of wind direction occurs. To avoid discontinuities in the concentration distribution in those regions where the trajectory changes its direction, it is necessary to consider also reference points with $\xi_k < 0$ and $\xi_k > u_k \Delta t$. For this purpose a circular region is defined around the endpoint $\xi_i = u_i \Delta t$, $i = 1, \ldots, n$, of each trajectory segment (Figure 23b). The radius, r_i, is defined as the distance from the plume's axis where the concentration on the plume' centreline, C_{pl} , has reduced to a minimum (or cut-off) concentration, C_{min}:

$$r_i = \sigma_{y,eff} \sqrt{-2 \ln\left(\frac{C_{pl}}{C_{min}}\right)} \quad , \; i = 1, \ldots, n \tag{2.35}$$

Then all reference points will also be considered whose ξ_k coordinates fulfill the conditions

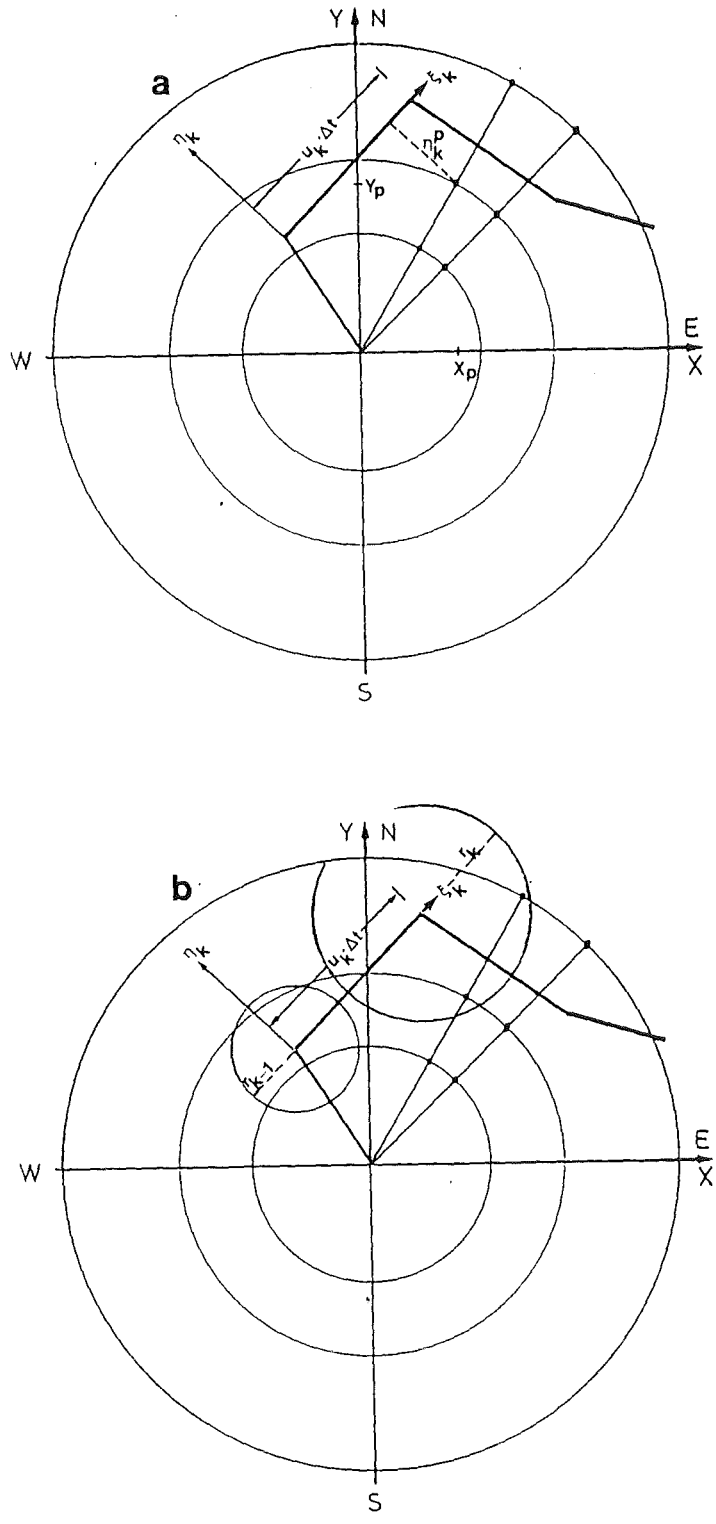

Figure 23. Geometrical relationships in the segmented plume model MUSEMET

$$u_k \Delta t < \xi_k \leq u_k \Delta t + r_k$$
$$-r_{k-1} \leq \xi_k < 0$$

2.11 *Output of the atmospheric dispersion models*

Each atmospheric dispersion model applied in the UFOMOD system has to provide normalized time-integrated air and ground concentrations with respect to the polar grid system. A correction factor for γ-radiation from the cloud in the near range has also to be determined at each grid point affected by the plume (see Chapter 4). In addition, the arrival times of the radioactive plume at a certain grid point has to be calculated. It is defined as the time interval from the beginning of the release phase when the cut-off concentration in the air near to the ground is exceeded for the first time. The time spent until a repeated passage of the plume over the same grid point will not be considered because it is assumed that the contributions to the concentration during a second or subsequent passage is much lower than during the first crossing.

All these quantities are then transferred to and processed in a subsequent UFOMOD submodule named CONCEN to calculate the initial air and ground activity concentrations of individual radionuclides at each grid element and to correct for radioactive decay during dispersion and the build-up of radionuclides from radioactive decay chains. Both normalized and actual concentration levels and the areas contaminated with concentration levels can be presented as complementary cumulative frequency distributions (CCFDs) and statistical quantities. A list of possible presentations is given in Table 16.

Type of results	Presentations
time integrated concentrations in air and on ground surface	CCFDs, expectation values, percentiles as a function of distance for each radionuclide
areas contaminated with concentration levels	CCFDs, expectation values, percentiles for a preselected concentration interval, radionuclide and distance band

Table 16. UFOMOD: possible presentations of results of atmospheric dispersion modelling: (from [9])

3. MODELLING OF PLUME RISE, LIFT-OFF, AND THE INFLUENCE OF BUILDINGS

As a function of the properties of the underlying source term and the meteorological conditions during the release, there may be plume rise and building effects. Both phenomena affect the concentration distributions and, hence, the consequences arising in the vicinity of a nuclear facility. It is for this reason that they must be taken into account in the dispersion model. This chapter only describes their modelling in MUSEMET.

In MESOS building effects at the source location are not considered because they will not influence the concentration in far distances. Also the rising phase of a thermal plume will not be taken into account. Only the final rise height is calculated.

In ISOLA "cold" releases are assumed. Therefore, plume rise is not modelled. The effects buildings might have on the concentration distribution in the vicinity of the source are modelled similar as in MUSEMET [26].

A new modelling of plume rise in RIMPUFF is under development. It will be described in [25].

3.1 Modelling thermal plume rise

The best known model equations dealing with thermal plume rise were derived by [57], and they are the basis for the plume rise model in MUSEMET. They describe in particular the end of the rise phase by turbulent mixing with the ambient air for the cases of neutral and unstable (convective) stratification of the atmosphere.

A plume rises above its source mainly for two reasons. On the one hand, it may have a certain escape velocity and, thus, a component of momentum directed vertically upward. On the other hand, it may be warmer than the ambient air, which means that an upward buoyancy force becomes effective because of the lower density. Generally, plume rise due to the initial momentum is neglected in favor of thermal buoyancy. Heating may occur already inside the plant by the input of sensible heat. However, heat may also be generated outside, on the one hand, by self-absorption of radiation in the radioactive plume [58] and, on the other hand by condensation in the cooling process, if the plume contains water vapor. The two heating processes mentioned last are not being considered at present in the dispersion models of the UFOMOD program system.

3.1.1 Model equations

Most models describing plume rise are based on the fundamental physical principles of the conservation mass, enthalpy, and momentum [57], [59]. It is from these conservation laws that Briggs [57]derives the following differential equation for thermal plume rise above a point source:

$$\frac{d^2\xi}{dt^2} + \beta_T \xi = \frac{3F}{\beta_e^2 x} t \qquad (3.1)$$

In this equation, the plume rise is $z = \xi^{1/3}$ (m), and t is the time (s) which, together with the advection speed, $\bar{u}$ (m s^{-1}), averaged over the height, results in the distance, $x = \bar{u}t$. Briggs parametrizes the turbulence in the plume by a simple entrainment relation, which links the increase in the plume radius, R, with the height by means of the entrainment constant, $\beta_e \simeq 0.4$ to 0.6 :

$$\frac{dR}{dt} = \beta_e \frac{\Delta z}{dt}$$
$$R(x) = \beta_e z(x) \qquad (3.2)$$

The buoyancy parameter depends on the emission of sensible heat, Q_H , and on the atmospheric ambient conditions. It can approximately be indicated as

$$F = \frac{gQ_H}{\pi c_p \rho T} = 8.84\, Q_H \quad , \quad (m^4 s^{-3}) \qquad (3.3)$$

with

g	acceleration under gravity (m s^{-2}),
c_p	specific heat of air at constant pressure (J kg^{-1} K^{-1})
ρ	air density (kg m^{-3})
T	absolute ambient temperature (K)
Q_H	sensible heat emission (MW).

The stratification of the atmosphere is represented by the stability parameter, β_T.

$$\beta_T = \frac{g}{T} \frac{\partial \Theta}{\partial z} \quad , \quad (s^{-2}) \qquad (3.4)$$

In this formula, Θ is the potential temperature of the ambient air (K).

For different atmospheric stability conditions, the following solutions of Eq. (3.1) can be indicated:

(a) $\beta_T > 0$ (stable stratification):

$$\xi = z^3 = \frac{3}{\beta_T \beta_e^2 \bar{u}} F \left(1 - \cos\left(\sqrt{\beta_T}\, \frac{x}{\bar{u}}\right)\right) + z_a^3 \qquad (3.5)$$

(b) $\beta_T = 0$ (neutral stratification):

$$\xi = z^3 = \frac{3}{2\beta_e^2 \bar{u}} F \left(\frac{x}{\bar{u}}\right)^2 + z_a^3 \qquad (3.6)$$

This equation also results from Eq. (3.5) for $\beta_T \rightarrow 0$, if the cosine term is developed up to the second term.

For point sources ($z_a = 0$), the well known $x^{2/3}$ law follows.

(c) $\beta_T < 0$ (unstable, convective stratification):

$$\xi = z^3 = \frac{3}{\beta_T \beta_e^2 \bar{u}} F \left(1 - \cosh\left(\sqrt{|\beta_T|}\, \frac{x}{\bar{u}}\right)\right) + z_a^3 \qquad (3.7)$$

In these equations, z_a is the initial vertical displacement of an area source above a virtual point source (Figure 24).

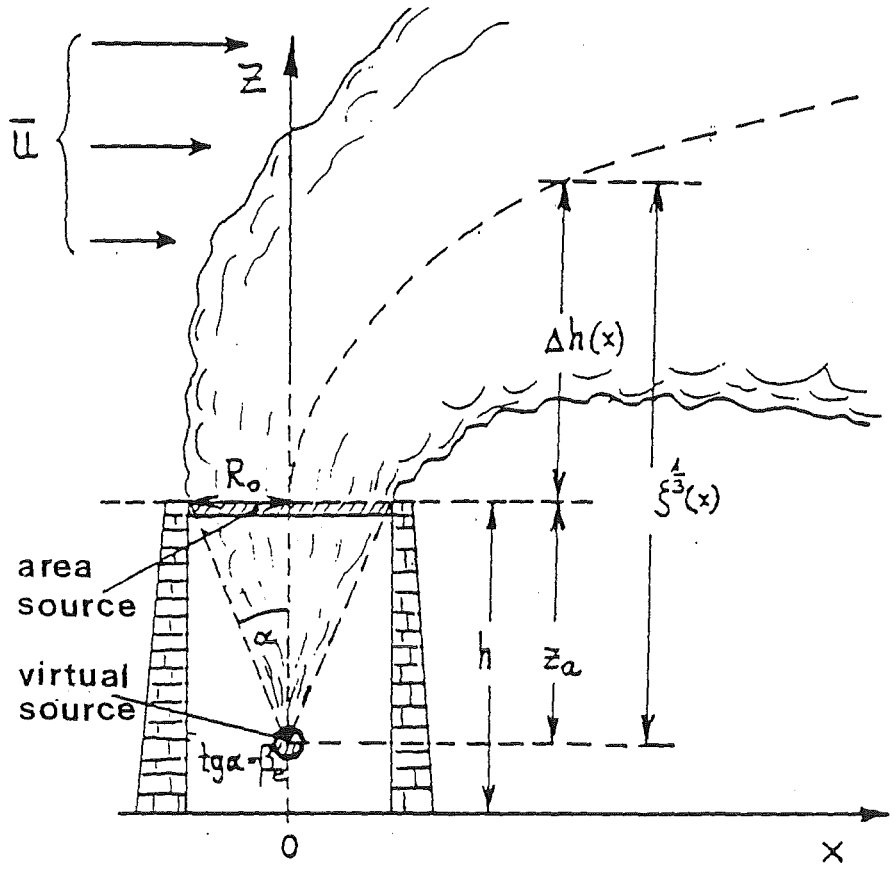

Figure 24. Diagram explaining the quantities dealing with plume rise

It results from the radius of the plane source, R_0, according to Eq. (3.2) :

$$z_a = \frac{R_0}{\beta_e} \qquad (3.8)$$

In case of a stack release, R_0 is the inner radius of the stack opening. If the accidental release occurs from a building, the source also must be treated as an area source. However, the orientation in space of this source is unknown. Therefore, the initial plume rise is defined as a characteristic length of the building, e.g., the "diameter",

$$2\sqrt{\frac{B\,H_B}{\pi}} \simeq z_a \qquad (3.9)$$

of a circle with the same area as the building assumed to be rectangle with the effective width, B (see Section 3.2.2), and the height, H_B [36]. The thermal plume rise above a real plane source in that case is

$$\Delta h = \xi^{1/3} - z_a \tag{3.10}$$

3.1.2 Formulae for the rise phase and for rise limitation

Except for the stable case, Eq. (3.5 - 3.7) do not limit thermal plume rise. Aside from external limitations to rise, such as inversion layers, there are effects restricting plume rise as a result of continuous turbulent broadening of the plume and the associated decrease of thermal energy density within the plume. According to [57], the final height has been reached when the dissipation rates of the internal turbulent energy of the plume and of the ambient air become identical.

For neutral stratification, this setup, with the approximation of a source height which is low compared to the ultimate height, results in the equation

$$\Delta h_{end} = 1.3 \frac{F}{\bar{u} u_\star^2} \tag{3.11}$$

$u_\star$ is the friction velocity in (m s^{-1}) calculated as a function of the surface roughness of the ground from the logarithmic wind profile. It is assumed to be constant over the entire height of rise.

The trajectory of the thermal plume in a neutral environment, prior to reaching the final height, is calculated in accordance with Eq. (3.6). If unstable conditions prevail, the dissipation rate of turbulent energy in the ambient convective atmosphere is proportional to the turbulent heat flow. From this [57] derives the relation,

$$\Delta h_{end} = 4.3 \left(\frac{F}{\bar{u}} \right)^{3/5} H_F^{-2/5} \tag{3.12}$$

where H_f is the turbulent heat flow multiplied by $g c_p^{-1} \rho^{-1} T^{-1}$, with the dimension of ($m^2 s^{-3}$). Typical values of H_F in the geographic latitudes of Europe are found in Table 17.

Diffusion category	H_F (m^2/s^3)
A	0.008
B	0.006
C	0.003

Table 17. Turbulent heat flow, H_F, under unstable conditions

To calculate the trajectory during the rise phase, Kaiser [59] recommends the use of Eq. (3.6) as a conservative approximation under neutral conditions, as there was shortage of observation data of plume rise in convection situations.

From Eq. (3.5) for stable stratification it can be seen that the plume rise has a peak for

$$t = \frac{x}{\bar{u}} = \frac{1}{\sqrt{\beta_T}}$$

For longer periods of time, ξ as well as the plume radius, R(x), oscillate (Eq. (3.2)). The latter finding, however, is physically unrealistic. In reality, the oscillation of the plume trajectory will be damped very quickly by stable ambient conditions. Briggs [57] recommends to define the final rise so that the temperature of the plume is identical to the ambient temperature. From this postulate, he derives as the final height,

$$\Delta h_{end} = 2.6 \left(\frac{F}{\bar{u}\beta_T} \right)^{1/3} \tag{3.13}$$

In the model, possible oscillations are suppressed. The rise phase up to the final height has been approximated from graphic plots of observed heights of rise [57].

$$\xi = z_a^3 + (2.6)^3 \frac{F}{\bar{u}\beta_T} \left(1.32 - \frac{1.26}{\sqrt{\beta_T}\,\frac{x}{\bar{u}} + 0.956} \right)^3 , \quad \sqrt{\beta_T}\,\frac{x}{\bar{u}} < 3 \tag{3.14}$$

Figure 25a and Figure 26a show two examples of thermal plume rise under neutral and stable conditions. The underlying assumptions were a release height, H = 30 m, and a heat emission, Q_H = 50 MW. The wind velocities at a height of 10 m are indicated in the diagrams.

The wind velocity, $\bar{u}$ and the stability parameter, β_T, are mean values over the rise interval, Δh.

According to Eq. (2.7) the wind velocity averaged over height is given as

$$\bar{u} = \frac{1}{\Delta h} \int_h^z u_0 \left(\frac{z'}{z_{ref}} \right)^p dz' = \frac{u_0}{z_{ref}^p\,(p+1)} \left(\frac{z^{p+1} - h^{p+1}}{\Delta h} \right) \tag{3.15}$$

if the effective release height is below 200 m. For heights above 200 m, the wind velocity is assumed to no longer increase with height, but to remain at its level, u_{200}, at 200 m altitude. Under this assumption, the mean wind velocity for effective source heights above 200 m is calculated as

$$\bar{u} = \frac{1}{\Delta h} = \left[\frac{u_0}{z_{ref}^p\,(p+1)} \left(200^{p+1} - h^{p+1} \right) + U_{200}(z - 200) \right] \tag{3.16}$$

To calculate the plume rise, Δh, in stable situations, gradients of the potential temperature, $\partial\Theta/\partial z$, averaged over Δh must be determined in order to find the stability parameter, β_T. In [36], the following height averaging procedure was used for this purpose:

$$\overline{\frac{\partial\Theta}{\partial z}} = \frac{1}{\Delta h} \int_{h_1}^{h_2} \frac{\partial\Theta}{\partial z}(z)\, dz = C\,\frac{2.5}{\Delta h} \left(h_2^{0.4} - h_1^{0.4} \right) \tag{3.17}$$

The parameter C is a "strength"-factor of the stable temperature gradient. Now, C is assumed to depend on the stability class SC (E or F) and on the measured wind velocity, u_0

$$C = C' f(SC, u_0) \tag{3.18}$$

The function, $f(SC,u_0)$, was determined on the basis of a classification scheme based on the wind velocity, u_0, and the vertical temperature gradient [60].

$$f(SC, u_0) = \frac{\Delta\Theta}{\Delta z}\Big|_{h_1}^{h_2} = \left\{ \begin{array}{l} 0.5u_0 + 0.2 \text{ , in category E} \\ \\ 0.7u_0 + 1.1 \text{ , in category F} \end{array} \right\} , \quad \left(\frac{K}{100m}\right) \tag{3.19}$$

where $f(SC,u_0)$ represents a gradient of the potential temperature averaged over the interval, $\Delta h = h_2 - h_1$. The constant, C', is determined so as to hold for the interval, Δh

$$\overline{\frac{\partial\Theta}{\partial z}}\Big|_{h_1}^{h_2} = \frac{\Delta\Theta}{\Delta z}\Big|_{h_1}^{h_2} \tag{3.20}$$

With $h_1 = 20$ m and $h_2 = 120$ m [60], it follows that $C' = 11.5$ [$K/100m^{0.4}$].

Consequently, according to Eq. (3.17), the mean gradient of the potential temperature is found to be

$$\overline{\frac{\partial\Theta}{\partial z}} = 11.5 \frac{2.5}{\Delta h}\left((h + \Delta h)^{0.4} - h^{0.4}\right) f(SC, u_0) \ , \quad \left(\frac{K}{100m}\right) \tag{3.21}$$

3.1.3 Approximation to the rise phase

As the mean wind velocity and the stability parameter depend on the averaging interval, Δh, the plume rise and the final height can be calculated only iteratively. Under the large variety of different atmospheric conditions to be taken into account in a probabilistic calculation of the consequences of an accident, such iterations take very much computer time. Consequently, the heights of the plume trajectory in the rise phase were determined approximately by means of the above formulae, but without iterations. Merely the final height is calculated iteratively for the first hour of diffusion, for test calculations have shown the final height to be reached within one hour even if the thermal power, Q_H, and the wind velocities are low. From this iteration process, a wind velocity and, in stable situations, a stability parameter are known which were averaged over the entire plume rise interval. They are then used in the corresponding equations to calculate the rise phase, thus obviating the need for iteration. For comparison with the plume rises following from an iteration, the approximated rise heights are shown in Figure 25a to Figure 26a. It is seen that approximation tends to slightly underestimate plume heights in the rise phase. This leads to overestimated concentrations, with the consequences that this approximation may be considered to be conservative.

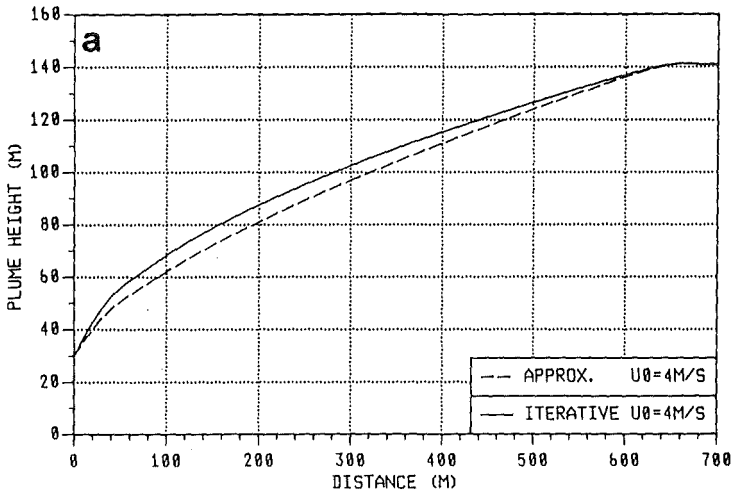

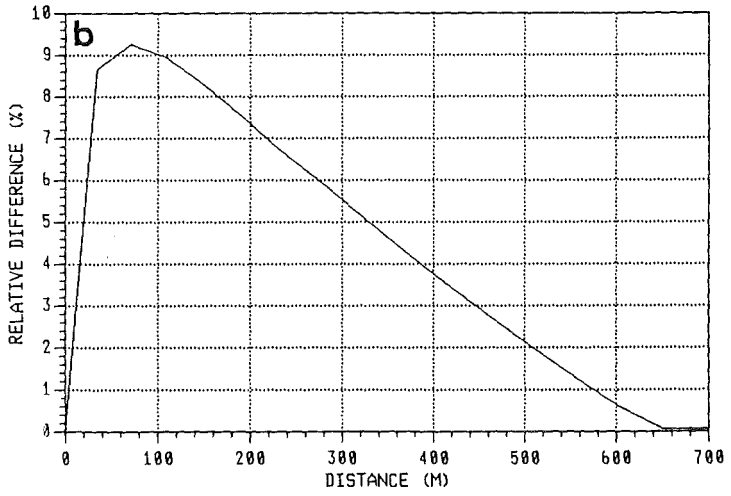

Figure 25. Comparison between iterative and approximate calculation of plume rise: release height, h = 30m; thermal capacity, Q_H = 50 MW; diffusion category D;
(a) rise curves
(b) relative difference with respect to iterative calculation.

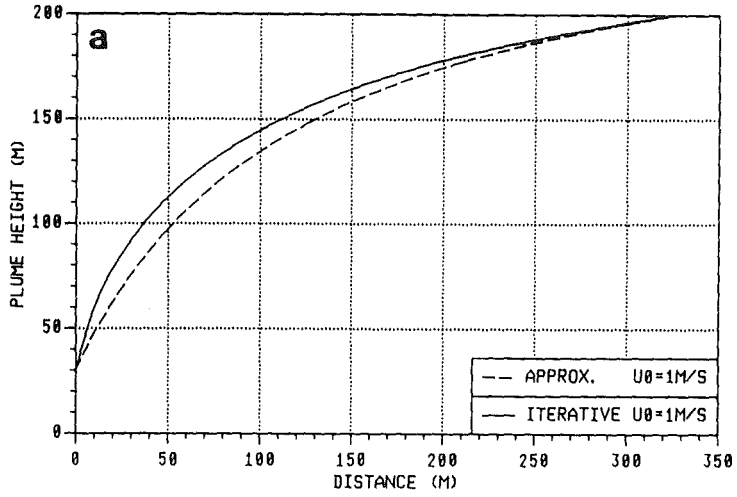

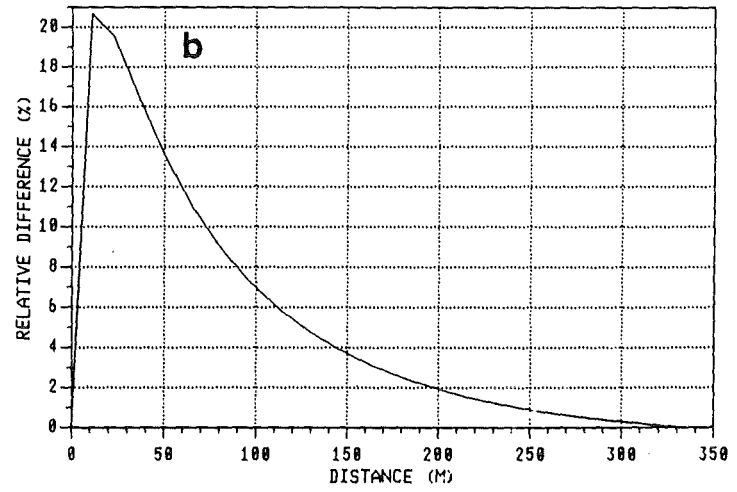

Figure 26. Analogous to Figure 25, but for diffusion category F

3.2 *Modelling the influences of buildings*

3.2.1 General structure of a flow disturbed by a building

The structure of the flow field in the immediate vicinity of a building is determined by aerodynamic forces. It has been sketched schematically in Figure 27 for a single building of simple geometric shape. A detailed representation can be found, e.g., in Halitsky [61]. He subdivides into three zones the area influenced by the building:

1. On the windward side, i.e., the side of the building facing the wind, a zone is produced in which the flow lines are displaced from their original direction(displacement zone);
2. on the lee side, i.e., the side of the building facing away from the wind, a turbulent wake zone is produced which incorporates the
3. cavity zone.

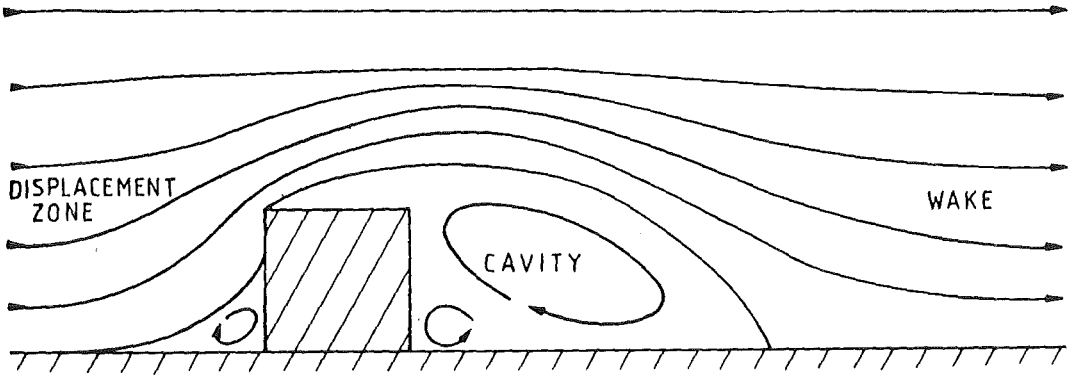

Figure 27. Schematic diagram of the flow around a simple building (from [62]).

The origin of the displacement zone is self-evident, as the flow must develop around the building. The wake zone and the cavity zone are based on the phenomenon of flow separation [63]. The wind velocities in the cavity zone are relatively low, while the turbulence intensity is very pronounced. Right behind the building there is an area of low, but nearly constant pressure. This produces the circulation in this zone, which is directed towards the building at ground level, i.e., opposite to the direction of the ambient flow. Halitsky [61]regards the cavity zone as a closed region in which there is an exchange of pollutants with the environment only by turbulent processes. However, more recent studies indicate that exchange of masses between this zone and the environment is also caused by advection (open model of the cavity zone) [64]. The cavity zone has an extension of about 1.5 H_B (H_B = building height). The wake zone is characterized by an

increased turbulence brought about by shear forces. These forces are active because of the different flow velocities in the wake zone and the undisturbed environment. The wind velocity is lower in the wake zone. Turbulence produces an exchange of momentum between the environment and the wake zone; consequently, the difference in velocities disappears with increasing distance from the building, and the wake zone dissolves. It has a typical extension of about 5 H_B to 10 H_B [62]

3.2.2 Model equations

The influences buildings may exert on atmospheric dispersion are normally taken in account by simple corrections in the dispersion equations. For this purpose, the building structure of a facility considered is reduced to one single, geometrically simple building. Figure 28 is a schematic diagram showing the parameters influencing dispersion close to a building.

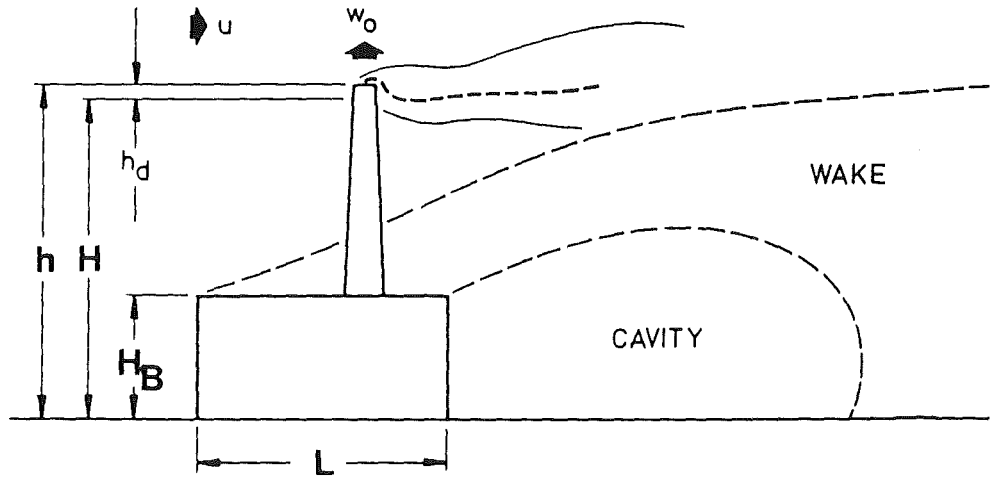

Figure 28. Diagram explaining the quantities influencing the flow around a building

The building has the height H_B, width W, and length L. It is located either near the source (e.g. a stack) or contains the source, e.g., as a door opening or a venting shaft. Under the assumption of the wind impinging in a normal direction on the area, WH_B, at the wind velocity, u, the width is defined as the extension of the building at right angles to the wind direction, while the length extends parallel to the wind. Assessment of accident consequences deal with a multitude of weather situations with the flow coming from various directions. Consequently, no distinction can be made as to which of the horizontal extensions of the building is the width and which is the length relative to the prevailing direction of the wind. The diameter of a circle with an area equal to the floor area, WL, of the building therefore is defined as the effective width of the building.

$$B = 2\sqrt{\frac{L\,W}{\pi}}$$

In the model, the wind is assumed to impinge on an effective area, BH_B, in a normal direction. By way of example, most probably the following building dimensions will be used to assess accident consequences in the German Risk Study Phase-B (DRS-B).
$W = 47$ m, $L = 85$ m, $H_B = 21.5$ m.
For the effective width, this results in $B \simeq 71$ m.

Lift-off criterion:

After there has been a release into the atmosphere, an investigation is conducted first of all to see whether the thermal buoyancy of the plume is sufficient to compensate for the influence of the building. This is decided by the lift-off criterion, which can be represented by a Richardson number, L_p [9]:

$$L_p = \frac{28\,Q_H}{u(H_B/2)\,u_\star^2 W_p} \tag{3.22}$$

with:

W_p	initial plume width (m), defined as $2 * \sigma_{y_0}$ (see Eq. (3.28 - 3.29))
Q_H	thermal power of the emission (MW),
$u(H_B/2)$	mean wind velocity at half the building height, $H_B/2$ (ms^{-1})
$u_\star$	friction velocity (ms^{-1}).

Briggs [65] indicated that thermal buoyancy dominates for $L_p > 30$; the effective release height in that case is calculated by model equations for the plume rise (see Section 3.1). In the case of $L_p \leq 30$, the aerodynamic perturbation effects dominate. The value $L_p = 30$ has recently been reconfirmed by wind tunnel experiments conducted at the Warren Spring Laboratory in the U.K. [66].

Eq. (3.22) shows the wind velocity, the extension of the building, and the mechanical turbulence to counteract thermal plume rise from the wake zone of the building (lift-off). When a mean wind velocity of $u = 4$ ms^{-1} at a height of $H_B/2 \simeq 11$ m, a friction velocity, $u_\star = 0.8 ms^{-1}$, and an initial plume width, $W_p = 33$m, is assumed for neutral atmospheric stratification, the release must have a thermal power of $Q_H \approx 90$MW in order for the plume to be able to leave the wake zone. The friction velocity, $u_\star$, can be calculated from the vertical wind profile by the planetary boundary layer theory (see, e.g., [35]). It is calculated for the cavity zone on the lee side of the building. This is where the mechanical turbulence is determined exclusively by the existence of the building. Consequently, a roughness length of $z_0 = 1.5$m is assumed independent of the roughness of the environment.

In the case of $L_p \leq 30$, the influence of the building dominates, with mainly two effects resulting:

- Downwash of the material released into the wake zone by the wakes on the lee side. This effect decreases the release height.

- Initial broadening of the pollutant plume as a result of the turbulent processes in the cavity zone. This influences the position and the amount of peak concentration.

Influence of buildings on stack releases:

A stack on top of a building or close to it also represents an obstacle to an atmospheric flow, which can alter the flow conditions in its close environment. On the lee side of the stack, in a way analogous to the building, a cavity zone is produced into which the material released is pulled (downwash effect). The value of h_d (Figure 28), by which the release height, h, must be reduced because of this effect, can be calculated according to [35]:

$$h_d = 2\left(\frac{w_0}{u} - 1.5\right) D$$

with

w_0	release velocity of the pollutants (ms^{-1})
u	mean wind velocity at height h (ms^{-1})
D	inside diameter of the stack (m).

The pollutants will be washed down only at low discharge velocities, w_0 , and high wind velocities, u, respectively, with $w_0/u < 1.5$. Typical values for D = 2.6 m and $w_0 = 0.26 ms^{-1}$ can be used to estimate from characteristic wind velocities for all diffusion categories that h_d will assume a value of 7m to 8m. In modelling, this is neglected compared to a typical stack height of h = 100 m. Consequently, only the existence of aerodynamic perturbation effects on the lee side of the building will be assumed below.

Substances released into the atmosphere do not enter the wake zone of a building, if the release height, h, exceeds a certain level, h'; in this way, h' defines the vertical region of influence of the wake zone. There is a rule saying that the release height must greater than the height of the building, H_B , plus 1.5 times the minimum of H_B and B, the effective width of the building, in order for the dispersion process not to be influenced by the turbulent zone of a building [67].

$$h' = H_B + 1.5\,\xi \qquad (3.23)$$

with $\xi = \min(H_B, B)$

If the height of the building is less than the effective width of the building, the condition is equivalent to the well known 2.5 H_B rule [35].

If the $h > h'$ condition is met, which is true of a stack release using the figures above, the effective release height, H, is determined solely by the plume rise model. However, if $h \leq h'$, the dispersion is influenced by the aerodynamic effects of the building. In this case, it must first be decided by means of the lift-off criterion whether the influence of the building can be overcome as a result of thermal buoyancy.

For $L_p > 30$, thermal buoyancy dominates, and the effective release height, H, is calculated in the plume rise model.

If the lift-off criterion is not fulfilled, it is seen for the effective release height, H, that [67]

$$H = 2\,h - h' \tag{3.24}$$

Releases from buildings:

If the source height, h, is less than, or equal to, the height of the building, H_B, the release is assumed to be from the building proper. The precise location of the discharge opening in the building is not known. First of all, again the lift-off criterion is verified. If it is fulfilled, i.e., if $L_p > 30$, the effective release height, H, is calculated in the plume rise model. Otherwise it holds that [67]

$$H = H_B - 1.5\,\xi \tag{3.25}$$

If H is less than 0.5 ξ, release close to the ground with an effective emission height, $H = 0.5\,\xi$, is assumed. For $H < 10$m , $H = 10$ m is used.

Initial mixing:

If a pollutant release occurs in the region of the wake zone on the lee side of a building, it undergoes rapid initial broadening because of the turbulence prevailing there. This is modeled by the virtual-source method. This source is assumed to exist on the windward side of the building. In this way, it is ensured that the diffusion parameters, σ_y and σ_z, assume values different from zero at the building. Close to the building, the method is equivalent to Gifford's modelling of initial broadening [68], which was used also in the atmospheric dispersion model of UFOMOD in DRS-A for effective release heights below 20 m [36]. Gifford's proposal suffers from the drawback that his correction factor, taking into account initial dilution, fails to change the diffusion parameters and, hence, the shape of the plume, while the concentrations are reduced by the correction term. As a consequence, the law of mass conservation

$$\int_0^\infty dz \int_{-\infty}^{\infty} C\,u\,dy = Q$$

no longer applies. The assumption of a virtual source, however, guarantees the conservation of mass, as the corrections are applied to the σ-parameters.

In the case of initial mixing, a new system of sigma parameters is defined as follows:

$$\sigma'_y(x) = \sigma_y(x + x_{y0}) \quad , \quad \sigma'_z(x) = \sigma_z(x + x_{z0}) \tag{3.26}$$

with the condition equations,

$$\begin{aligned} \sigma'_y(0) &= \sigma_y(x_{y0}) = \sigma_{y0} \\ \sigma'_z(0) &= \sigma_z(x_{z0}) = \sigma_{z0} \end{aligned} \tag{3.27}$$

In determining the initial values, σ_{y0} and σ_{z0}, they are assumed, according to Turner [49], to be part of a Gaussian plume whose lateral and vertical boundaries are defined by the effective width and height of the building. The concentration at the boundaries is

assumed to have dropped to 1/10 compared to the level in the axis of the plume. This concentration in the axis of the plume is assumed to exist in the middle of the building at ground level, the release height being neglected. In this case, the following equations can be derived for the initial values of the diffusion parameters:

$$\sigma_{y0} = \frac{B}{4.3} \quad , \quad \sigma_{z0} = \frac{H_B}{2.15} \tag{3.28}$$

In case the effective release height is less then, or equal to, the height of the building ($H \leq H_B$), initial mixing is assumed to exist both in the lateral and in the vertical directions. Initial lateral mixing is neglected for $H > H_B$:

$$\sigma_{y0} = 5\text{m} \quad , \quad \sigma_{z0} = \frac{H_B}{2.15} \tag{3.29}$$

The coordinates, x_{y0} and x_{z0}, in Eq. (3.26) and Eq. (3.27) indicate the position of the virtual source on the windward side of the building. They can be calculated from Eq. (2.5 - 2.6) and Eq. (3.27 - 3.29), respectively. Figure 29 und Figure 30 show the σ' -systems from Eq. (3.26). $H_B = 22$m and B = 71 m have been assumed for the building height and the effective building width, respectively. It is evident from the diagrams that initial mixing loses its influence with increasing source distance, x, and that the σ'-system asymptotically approaches the σ-system from Eq. (2.5 - 2.6).

3.3 Influences of the building factor upon the position and amount of the peak ground level concentration

It can be seen from Eq. (3.28 - 3.29), respectively, that σ_{y0} and σ_{z0} and, thus, x_{y0} and x_{z0}, are not necessarily identical. As a result, both the position and the amount of the peak ground level concentration may change as a result of initial mixing. A shift towards the source in the position of the peak is directly evident as a result of initial vertical broadening and the associated vertical dilution of the plume. If one considers the dispersion factor,

$$S = C(x, y, z)\,\frac{u}{Q_0} \quad , \quad (\text{m}^{-2})$$

with

C time integrated concentration, in Bq s m^{-3}
Q_0 source strength in Bq,

Eq. (2.3) can be written in the following way:

$$S(x,y,z) = \frac{1}{2\pi\sigma_y\sigma_z u}\exp\left(-\frac{y^2}{2\sigma_y^2}\right) \left\{\exp\left(-\frac{(z-H)^2}{2\sigma_z^2}\right) + \exp\left(-\frac{(z+H)^2}{2\sigma_z^2}\right)\right\} \tag{3.30}$$

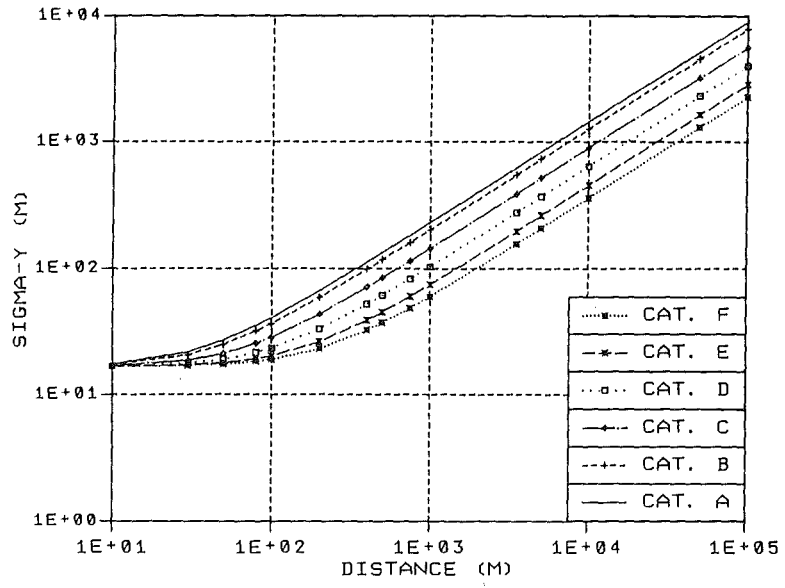

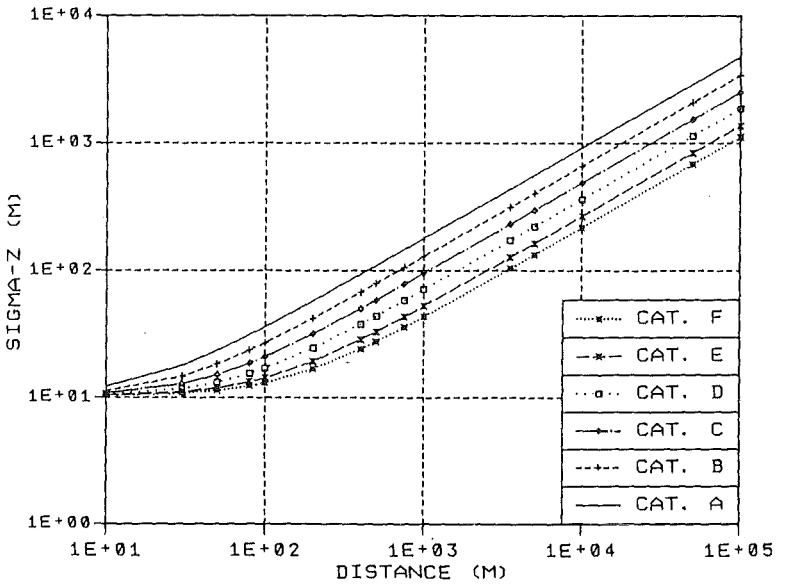

Figure 29. Diffusion parameters in UFOMOD taking into account building effects:
- smooth surfaces
- building dimensions: H_B = 22 m, B = 71 m.

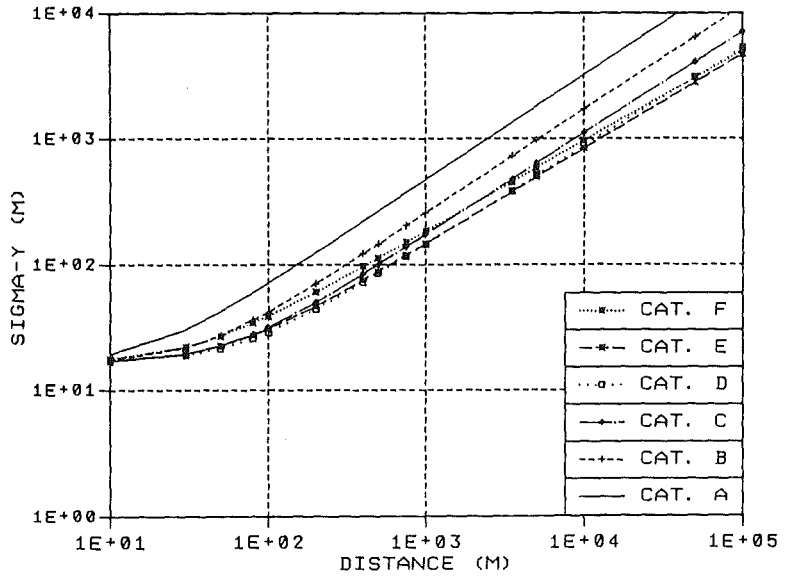

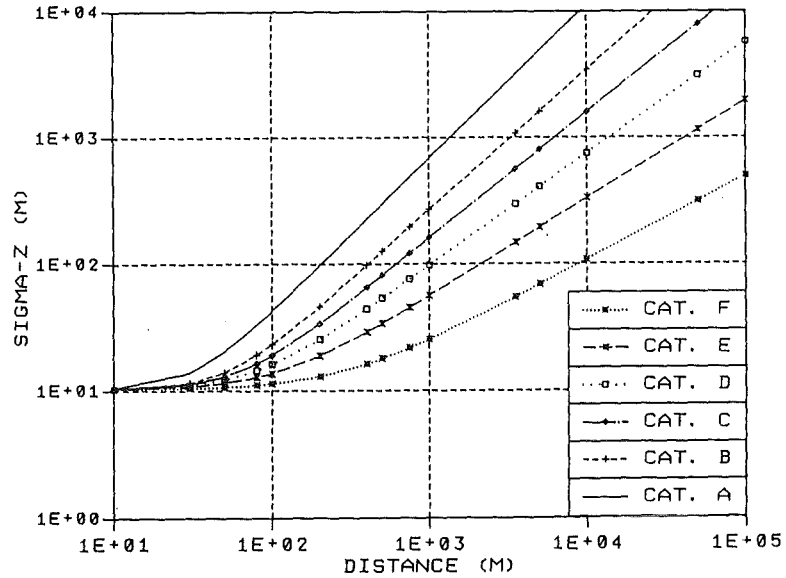

Figure 30. Diffusion parameters in UFOMOD taking into account building effects:
- rough surfaces
- building dimensions: H_B = 22 m, B = 71 m.
- source height: h = 50 m.

From this, it follows for the dispersion factor at ground level (z = 0) and under the plume axis (y = 0):

$$S(x, 0, 0) = \frac{1}{\pi \sigma_y \sigma_z} \exp\left(-\frac{H^2}{2\sigma_z^2} \right) \tag{3.31}$$

The position of the maximum of S is obtained by differentiating S in Equation (4.2) with respect to x. The formal procedure, taking into account $\sigma_{y,z} = \sigma_{y,z}(x)$, results in the following equation:

$$\frac{\partial S}{\partial x} = S(x, 0, 0) \left[-\frac{\partial}{\partial x} \ln \sigma_z - \frac{\partial}{\partial x} \ln \sigma_y + \frac{h_e^2}{\sigma_z^2} \frac{\partial}{\partial x} \ln \sigma_z \right] \tag{3.32}$$

If there is initial mixing, the σ'-parameters from Eq. (3.26) must be used. With Eq. (2.5 - 2.6) taken into account, and by substitution in Eq. (3.31), one then obtains a condition equation for the position, x'_m, of the maximum S'_m:

$$\frac{H^2}{\sigma_z^2(x'_m + x_{z0})} = 1 + \frac{q_y}{q_z} \frac{x'_m + x_{z0}}{x'_m + x_{y0}} \tag{3.33}$$

No general analytical solution can be found for this equation. Consequently, the assumption is made of $x'_m \gg x_{y0}$ and $x'_m \gg x_{z0}$. A corresponding first order Taylor expansion of the fraction on the right side of Eq. (3.33) leads to an equation for the source distance of the maximum,

$$x'_m = \left(\frac{H}{p_z \sqrt{2r}} \right)^{1/q_z} - x_{z0} \tag{3.34}$$

$$\text{with:} \quad 2r = 1 + \frac{q_y}{q_z}$$

For the maximum of the dispersion factor it follows,

$$S'_m = \frac{\exp(-r)}{\pi \sigma_z(x'_m + x_{z0})\, \sigma_y(x'_m - x_{y0})} = \frac{\exp(-r)}{\pi p_y \frac{H}{\sqrt{2r}} \left[\frac{H}{p_z \sqrt{2r}} - x_{z0} + x_{y0} \right]^{q_y}} \tag{3.35}$$

It is now possible to obtain, from Eq. (3.33 - 3.35), information about the position and the amount of the peak concentration for various positions of the virtual source.

(i) $x_{y0} = x_{z0} = 0$

In case there is no perturbation of the atmospheric flow, and the influence of the building and thus also initial mixing is missing, the familiar equations result (cf, e.g., [2]):

$$x'_m = x_m = \left(\frac{H}{p_z \sqrt{2r}} \right)^{1/q_z} \tag{3.36}$$

and

$$S'_m = S_m = \frac{p_z^{2r-1}}{\pi p_y} \frac{(2r)^r}{H^{2r}} \exp(-r) \tag{3.37}$$

(ii) $x_{y0} = x_{z0} \neq 0$

Modelling initial mixing, from which results $x_{y0} = x_{z0} \neq 0$ for the positions of the virtual source, leads to Eq. (3.34) and Eq. (3.37) as the exact solutions for the position and the amount of the peak. Compared to the case without initial broadening, the peak is shifted in the direction of the source by the same distance by which the virtual source is removed from the real source. The amount of the peak, however, does not change. This depends on the lateral dilution of the pollutant plume, which does not change. This can also be derived from Eq. (3.35) and Eq. (3.37). If one establishes a ratio between S_m and S'_m, one finds

$$\frac{S_m}{S'_m} = \frac{\sigma_y(x_m - \Delta x_0)}{\sigma_y(x_m)} \tag{3.38}$$

with $\Delta x_0 = x_{z0} - x_{y0}$ and x_m in accordance with Eq. (3.36). For $x_{y0} = x_{z0}$ it immediately follows that $S_m = S'_m$.

(iii) $x_{y0} \neq x_{z0}$, $x_{y0} \geq 0$, $x_{z0} > 0$

As mentioned above at the beginning of this section, the positions x_{y0} and x_{z0} of the virtual source normally do not agree in case of initial mixing. In that case, Eq. (3.34 - 3.35) represent approximate solutions. The position of the peak concentration is corrected by the line segment of x_{z0}. Compared to the two cases described above, the amount of the peak changes. First of all, the position, x_{y0}, is assumed to be located between the real source and x_{z0}; this includes the case of $x_{y0} = 0$. The lateral dilution of the plume at the position of peak concentration has not progressed as far as in the cases mentioned above. Consequently, the value of S'_m of the peak must be higher than S_m. This can also be seen from Eq. (3.38), as $\Delta x_0 > 0$ and, thus, $\sigma_y(x_m - \Delta x_0) < \sigma_y(x_m)$. However, in the case of $x_{y0} > x_{z0}$, lateral dilution at the position of the peak is already more pronounced, and it holds that $S'_m < S_m$.

Although Eq. (3.33) determining the position of peak concentration cannot be solved analytically in the absence of assumptions about x_{y0} and x_{z0}, almost exact values, S_{mE} and x_{mE}, can be indicated by numerical techniques for the amount and the associated source distance. For this purpose, the source distance, x, in Eq. (3.31) is increased successively, e.g. in steps of 1 m, by means of Eq. (3.26) and the peak is looked for. In Table 18 and Table 19, respectively, the approximate values, x'_m and S'_m, according to Eq. (3.34 - 3.35), and the exact numerical values, x_{mE} and S_{mE}, respectively, are given for the case of $x_{y0} \neq x_{z0}$, $x_{y0} > 0$, $x_{z0} > 0$. Comparing the tables indicates excellent agreement for the peak of the dispersion factor. Some small differences arise with respect to the position of the maximum.

Diffusion category	Roughness II $0.1\ m \leq z_0 < 1\ m$		Roughness III $z_0 \geq 1\ m$					
	H = 69 m		H (m)					
			50		100		180	
	x'_m (m)	S'_m ($10^{-5}\ m^{-2}$)	x'_m (m)	S'_m ($10^{-5}\ m^{-2}$)	x'_m (m)	S'_m ($10^{-5}\ m^{-2}$)	x'_m (m)	S'_m ($10^{-6}\ m^{-2}$)
A	136	4.1	63	6.1	188	0.9	264	8.7
B	216	3.4	119	6.4	342	1.2	479	8.1
C	332	3.4	167	6.7	506	1.5	1181	6.3
D	504	3.4	251	5.9	838	1.2	3301	2.7
E	778	3.4	452	3.8	1720	0.5	13775	0.4
F	1040	3.4	1528	1.3	7639	0.04	48643	0.06

Table 18. Source distance, x'_m, and amount, S'_m, (approximate values) of the peak dispersion factor, S:
influence of the building included

Diffusion category	Roughness II $0.1\ m \leq z_0 < 1\ m$		Roughness III $z_0 \geq 1\ m$					
	H = 69 m		H (m)					
			50		100		180	
	x_{mE} (m)	S_{mE} ($10^{-5}\ m^{-2}$)	x_{mE} (m)	S_{mE} ($10^{-5}\ m^{-2}$)	x_{mE} (m)	S_{mE} ($10^{-5}\ m^{-2}$)	x_{mE} (m)	S_{mE} ($10^{-6}\ m^{-2}$)
A	142	4.1	60	6.1	183	0.9	261	8.7
B	221	3.4	115	6.4	335	1.2	476	8.1
C	340	3.4	165	6.7	502	1.5	1184	6.3
D	517	3.4	247	5.9	833	1.2	3303	2.7
E	798	3.4	431	3.8	1703	0.5	13711	0.4
F	1065	3.4	1412	1.3	7503	0.04	48396	0.06

Table 19. Source distance, x_{mE}, and amount, S_{mE}, (numerically exact values) of the peak dispersion factor, S:
influence of the building included

4. CLOUD CORRECTION FACTORS FOR γ-DOSE CALCULATION

External irradiation from the radioactive cloud as it passes overhead contributes to the acute exposure as well as to the lifetime exposure [9]. Important quantities influencing the calculation of external radiation doses from the passing cloud are summarized in Figure 31.

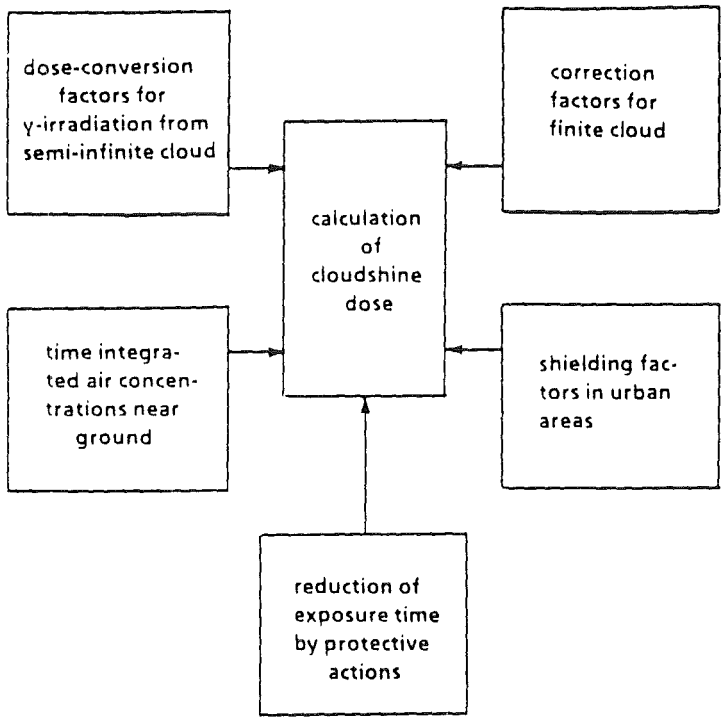

Figure 31. Quantities influencing the calculation of cloudshine doses: (from [9])

Shielding factors in urban areas and protective actions to reduce the exposure time are described elsewhere (for example [9]). Mathematically, the γ-dose at a reference point (i,j) (radial distance i and angle j refer to a grid point in the UFOMOD polar concentration grid; see Section 2.10) is expressed as

$$D_{i,j} = g_\gamma C_{i,j} \qquad (4.1)$$

with

$D_{i,j}$ γ-dose, expressed in Sievert (Sv), at reference point (i,j) due to external irradiation from the cloud
g_γ dose conversion factor (Sv m^3 Bq^{-1} s^{-1})
$C_{i,j}$ T.I.C. near the ground at reference point (i,j) (Bq s m^{-3})

The dose conversion factors have been derived at the Gesellschaft für Strahlen- und Umweltforschung mbH (GSF) using Monte-Carlo methods [70]. They are calculated under

the assumption of immersion in a semi-infinite cloud of uniform activity concentration with inclusion of anisotropy of the irradiation field and the influence of the ground surface. Thus, Eq. (4.1) is only valid if the dispersing cloud resembles an semi-infinite cloud with uniform concentration distribution as it is the case in farther distances where the activity is well mixed over the depth of the mixing layer and also the horizontal dimensions are large compared to the distance that the γ-rays travel (' a few hundred metres in air, dependent on energy). Or in other words, the dimensions of the cloud of γ-emmitting material have to be large compared to $1/\mu$, ($\sigma \gg 1/\mu$), where μ denotes the energy dependent γ-ray absorption coefficient (m^{-1}) [71]. In the near range (up to 20 km) the finite extent of the plume and the bi-Gaussian concentration distribution has to be taken into account. Therefore, cloud correction factors, $F^{Cl}_{i,j}$, have to be calculated for each grid point (i,j) affected by the cloud. To that purpose, basic plume correction factors evaluated by the GSF applying Monte-Carlo methods have been implemented [70]. They are available for an energy level of 1 MeV as functions of the location of the target with respect to the centre-line of a straight-line Gaussian plume, of the spread over the vertical and horizontal directions of the plume, and of stability class for four different release heights and two different types of surface roughness (Table 20).

release height (m)	10, 50, 100, 200
Pasquill-Gifford stability class	A, B, ... ,F
radial distance from the source (m)	100, 200, 500, 1000, 2000, 5000, 10000, 20000
azimuthal distance from the source (°)	0, 10, 20, ... ,90
surface roughness	smooth surface: 0.1m $\leq z_0 <$ 1m rough surface: $z_0 \geq$ 1m

Table 20. Quantities influencing the basic plume correction factors for γ-dose calculation

The influence of surface roughness has been considered by applying the two different dispersion parameters sets described in Section 2.6 (Table 6, and Table 7). Therefore, the correction factors presently available are only valid in conjunction with the use of these dispersion parameter systems.

Taking into account the plume correction factors, the γ-dose is calculated according to

$$D_{i,j} = g_\gamma F^{Cl}_{i,j} = g_\gamma f_{i,j} C_{s,0} \qquad (4.2)$$

with

$f_{i,j}$	basic plume correction factor
$C_{s,0}$	plume centre-line concentration in effective source distance s
$F^{Cl}_{i,j}$	cloud correction factor, $F^{Cl}_{i,j} = f_{i,j} C_{s,0}$

In the following, the evaluation of $f_{i,j}$ and thus the calculation of $F^{Cl}_{i,j}$ in MUSEMET is described. The centre-line concentrations corresponding to each reference point affected by the passing cloud are known from Eq. (2.8) for $\eta = 0$ and $z = H$. The plume correction factors have to be interpolated vertically if the release height H lies between two heights given in Table 20; for heights above 200 m the 200 m values will be used. Then

the plume correction factors are evaluated in the horizontal plane as it is illustrated in Figure 32.

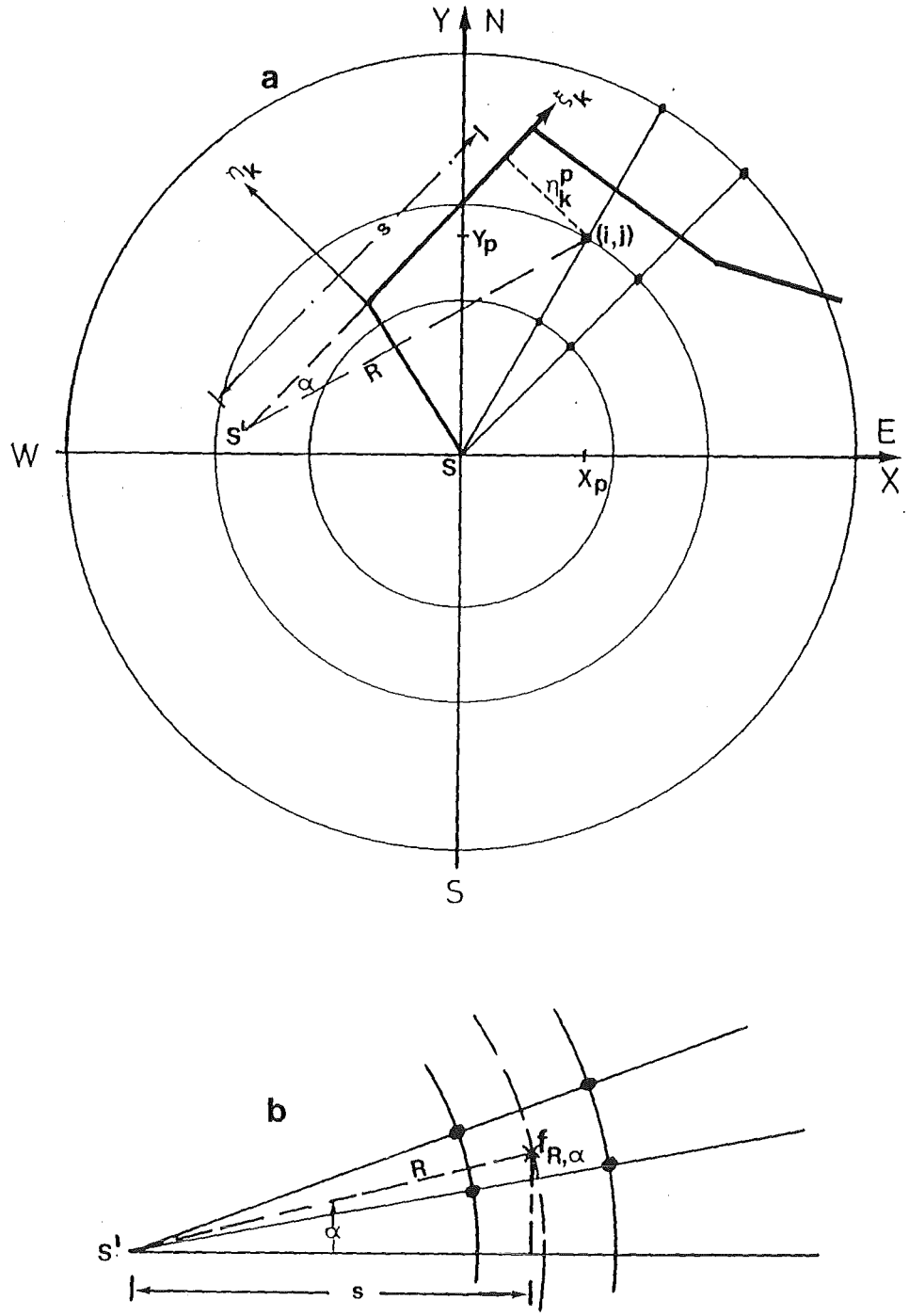

Figure 32. Illustration of horizontal evaluation of plume correction factor

Because the correction factors are derived for straight-line Gaussian plumes, a virtual source S′ is defined which is located in the upwind direction of the current trajectory segment. The distance, s, from the image source to the projection point of a grid point onto the current trajectory segment (onto the plume's centre-line) is given by the sum over the lengths of all previous segments and the known ξ-coordinate of the grid point with respect to the trajectory frame of reference. Thus, s is identical to the effective distance from the real source covered by the plume. Knowing this distance s and the lateral distance η of the grid point from the trajectory, the radial distance, R, and the angle, α, with respect to the virtual source S′ can easily be calculated:

$$R = \sqrt{s^2 + \eta^2}$$

$$\alpha = \sin^{-1}(\eta/R)$$

Generally, the polar point (R, α) in the virtual source system will not coincide with a reference point for whom a correction factor is available. Therefore, if $R \leq 20$km, an interpolated correction factor, $f_{R,\alpha}$, is calculated taking into account the four neighbouring grid points in the S′ -system where plume correction factors are available. Since the polar point (R, α) corresponds to the polar point (i,j) of the UFOMOD concentration grid, the resulting correction factor $f_{R,\alpha}$ is identical to $f_{i,j}$ and can be applied in Eq. (4.2).

5. THE METEOROLOGICAL SAMPLING SCHEME METSAM

METSAM is a program package which is used to select samples of weather sequences for the probabilistic assessments of the consequences after accidental releases of radionuclides from nuclear facilities into the atmosphere. It has been adopted from [18] and modified for the application as a preprocessing system within the framework of the new UFOMOD code [9].

In probabilistic accident consequence assessments, it is necessary to repeat the atmospheric dispersion calculations with several hundreds of weather sequences to predict the full distribution of consequences which may occur following a postulated accidental release. Ideally, the ACA should be performed with every possible sequence of weather conditions, that means dispersion calculations should be started at every time meteorological data are available. In practice, time and computer constraints prevent this because the number of possible different sequences of weather conditions is large. However, many of the sequences would result in similar dispersion of activity and consequently in similar accident consequences. Therefore, it is desirable to select a representative sample of weather sequences from a meteorological record which is typical of the area over which the released radionuclides will disperse and which spans a sufficiently long period.

Generally, the meteorological record will include windspeed, wind direction, rainfall and atmospheric stability category which are extracted from routine observations recorded and reported from meteorological stations. The assignment of meteorological stations with continuous longterm records of meteorological conditions to the nuclear site considered in an ACA should take into account the topographical and regional climatological characteristics of the areas where they are located. For risk assessments within the framework of the DRS-B, the assignment of meteorological stations to nuclear sites taking into account these requirements has been carried out by the German Weather Service. The procedure used to select the sample of weather sequences should ensure that the full range of weather conditions which might occur is included. Especially infrequent sequences which might lead to severe consequences in the region close to the site should not be overlooked. In order to present the consequences probabilistically, the procedure should also be capable of determining the probability with which each chosen sequence occurs.

5.1 Sampling techniques

A meteorological sequence within a database of continuous records is defined by specifying the time at which it starts. The most straightforward methods of sampling these times are the random and cyclic sampling techniques, respectively [16]. Both methods tend to sample similar sequences frequently, whilst overlooking the more unusual (and potentially more serious) ones and neither of these sampling schemes is adequate for predicting the probabilities of severe consequences. Despite of these disadvantages cyclic sampling can be selected optionally in UFOMOD. Each weather sequence then has the same probability.

A more refined method is called stratified sampling. This technique is potentially capable of selecting meteorological sequences from the full spectrum of weather situations and associating more realistic probabilities of occurrence to them. The intention is to group together all weather sequences present in the meteorological database which give rise to similar consequences. By categorizing the recorded weather sequences, the probabilities of occurrence of each category may be determined directly. Meteorological sequences, identified by the time of their start, are then selected randomly from each category, thus ensuring that the full range of possible weather situations is covered. A more comprehensive discussion of stratified sampling, especially of grouping weather sequences with rainfall, is given in [16].

5.2 *Outline of sampling scheme of METSAM*

As already mentioned above, a sampling scheme should ensure that the numbers of health effects and the extent of countermeasures taken to limit the radiological exposure of the population together with the corresponding frequencies are predicted as realistically and comprehensively as possible. Besides on the weather situation, these consequences also depend on the distribution of the population in the surroundings of the site. Therefore, meteorological sampling schemes used for instance in CRAC2 [4] or MARC [6]select weather sequences for site-specific ACAs in correlation with population distributions [73].

The procedure of weather sampling developed within the framework of UFOMOD and its application in the DRS-B is more aiming at generic ACAs which consider a larger number of sites. Therefore, the correlation with population distributions is not taken into account. But because METSAM is a stand-alone program package which is not integrated in the UFOMOD system it can be substituted by any other stratified sampling procedure developed for site-specific ACAs. The method for grouping weather sequences in METSAM has been adopted from [18]. For every possible sequence of weather situations the travel time of the plume is determined depending on the wind conditions prevailing during each time interval, and on the distance out to which severe early consequences are to be expected (e.g. 20 km). Additionally, the total amount of rainfall occurring within the travel time of the plume is calculated and the initial wind direction is registered. Then defining certain categories characterized by the initial wind direction, the total rainfall and the travel time, several hundreds of groups may be obtained. From each of these groups at least one weather sequence is selected randomly.

The probability of occurrence, P_j^k, of a weather sequence j selected from a class k, k = 1, ..., K, is given by

$$P_j^k = \frac{f_k}{Z_k} = \frac{N_k}{Z_k M} \quad , \; j = 1, \ldots, Z_k. \tag{5.1}$$

In this equation M denotes the total number of weather sequences which are classified in K classes and N_k gives the absolute frequency of each class k, so that

$$\sum_{k=1}^{K} N_k = M$$

Thus, $f_k = \frac{N_k}{M}$, is the relative frequency of class k. It is identical to the probability of occurrence of weather sequences representing the meteorological conditions which are grouped in class k. If $Z_k \geq 1$ weather sequences are selected from class k the probability of occurrence of each of these sequences is given by the equation above to avoid an overweighting of class k in the complete set of weather sequences for the ACA calculations. Thus, the sum over all probabilities, P_j^k, in a class k is identical to f_k:

$$\sum_{j=1}^{Z_k} P_j^k = \sum_{j=1}^{Z_k} \frac{f_k}{Z_k} = \frac{f_k}{Z_k} Z_k = f_k$$

And the sum over all probabilities of all weather sequences selected from K classes equals one.

As an illustration of the sampling method currently used in UFOMOD, Table 21 shows one part of the whole classification scheme of meteorological data recorded at Karlsruhe (FRG). The initial wind directions are grouped into twelve 30° sectors. The travel times of the plume are categorized in three groups. In the example the trajectory calculations are performed out to a distance of 20 km and the following boundaries are chosen for the three groups of travel time.

1. $0 < T \leq 3$ h
2. 3 h $< T \leq 6$ h
3. $T > 6$ h

Additionally, four classes of the total amount of precipitation are distinguished:

1. $I = 0$ mm
2. 0 mm $< I < 1$ mm,
3. 1 mm $\leq I < 3$ mm,
4. $I \geq 3$ mm

In this way 12 x 3 x 4 = 144 different classes of weather conditions are obtained. Table 21 shows the precipitation intensity/travel time classification for the most frequent initial wind direction sector with the numbers of weather situations per category. The probability of occurrence of each categorized sequence can be determined from the known total number of weather sequences.

Travel time T (h)	Precipitation intensity I (mm)			
	$I = 0$	$0 < I < 1$	$1 \leq I < 3$	$I \geq 3$
$0 < T \leq 3$	2905	618	301	22
$3 < T \leq 6$	150	19	12	3
$T > 6$	79	13	6	6

Table 21. Illustration of classification scheme of stratified sampling

6. SUMMARY

During the development of the new program system UFOMOD for assessing the consequences of nuclear accidents special demands on the modelling of the atmospheric dispersion emerged from the broad spectrum of possible source terms. The incorporation of different trajectory models with ranges of validity near to the site and at far distances, respectively, is a significant step foreward to an appropriate treatment of site-specific problems and questions arising in connection with the transportation of radioactive material over large land areas up to thousands of kilometres. The new structure of UFOMOD clearly reflects this problem-oriented modelling by the division into three subsystems each built to assess accident consequences resulting from acute or chronic exposure.

In the two near range versions UFOMOD/NE and UFOMOD/NL the segmented plume model MUSEMET and the puff model RIMPUFF can be applied. Both are Gaussian-like trajectory models. MUSEMET, as the standard atmospheric dispersion model of the UFOMOD system, is implemented as a subroutine in the UFOMOD code. RIMPUFF is a stand-alone code with an appropriate interface to UFOMOD.

The only long-range dispersion model available at the time of designing the new UFOMOD was the trajectory-puff model MESOS.

In addition, the special straight-line Gaussian model ISOLA has been implemented to estimate the spatial concentration distribution for low-level long-duration (weeks or months) releases of radioactive material.

Due to its modular structure the program system UFOMOD is universal in such a sense, that any other atmospheric dispersion model can be used which provides time-integrated air and ground concentrations in a polar coordinate grid around the source.

The atmospheric dispersion models mentioned above predict the spatial and temporal distributions of activity in the air near to the ground and on the ground surface, thereby taking into account the meteorological conditions during the release and time of travel of the radioactive cloud, which determine the transport direction of the acitivity and the rate and extent of its dispersion. Mechanisms for removal of activity from the cloud are considered by each of the models, these being mainly dry and wet deposition processes. The source depletion model is applied to account for the reduction of activity in the plume due to the removal processes. Radioactive decay during the dispersion and the built-up of radionuclides from radioactive decay chains are not considered in the atmospheric dispersion models themselves but in a subsequent module of the UFOMOD system. Dependent on the release characteristics special features are modelled, for example the effect of plume rise due to the buoyancy of the released activity and the behaviour of plumes released into building wakes (the latter is not considered in MESOS because a building loses its influence in farther distances).

To consider external irradiation from the radioactive cloud in the near range ($\leq$ 20 km), it is necessary to evaluate cloud correction factors, which correct the dose conversion factors with respect to the finite extent of the cloud and the non-uniform activity distribution in the cloud in the near range. For this purpose, new basic plume correction factors

have been implemented (presently only in the MUSEMET model) which have been derived by the GSF/Munich using Monte Carlo techniques.

To define starting times of weather sequences and the probabilities of occurrence of these sequences, it is convenient to apply stratified sampling. Therefore, the preprocessing program package METSAM has been developed to perform the sampling. METSAM is designed in such a way that all possible weather situations are classified according to the initial wind direction, the time a plume need to leave a predefined area around the source, and the total amount of precipitation fallen during the dispersion. Afterwards, at least one weather sequence is sampled randomly from each class. This procedure ensures that the whole spectrum of weather conditions is taken into account. Especially infrequent sequences which might lead to severe consequences near to the plant will not be overlooked. In order to present the consequences probabilistically, the METSAM procedure is able to determine the probability of each chosen weather sequences.

The weather sampling procedure METSAM is more aiming at generic ACAs. Therefore, the correlation with population distributions is not taken into account. But for site-specific ACAs it is inevitable to apply meteorological sampling schemes to select weather sequences in correlation with the population distribution around the site. Therefore, as a further improvement of the UFOMOD system and with regard to the development of the program package COSYMA [72], it is planned to implement such a sampling scheme which has been developed at the National Radiological Protection Board (NRPB, Chilton/UK) [73]. COSYMA (Code System from MARIA) emerges from the MARIA (Methods for Assessing the Radiological Impact of Accidents) program of the Commission of the European Communities (CEC). It represents a fusion of ideas and modules from the NRPB program MARC [6], the program system UFOMOD [9], and new developments and input from other MARIA contractors. The skeleton of COSYMA will be the UFOMOD sytem and, therefore, also the atmospheric dispersion models described in this report will be parts of it.

Further improvements of the atmospheric dispersion models which should be examined with respect to the development of COSYMA are the updating of the modelling of removal processes from the cloud and the applicability of the models in complex terrain. To improve the deposition modelling it will certainly be necessary to substitute the source depletion model by a more realistic model. The implementation of Horst's corrected source depletion model could be a step in this direction [53]. Also gravitational settling of large particles as a further important deposition process should be included. Additionally, the importance of fog as a depletion factor should be studied. A step in the direction of atmospheric dispersion modelling over complex terrain has already been made by the puff-splitting technique developed for RIMPUFF [21]. This procedure will certainly suffer from the constraints of reasonable computer time. But on the other hand, anybody aiming at the more realistic assessments of the consequences emerging from accidents in nuclear facilities and the detailed scientific evaluation and presentation of intermediate and final results should be aware that powerful computer systems are necessary. Codes like UFOMOD or COSYMA will never run on a Personal Computer with their full range of complexity.

In the meantime the program system UFOMOD has been used for a variety of studies. These comprise for example

- an examination how a depressurization of the containment by controlled venting through aerosol and iodine filters influences the radiological consequences of releases from PWRs and BWRs;
- dose assessments in the cities of Svetlogorsk and Mogilev (both USSR) for the first 48 hours after the accident in Chernobyl, and the comparison with measurements;
- assessments of the radiological consequences in Austria due to normal operation and accidental releases from the planned reprocessing plant in Wackersdorf/FRG.

A detailed discussion of these studies can be found in [74].

7. APPENDIX A: EVALUATION OF THE PRESENT WEATHER CODE WITH RESPECT TO PRECIPITATION

An hourly interpretation of precipitation is generally only available in the qualitative form of the present weather code which contains 100 different weather specifications (Figure 33).
The code numbers 50 to 99 are used to indicate various types of preciptiation occurring at the time of observation, whilst codes 20 to 29 are reserved for precipitation in the previous hour. Quantitative measurements of precipitation only exist in general as the sum over the previous 6 or 12 hours. But to apply the washout model as it is described in Section 2.8, it is necessary to have the hourly precipitation rate in mm/h. Thus, the code numbers have to be converted into figures which represent the different types of preciptitation quantitatively.

The procedure used in the evaluation of the meteorological data base for MESOS is described in detail in [15]. A rain index,I, in the range from 0 to 9 is assigned to each present weather code to quantify the intensity of precipitation (Figure 33). The interrelation between rain index I and the intensity, R, is given by

$$\begin{aligned} R &= 0.25\, I \ , \ \text{mm/h} \ , \ \text{if } I = 1 \\ R &= 0.5\, I \ , \ \text{mm/h} \ , \ \text{if } I > 1 \end{aligned} \qquad (7.1)$$

Precipitation observations coded in the present weather code can be classified according to rainfall rates. Table 22 shows typical ranges of rainfall rate for common precipitation types, and values of rain index I.

Type of preciptiation		Rainfall rate (mm/h)	Rain index, I
rain	slight	0.0 - 0.5	1
	moderate	0.5 - 4.0	5
	heavy	> 4.0	9
showers	slight	0.0 - 2.0	1
	moderate	2.0 - 10.	2
	heavy	10. - 50.	6
drizzle	slight	0.20	1
	moderate	0.50	2
	heavy	0.75	2

Table 22. Rainfall rates for common precipitation types: (from [15])

Comparing the typical rainfall rates in Table 22 with those being calculated according to Eq. (7.1), it is conspicuous that the rain index of showers has been scaled down by a factor of ten to account for short duration and locality of showers. In [15] it has been shown that then the agreement between measured and calculated annual rainfall rates is generally good. Relatively low rainfall totals over the sea where both convective and

Code-No. Group	General Description
00-19	no preciptiation at the station at the time of observation
20-29	preciptiation, fog, or thunderstorm at station during the last hour but not at time of observation
30-39	duststorms, sandstorms, drifting or blowing snow
40-49	fog or ice fog at time of observation
50-59	drizzle at time of observation
60-69	rain at time of observation
70-79	solid precipitation not showers
80-90	showery precipitation
91-99	precipitation with current or recent thunderstorm

WW	0	1	2	3	4	5	6	7	8	9
00	0	0	0	0	0	0	0	0	0	0
10	0	0	0	0	0	0	0	0	0	0
20	1	2	2	2	1	1	1	1	0	1
30	0	0	0	0	0	0	0	0	0	0
40	0	0	0	0	0	0	0	0	0	0
50	1	1	1	2	1	2	1	2	1	4
60	1	1	2	5	4	4	1	3	1	4
70	1	1	2	5	4	9	3	3	3	3
80	1	4	6	1	4	1	4	1	4	1
90	4	1	6	1	6	4	4	5	0	5

Figure 33. The present weather code and MESOS data base indices: (from [15])

orographic processes are absent could be simulated with a fairly good agreement as well as the high rainfall in mountainous areas due to orographic rain.

To evaluate the German meteorological data bases presently available for MUSEMET, RIMPUFF, and ISOLA, a procedure described in [56] has been used. It has been slightly modified in that sense that weather code numbers 20 to 29 has also been considered. In accordance with [56] the code figures 50 to 99 are assigned to four typical ranges of rainfall rates which then can be represented by typical precipitation intensities (Table 23).

Index of precipitation intensity class	Rainfall rate (mm/h)	Representative intensity (mm/h)
0	< 0.02	0
1	0.02 - 1	0.15
2	1 - 3	1.2
3	≥ 3	4.2

Table 23. Rainfall rates in the German meteorological data bases

Figure 34 shows the correlation between the present weather code and the indices of precipitation classes.
A kind of reliability test of this correlation can be performed by calculating the annual sum of precipitation and comparing it with measured values. Table 24 shows the calculated and measured annual precipitation rates for 10 synoptic stations in the FRG. These are the stations whose meteorological data of the years 1982/1983 had been made available by the German Weather Service for the ACAs within the framework of the German Risk Study - Phase B.

Synoptic station	Rainfall rate 1982 (mm/h)		Rainfall rate 1983 (mm/h)	
	measured	calculated	measured	calculated
Augsburg	776.1	551.4	695.5	569.6
Frankfurt / Main	608.0	609.9	700.5	718.1
Regensburg	544.6	553.2	561.8	530.4
Hamburg	700.8	701.3	809.7	756.5
Karlsruhe	913.4	708.8	711.9	687.2
Kassel	547.2	639.0	635.1	730.8
Köln	884.6	906.8	707.1	857.6
Münster	656.7	671.3	708.5	697.4
Nürnberg	614.4	648.8	629.1	688.4
Stuttgart	857.8	787.5	706.7	846.3

Table 24. Calculated and measured annual rainfall rates at 10 stations in the FRG

Code-No. Group	General Description
00-19	no preciptiation at the station at the time of observation
20-29	preciptiation, fog, or thunderstorm at station during the last hour but not at time of observation
30-39	duststorms, sandstorms, drifting, or blowing snow
40-49	fog or ice fog at time of observation
50-59	drizzle at time of observation
60-69	rain at time of observation
70-79	solid precipitation not showers
80-90	showery precipitation
91-99	precipitation with current or recent thunderstorm

WW	0	1	2	3	4	5	6	7	8	9
00	0	0	0	0	0	0	0	0	0	0
10	0	0	0	0	0	0	0	0	0	0
20	1	2	0	1	1	2	1	1	0	2
30	0	0	0	0	0	0	0	0	0	0
40	0	0	0	0	0	0	0	0	0	0
50	0	1	0	1	1	2	0	1	1	2
60	1	1	1	2	2	3	1	2	1	2
70	0	0	1	1	2	3	0	0	0	2
80	2	3	3	1	3	1	3	1	3	2
90	3	2	3	2	3	3	3	3	0	3

Figure 34. The present weather code and correlated rainfall rate indices: (adapted from [56])

To achieve the rather good agreements it was necessary also to consider the code numbers 20 to 29 representing the precipitation in the hour before the observation. If at a time n of observation a code number between 20 and 29 has been reported but there was no precipitation one hour earlier (no code > 50 for the previous observation time (n-1)), then codes shown in Table 25 have been assigned to the (n-1)-th hour. They correspond to the most frequent precipitation phenomena of the different groups of precipitation types.

Code number	Weather in the previous hour	corresponding precipitation groups	most frequent precipitation type	Index of precipitation intensity class
20	drizzle (not freezing)	50 - 55	51	1
21	rain (not freezing)	60 - 65	61	1
22	snow	70 - 75	71	0
23	rain and snow or ice pellets	68, 69, 79	68	1
24	freezing drizzle or freezing rain	56, 57, 66, 67,	66	1
25	showers of rain	80 - 82	80	2
26	showers of rain, or of rain and snow	83 - 86	85	1
27	showers of hail, or of hail and rain	87 - 89	87	1
28	fog or ice fog	40 - 49	40	0
29	thunder-storm (with or without parecipita-tion)	90 - 94	91	2

Table 25. Assignment of weather code of the previous hour to a representative precipitation type

With respect to a harmonization of the evaluation of meteorological data bases it might be advantageous only to apply one of the two procedures to convert the qualitative pre-

ciptiation coding into quantitative figures of intensity. Therefore, the MESOS procedure has also been used to translate the rainfall codes of the German data, and the reliability test also has been repeated. For nearly all stations shown in Table 24 the measured annual precipitation has been overestimated and the difference between measured and calculated values was getting worse. The MESOS procedure is only applicable in conjunction with a three-hourly data base.

8. APPENDIX B: STRUCTURE OF MUSEMET

8.1 *Integration in the UFOMOD system*

Figure 35 shows schematically how the atmospheric dispersion models described so far are integrated in the UFOMOD system.

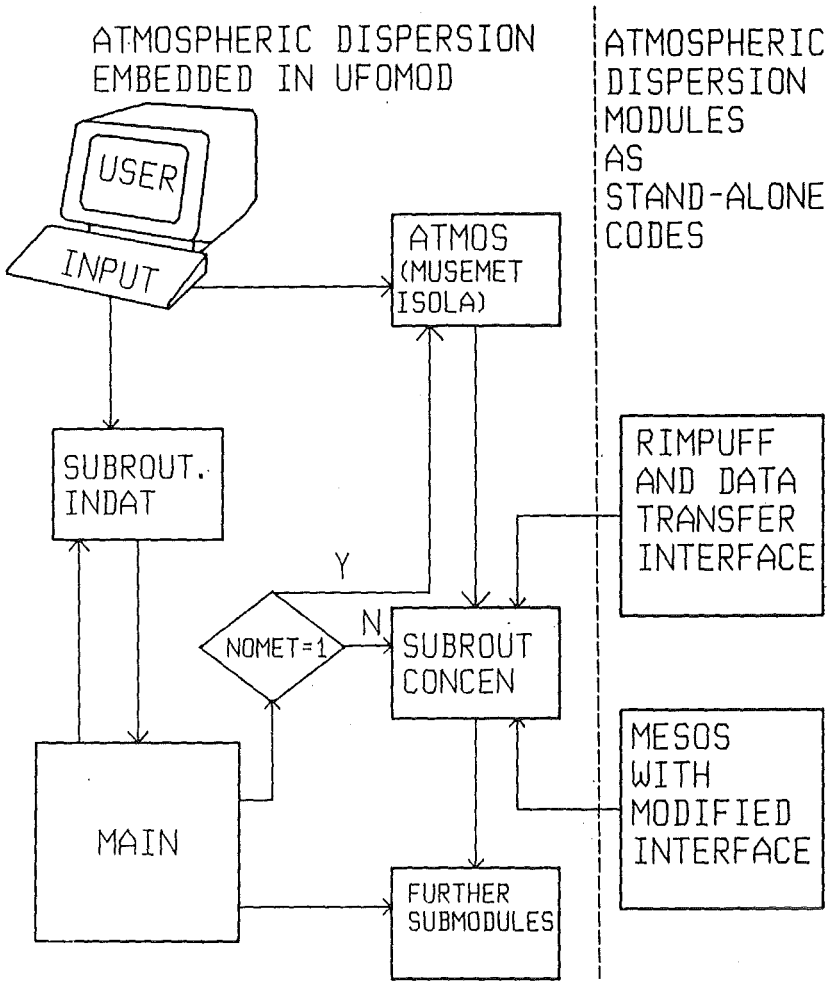

Figure 35. Atmospheric dispersion modules within the UFOMOD system

The trajectory model MUSEMET and the straight-line Gaussian model ISOLA are embedded as subroutines in the UFOMOD code. The value of a steering variable defines

whether they are processed or not. Once ATMOS has been performed, its results are stored and transferred to the subsequent module CONCEN (see also Section 2.11).

RIMPUFF and MESOS are both stand-alone codes which are not integrated in the UFOMOD program. The connection between these models and UFOMOD is established by data transfer interfaces which prepare and store the necessary results. Performing UFOMOD in subsequent steps then needs the steering variable NOMET to be set to zero.

Figure 35 also demonstrates that the general structure of the UFOMOD systems allows to exchange each atmospheric dispersion model by another model provided that an appropriate interface exists to transfer the results to the UFOMOD program.

8.2 General I/O-structure of MUSEMET

Figure 36 illustrates the input/output (I/O) structure of the UFOMOD module ATMOS (=MUSEMET).

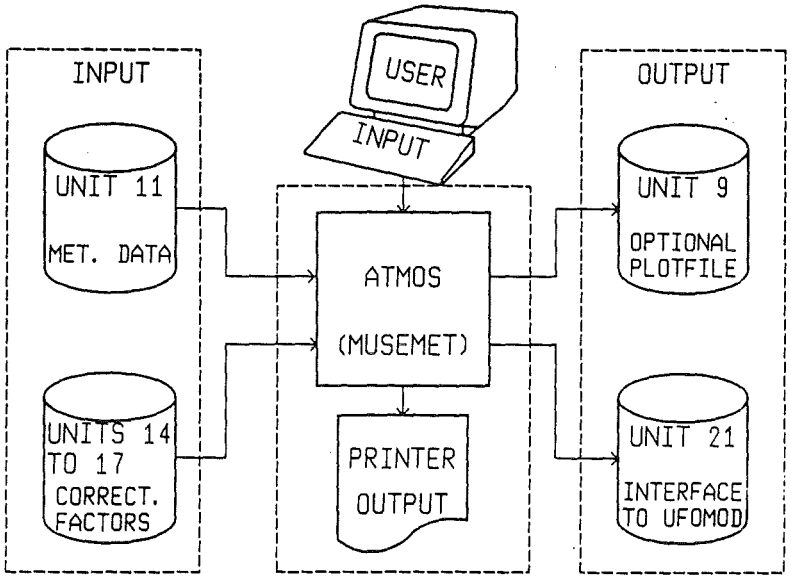

Figure 36. I/O-stucture of UFOMOD module ATMOS (MUSEMET)

The input part consists of user defined variables which define the boundary conditions of each UFOMOD, and of external data sets which have to be available on permanent storage units (disk or magentic tape). The latter are the meteorological data base (see Section 2.10) and the basic plume correction factors (see Chapter 4) which must be resident on input units 11 and 14 to 16, respectively.

The output part consists of a printer output and two storage units. The printer output comprises an obligatory control of input data and, if it is desired, the normalized air and ground concentrations of a selected type of nuclide in different distances for selected weather sequences. To get a first graphical impression of the concentration distributions, a printer plot can also be performed. The output unit 21 represents the interface of ATMOS with the subsequent UFOMOD module CONCEN. On unit 21 all results obtained with the atmospheric dispersion module are stored and transferred to CONCEN. Output unit 9 is mentioned only for reasons of completeness. It represents an optional output file to store normalized air and ground concentrations of a selected type of nuclide so that they can be plotted by an isoline plot program which does not belong to the UFOMOD system.

For a comprehensive listing and description of all input variables being necessary to run MUSEMET within the UFOMOD system, the reader is referred to the UFOMOD user guide [69]. There he will also find a detailed description of all external input and output units.

8.3 Subroutines and flow chart of MUSEMET

A list of all subroutines called within the MUSEMET program and short descriptions of what they are doing is given in Figure 37.

The flow chart (Figure 38) is intended to help the user to understand the internal logic of MUSEMET.

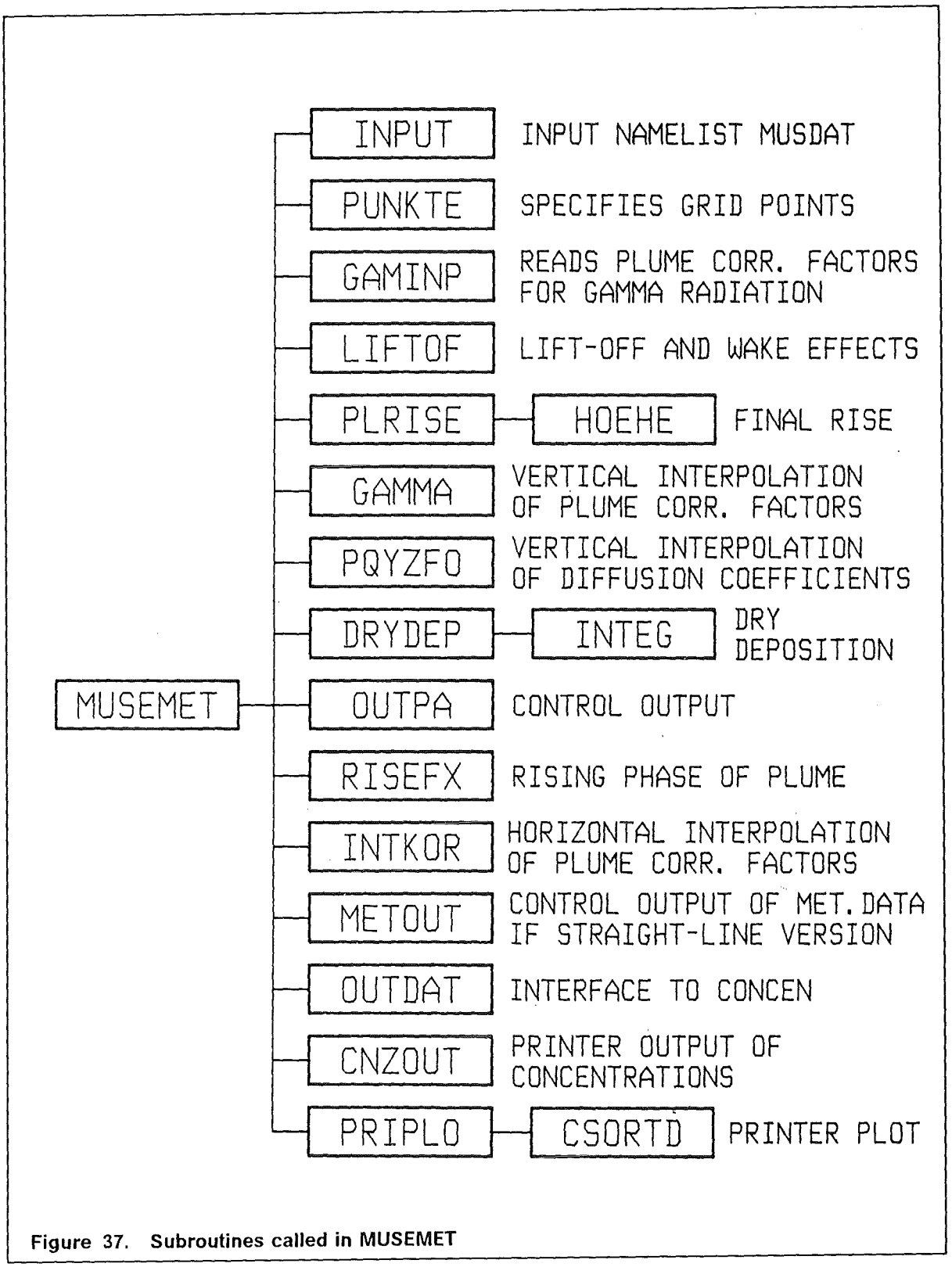

Figure 37. Subroutines called in MUSEMET

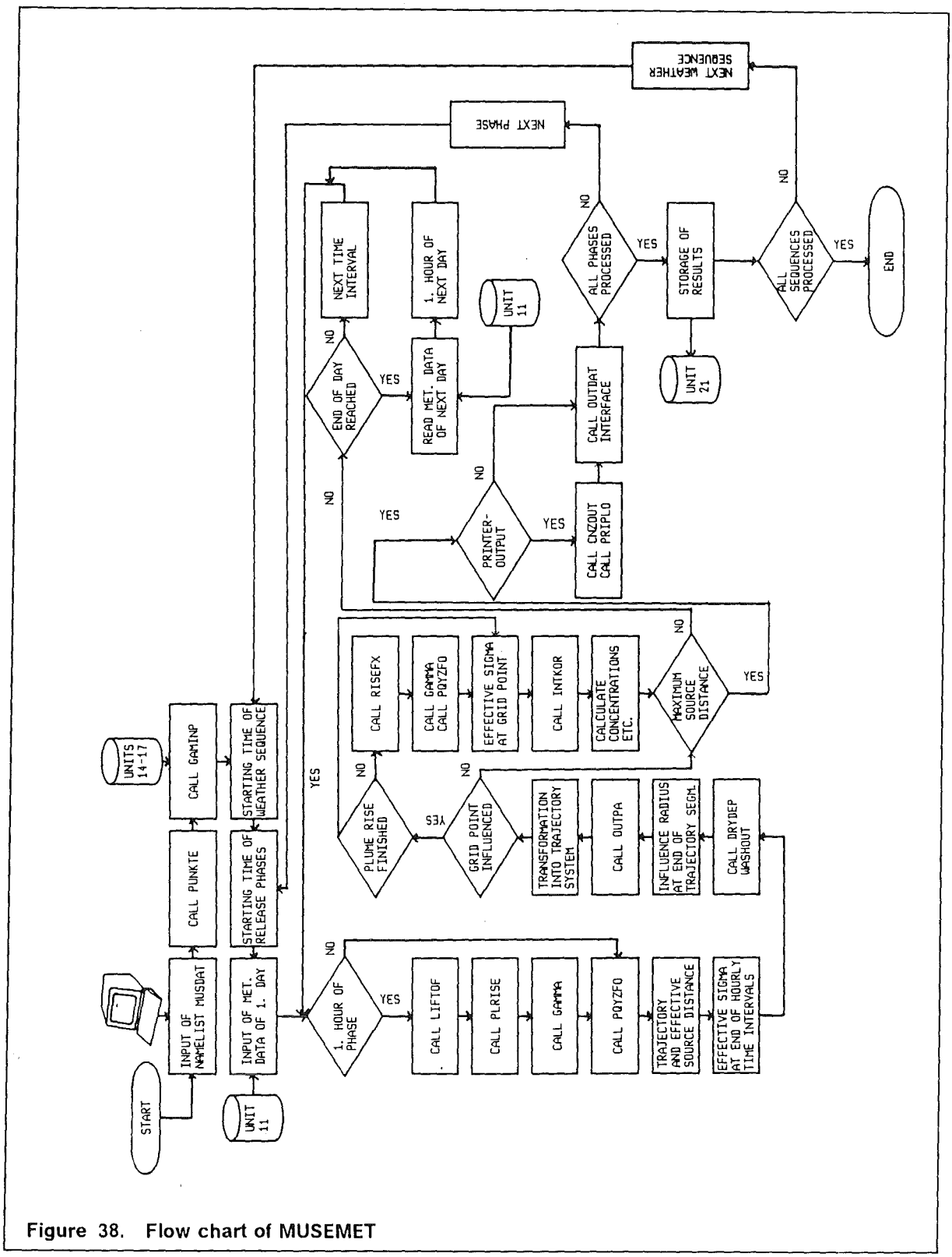

Figure 38. Flow chart of MUSEMET

9. APPENDIX C: STRUCTURE OF METSAM

The METSAM code system consists of three different programs.

9.1 The trajectory program TRAJEC

TRAJEC is a reduced version of the atmospheric dispersion model MUSEMET which is used within the METSAM system to calculate trajectories. These calculations are based on hourly recordings of wind direction and wind speed which should be available for at least one year from a meteorological station representative for the location of a nuclear facility itself and its surroundings. It is possible to consider different nuclear sites if the data of corresponding meteorological zones are available. At each hourly time interval a trajectory is started at the source site. The release height, the maximum source distance, the number of different trajectories desired, and the number of days with meteorological data available have to be defined by the user. Additionally, a stability dependent wind-profile exponent, because a power law according to Eq. (2.7) is used to calculate the wind profile, and the number of different nuclear sites have to be determined by the user. The prevailing meteorological conditions (stability category, wind direction, wind speed and precipitation intensity) as well as a counter for each trajectory are stored on an output unit for each hourly time interval until the trajectory has left the predefined area. Additionally, the horizontal coordinates of each trajectory relative to the cartesian coordinate system (see Section 2.1) with its origin at the source site are stored after each time interval. This last information is not relevant to the subsequent sampling procedure but it might be used for plotting of selected trajectories.

9.2 The statistic program STATIS

The second program, STATIS, is optional but it might help to find appropriate boundaries for the travel time and/or precipitation intensity classes. The program reads the results obtained in TRAJEC. For each 30° sector of initial wind direction it constructs a frequency distribution of the trajectories according to the total amount of precipitation fallen as a trajectory passes over the predefined area and according to the travel time. The sum of precipitation intensity is categorized in four groups. Their boundaries are user defined. The travel time is divided into hourly intervals. The maximum travel time considered can also be defined by the user. The resulting frequency distributions are printed.

9.3 The sampling program SAMPLE

SAMPLE performs the actual stratified sampling of weather sequences. The general procedure has been already described in Section 4. SAMPLE reads the output data sets obtained with TRAJEC. Each trajectory, defining a weather sequence, is categorized according to its initial wind direction, its travel time to leave a predefined area and the total amount of precipitation fallen in the course of the sequence. With the exception of

the twelve 30° wind direction sectors the boundaries of the three travel times and the four precipitation intensity classes can be defined by the user. The boundaries of the wind direction sectors are shown in Table 26 together with the corresponding sector index.

Sector boundaries (degree)	Sector index
15° - 44°	1
45° - 74°	2
75° - 104°	3
115° - 134°	4
135° - 164°	5
165° - 194°	6
195° - 224°	7
225° - 254°	8
255° - 284°	9
285° - 314°	10
315° - 344°	11
345° - 14°	12

Table 26. Boundaries and indices of wind direction sector: directions relative to the clockwise wind rose.

At least one weather sequence is chosen randomly from each of the resulting 144 classes. The number of 144 classes is fixed and cannot be changed without modifying the code, but the user can decide whether he would like to select more than one sequence with different starting times from each class.

If a certain class is empty, because the meteorological situation represented by this class does not occur, or if the class does not contain sufficient weather sequences, additional sequences will be selected by staying in the same travel time group but jumping to the lower precipitation intensity class.

The starting times and the probabilities of occurrence of the selected weather sequences are stored on an output data set. Additionally, the absolute class frequencies, the number of weather sequences selected from each class, and the starting times and probabilities of these sequences are printed. The whole procedure is repeated in one single computer run for all meterorological zones considered.

9.4 List and structure of I/O units of METSAM

For an application of the complete METSAM system some I/O units are required which are given in Table 27 and the data transfer is illustrated in Figure 39.

UNIT	used as INPUT-unit in	used as OUTPUT-unit in	Description
5	TRAJEC, STATIS, SAMPLE		reads input data defined in NAMELIST statements
6		TRAJEC, STATIS, SAMPLE	printout of input data, results, and additional informations
2		SAMPLE	output unit to store results of SAMPLE
11	TRAJEC		input unit to read meteorological data
20+IZ, IZ=1,...,NSTAT	STATIS, SAMPLE	TRAJEC	output and input units to store and read results of trajectory calculations for each meteorological zone IZ, IZ=1,...,NSTAT

Table 27. I/O units required for the METSAM system

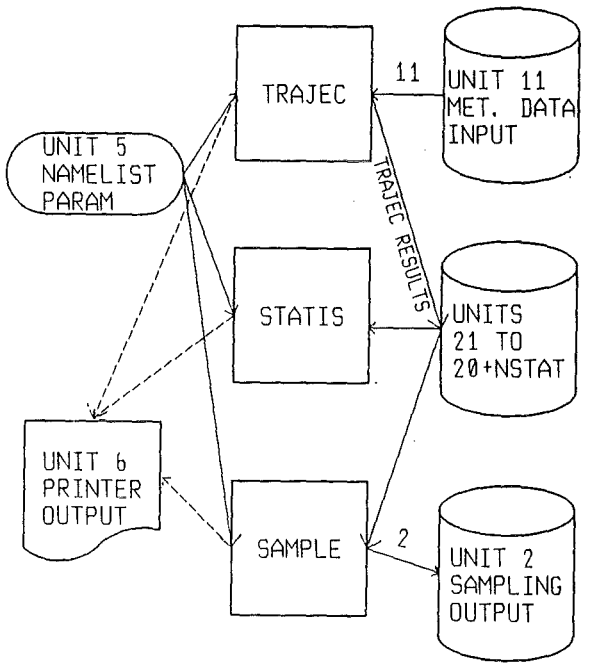

Figure 39. Illustration of data transfer within METSAM

9.4.1 Structure of I/O units of TRAJEC

9.4.1.1 Description of input namelist PARAM

To perform the trajectory calculations the user has to define some input data which are read using the **NAMELIST** statement. The Namelist statement does not belong to the standard FORTRAN-77, but it is an element of extended versions of the standard language. Because no default values are defined, the input of the namelist is obligatory. Its name is **PARAM**. The following Table 28 gives the parameters of namelist PARAM and their definitions.

PARAMETER	TYPE	DEFINITION
MEX(6)	REAL * 4	array of stability dependent wind profile exponents
H	REAL * 4	emission height (m)
NWETTR	INTEGER * 4	number of trajectories which are calculated for each meteorological zone
NSTAT	INTEGER * 4	number of different meteorological zones
ZONE(10)	CHARACTER * 10	array with names of meteorological zone or nuclear facilities
RMAX	REAL * 4	maximum source distance (m)
NDAYMX	INTEGER * 4	number of days with meteorological days available

Table 28. Parameters of input namelist PARAM of TRAJEC

9.4.1.2 Description of meteorological input data set

The hourly meteorological data which determine the path and length of each trajectory have to be available on unit 11 (Figure 39). The data should consist of hourly synoptic recordings of

- wind direction
- wind speed
- stability category according to the Pasquill-Gifford classification
- precipitation intensity

These data should be available at least for one year from one or several meteorological zones. Each zone can be assigned to several nuclear sites with respect to topographical and regional climatological properties of the site, so that the corresponding meteorological data can be considered representative for the site location and its environment.

The data set containing the data base has to be organized as a **DIRECT ACCESS** file with a fixed record length which is equal to the blocksize. The data must be coded binary. Each record of this file contains the meteorological data of one day measured at a certain meteorological station. The following FORTRAN statements show the READ-statement for a record and they also indicate the arrangement of the records if NSTAT meteorological zones are considered:

```
      DO 1 IZ=1, NSTAT

      DO 2 NDAY=1, NDAYMX
C
C     NDAYMX = number of days with meteorological data for each
C     meteorological zone
C
      L1 = (IZ-1) * NDAYMX + NDAY

      READ(11,REC=L1) (DIR(J),DIFF(J),RAIN(J),SPEED(J),J=1,24)

C
C     ATTENTION: all parameters in the READ statement above have
C     to be of type INTEGER
C
    2 CONTINUE

    1 CONTINUE
```

with:

L1	record counter
DIR	wind direction in degree
DIFF	Pasquill-Gifford stability class, coded as an integer in the range from 1 to 6; 1 = A, 2 = B, ..., 6 = F
RAIN	precipitation intensity (10^{-2} mm/h)
SPEED	wind speed (10^{-2} m/s) at 10 m height

Since each variable in the READ-statement has to be of type INTEGER with a length of four byte, the total length of a record equals 24 * 4 * 4 byte = 384 byte.

9.4.1.3 Description of the output data sets

The results of the trajectory calculations are stored on the output units 20 + IZ, IZ = 1,...,NSTAT, (Figure 39). For each meteorological zone, IZ, considered, a new data set has to be created. Each data set has to be organized sequentially with a variable record length and the data must be coded binary. The arrangement of the stored data is sketched in the following FORTRAN statements:

```
      DO 3 IZ = 1, NSTAT
      DO 4 IT = 1, NWETTR
      DO 5 IH = 1, NINTVL

C
C     NINTVL = number of hourly intervals a trajectory needed to
C     leave to the predefined area
C
      WRITE(20+IZ) (DIFF(IH), DIR(IH), SPEED(IH), RAIN(IH),
     +              IT, IH, XT(IH), YT(IH)

    5 CONTINUE

    4 CONTINUE

    3 CONTINUE
```

with:

DIFF(IH)	Pasquill-Gifford stability class for the IH-th hourly time interval along the path of trajectory IT
DIR(IH)	corresponding wind direction in degree
SPEED(IH)	corresponding wind speed (10^{-2} m/s) at 10 m height
RAIN (IH)	corresponding precipitation intensity (mm/h)
IT	index of the tracjectory
IH	index of time interval
XT(IH), YT(IH)	corresponding horizontal coordinates of the trajectory

The total amount of records in an output data set is variable. It depends on the number of time intervals, NINTVL, each trajectory needs to leave the area which is defined by the maximum source distance, RMAX. It might happen that the number of trajectories calculated and stored for a meteorological zone is less than NWETTR because the end of the meteorological input data is reached before the last trajectories have left the predefined area. The user will get an information on this on the printer output.

9.4.2 Structure of I/O units of STATIS

9.4.2.1 Description of input namelist PARAM

To construct the three dimensional frequency distribution of the trajectories according to the initial wind direction, the total amount of precipitation and the travel time, STATIS needs a few input data which are read using the namelist PARAM. The following list gives the parameter names, their definitions, and default values. Any of these parameters has only to be read if the user wants to change the default value.

PARAMETER	TYPE	DEFAULT	DEFINITION
NSTAT	INTEGER * 4	1	number of different meteorological zones
ZONE(10)	CHARACTER * 10	'.....'	array with names of meteorological zones
MAXTIM	INTEGER * 4	250	maximum number of hourly travel time intervals of the trajectories
PRECIP(4)	REAL * 4	0., 0.9, 2.9, 100.	array with boundaries of the precipitation intensity classes

Table 29. Parameters of input namelist PARAM of STATIS

The fixed boundaries of the twelve 30°-sectors of the initial wind direction and the corresponding sector indices are shown in Table 27.

9.4.2.2 Input of trajectory informations

STATIS reads the output data sets of TRAJEC which have to be available on the input units 20 + IZ, IZ = 1,...,NSTAT, (Figure 39).

9.4.2.3 Output of STATIS

STATIS only provides a printer output. The user gets the three-dimensional frequency distributions for each meteorological zone considered. The output example in Section 9.5 shows the frequency distribution of trajectories according to precipitation intensity and travel time for the most frequent initial wind direction sector calculated from hourly meteorological data of two years recorded at Karlsruhe, F.R.G.

9.4.3 Structure of I/O units of SAMPLE

9.4.3.1 Description of input namelist PARAM

To perform the classification of weather sequences, SAMPLE needs some input data which are read using the namelist PARAM. The following list gives the parameter names, their default values and definitions.

PARAMETER	TYPE	DEFAULT	DEFINITION
NSTAT	INTEGER * 4	1	number of different meteorological zones
ZONE(10)	CHARACTER * 10	'.....'	array with names of meteorological zones
PRECIP(4)	REAL * 4	0., 0.9, 2.9, 100.	array with boundaries of the precipitation intensity classes
TTIME(3)	REAL * 4	3.,6.,250.	array with boundaries of travel time classes
NSEQU	INTEGER * 4	1	number of weather sequences which has to be selected from each class

Table 30. Parameters of input namelist PARAM of SAMPLE

9.4.3.2 Input of trajectory informations

SAMPLE reads the output data sets of TRAJEC which have to be available on the input units 20 + IZ, IZ = 1,...,NSTAT (Figure 39).

9.4.3.3 Description of output data set

The resulting starting times and probabilities of occurrence of the selected weather sequences are stored on the output unit 2 (Figure 39). The data set has to be organized sequentially with a variable record length and the data must be coded binary. The following FORTRAN statements indicate the arrangement of the stored data.

```
      DO 1 IZ = 1, NSTAT

      WRITE(2) IZ, NWET, (STARTT(IJ), PROB(IJ), IJ=1, NWET)

    1 CONTINUE
```

with:

IZ	identifier of the meteorological zone
NWET	number of weather sequences selected
STARTT	starting times of selected weather sequences
PROB	probability of occurrence of selected weather sequences

This simple WRITE-statement within the loop over the meteorological zones is the interface of METSAM to the UFOMOD system. Therefore a potential user of the UFOMOD system who wants to apply his own procedure of meteorological sampling or to modify that one described here, has to ensure that the structure of the starting time / probability output data set is identical to that illustrated above.

9.4.3.4 Printer output of SAMPLE

In addition to the output of the results on a mass storage unit informations on the results of the sampling procedure are printed. These are mainly the absolute class frequencies, the number of weather sequences selected from each class, their starting times and probabilities. The printer output is given for each meteorological zone considered. An example is shown in the following section together with examples of the printer outputs of TRAJEC and STATIS.

9.5 Examples of the printer output of TRAJEC, STATIS, and SAMPLE

In the corresponding METSAM run 8 meteorological zone were considered. The emission height was 50 m and the area over which the trajectories passed had a maximum radial source distance of 20000m. Only 17400 trajectories should be considered for each station.

The TRAJEC output example shows the complete output while the examples for STATIS and SAMPLE are only parts of the corresponding output lists.

Example of T R A J E C printer output

```
 CONTROL OUTPUT OF INPUT DATA FOR

       THE PROGRAM TRAJEC


 NUMBER OF METEOROLOGICAL ZONES CONSIDERED:      8
 EMISSION HEIGHT (M)                        :    50.
 NUMBER OF TRAJECTORIES                     : 17400
 MAXIMUM SOURCE DISTANCE (KM)               :  20.00


     WIND PROFILE EXPONENTS

       DKAT     MEX

         A     0.07
         B     0.13
         C     0.21
         D     0.34
         E     0.44
         F     0.44

 METEOROLOGICAL ZONE: AUGSBURG
 -------------------

 NUMBER OF TRAJECTORIES CONSIDERED 17400


 METEOROLOGICAL ZONE: HAMBURG
 -------------------

 NO MORE METEOROLOGICAL DATA AVAILABLE FOR METEOROLOGICAL ZONE HAMBURG
 TO CONSIDER ALL 17400 TRAJECTORIES
 LAST TRAJECTORY 17400 REACHED SOURCE DISTANCE OF   15929.1M

 METEOROLOGICAL ZONE: KARLSRUHE
 -------------------

 NO MORE METEOROLOGICAL DATA AVAILABLE FOR METEOROLOGICAL ZONE KARLSRUHE
 TO CONSIDER ALL 17400 TRAJECTORIES
 LAST TRAJECTORY 17400 REACHED SOURCE DISTANCE OF   19164.7M
```

Example of T R A J E C printer output (cont'd.)

```
METEOROLOGICAL ZONE: KASSEL
-------------------

NO MORE METEOROLOGICAL DATA AVAILABLE FOR METEOROLOGICAL ZONE KASSEL
TO CONSIDER ALL 17400 TRAJECTORIES
LAST TRAJECTORY 17398 REACHED SOURCE DISTANCE OF   18233.7M

METEOROLOGICAL ZONE: KOELN
-------------------

NO MORE METEOROLOGICAL DATA AVAILABLE FOR METEOROLOGICAL ZONE KOELN
TO CONSIDER ALL 17400 TRAJECTORIES
LAST TRAJECTORY 17400 REACHED SOURCE DISTANCE OF   18710.7M

METEOROLOGICAL ZONE: MUENSTER
-------------------

NO MORE METEOROLOGICAL DATA AVAILABLE FOR METEOROLOGICAL ZONE MUENSTER
TO CONSIDER ALL 17400 TRAJECTORIES
LAST TRAJECTORY 17400 REACHED SOURCE DISTANCE OF   14983.1M

METEOROLOGICAL ZONE: NUERNBERG
-------------------

NO MORE METEOROLOGICAL DATA AVAILABLE FOR METEOROLOGICAL ZONE NUERNBERG
TO CONSIDER ALL 17400 TRAJECTORIES
LAST TRAJECTORY 17400 REACHED SOURCE DISTANCE OF   19164.7M

METEOROLOGICAL ZONE: STUTTGART
-------------------

NO MORE METEOROLOGICAL DATA AVAILABLE FOR METEOROLOGICAL ZONE STUTTGART
TO CONSIDER ALL 17400 TRAJECTORIES
LAST TRAJECTORY 17399 REACHED SOURCE DISTANCE OF   18710.7M


END OF PROGRAM      T R A J E C
```

Part of S T A T I S printer output

METEOROLOGICAL ZONE KARLSRUHE
NUMBER OF DIFFERENT TRAJECTORIES FOUND: 17400

METEOROLOGICAL ZONE 3
SECTOR 8 OF INITIAL WINDDIRECTION:
225. DEGREE - 254. DEGREE

	BOUNDARIES OF PRECIPITATION CLASSES			
TRAVEL TIME (H)	0.0	0.9	2.9	100.0
1	1795	426	180	16
2	893	162	112	5
3	217	30	9	1
4	71	12	8	1
5	39	6	1	2
6	40	1	3	0
7	21	3	2	1
8	17	5	1	2
9	14	2	1	1
10	7	0	2	2
11	6	0	0	0
12	2	0	0	0
13	3	1	0	0
14	5	0	0	0
15	2	2	0	0
16	2	0	0	0
SUM	3134	650	319	31

CLASS FREQUENCY: 4134

END OF PROGRAM S T A T I S

Part of S A M P L E printer output

STATION KARLSRUHE
NUMBER OF TRAJECTORIES CONSIDERED 17400

```
**************************************************************************
*                                                                        *
*     the following two tables have been shortened                       *
*     the second precipitation class has been omitted here               *
*     it appears of course in the original printer output                *
*                                                                        *
**************************************************************************
```

FREQUENCY DISTRIBUTION FOR ALL CLASSES

PRECIPTIATION CLASSES	0.0			0.9 < I <= 2.9			> 2.9			
TRAVEL TIME CLASSES	1 - 3	4 - 6	> 6	1 - 3	4 - 6	> 6	1 - 3	4 - 6	> 6	
SECTOR										SUM
1 (15- 44) :	1522	443	74	25	18	8	5	2	7	2242
2 (45- 74) :	1993	449	93	15	20	5	6	5	3	2687
3 (75- 104) :	403	209	50	11	9	4	5	8	3	759
4 (105- 134) :	103	146	46	8	12	7	0	7	2	402
5 (135- 164) :	80	162	62	7	10	2	2	3	2	390
6 (165- 194) :	307	257	61	39	14	5	6	2	3	804
7 (195- 224) :	2362	196	88	227	11	7	27	9	5	3563
8 (225- 254) :	2905	150	79	301	12	6	22	3	6	4134
9 (255- 284) :	457	83	40	73	6	2	13	2	1	789
10 (285- 314) :	145	84	19	28	12	3	10	1	4	332
11 (315- 344) :	73	92	25	13	16	1	5	1	0	260
12 (345- 14) :	520	267	50	57	7	4	5	8	5	1038

GWICHT: 1.00

CLASS 410 IS EMPTY
CLASS 1112 IS EMPTY

NUMBER OF WEATHER SEQUENCES SELECTED PER CLASS

PRECIPTIATION CLASSES	0.0			0.9 < I <= 2.9			> 2.9		
TRAVEL TIME CLASSES	1 - 3	4 - 6	> 6	1 - 3	4 - 6	> 6	1 - 3	4 - 6	> 6
SECTOR									
1 (15- 44) :	1	1	1	1	1	1	1	1	1
2 (45- 74) :	1	1	1	1	1	1	1	1	1
3 (75- 104) :	1	1	1	1	1	1	1	1	1
4 (105- 134) :	1	1	1	2	1	1	0	1	1
5 (135- 164) :	1	1	1	1	1	1	1	1	1
6 (165- 194) :	1	1	1	1	1	1	1	1	1
7 (195- 224) :	1	1	1	1	1	1	1	1	1
8 (225- 254) :	1	1	1	1	1	1	1	1	1
9 (255- 284) :	1	1	1	1	1	1	1	1	1
10 (285- 314) :	1	1	1	1	1	1	1	1	1
11 (315- 344) :	1	1	1	1	1	1	1	1	0
12 (345- 14) :	1	1	1	1	1	1	1	1	1

Part of S A M P L E printer output (cont'd.)

PROBABLITIES AND STARTING TIMES OF SELECTED WEATHER SEQUENCES

CLASS:	901	PROBABILITY:	0.263E-01	STARTING TIME	44	I:	1
CLASS:	407	PROBABILITY:	0.230E-03	STARTING TIME	64	I:	2
CLASS:	408	PROBABILITY:	0.690E-03	STARTING TIME	249	I:	3
CLASS:	107	PROBABILITY:	0.144E-02	STARTING TIME	502	I:	4
CLASS:	603	PROBABILITY:	0.351E-02	STARTING TIME	635	I:	5
CLASS:	803	PROBABILITY:	0.454E-02	STARTING TIME	1212	I:	6
CLASS:	503	PROBABILITY:	0.356E-02	STARTING TIME	1216	I:	7
CLASS:	1206	PROBABILITY:	0.345E-03	STARTING TIME	1306	I:	8
CLASS:	204	PROBABILITY:	0.253E-02	STARTING TIME	1528	I:	9
CLASS:	511	PROBABILITY:	0.172E-03	STARTING TIME	2047	I:	10
CLASS:	607	PROBABILITY:	0.224E-02	STARTING TIME	2067	I:	11
CLASS:	1105	PROBABILITY:	0.977E-03	STARTING TIME	2140	I:	12
CLASS:	1110	PROBABILITY:	0.287E-03	STARTING TIME	2346	I:	13
CLASS:	104	PROBABILITY:	0.552E-02	STARTING TIME	2360	I:	14
CLASS:	201	PROBABILITY:	0.115E+00	STARTING TIME	2754	I:	15
CLASS:	302	PROBABILITY:	0.120E-01	STARTING TIME	2791	I:	16
CLASS:	203	PROBABILITY:	0.534E-02	STARTING TIME	2882	I:	17
CLASS:	310	PROBABILITY:	0.287E-03	STARTING TIME	3257	I:	18
CLASS:	108	PROBABILITY:	0.103E-02	STARTING TIME	3328	I:	19
CLASS:	109	PROBABILITY:	0.460E-03	STARTING TIME	3358	I:	20
CLASS:	702	PROBABILITY:	0.113E-01	STARTING TIME	3490	I:	21
CLASS:	902	PROBABILITY:	0.477E-02	STARTING TIME	3588	I:	22
CLASS:	101	PROBABILITY:	0.875E-01	STARTING TIME	3780	I:	23
CLASS:	301	PROBABILITY:	0.232E-01	STARTING TIME	3826	I:	24
CLASS:	1007	PROBABILITY:	0.161E-02	STARTING TIME	3914	I:	25
CLASS:	711	PROBABILITY:	0.517E-03	STARTING TIME	4019	I:	26
CLASS:	810	PROBABILITY:	0.126E-02	STARTING TIME	4142	I:	27
CLASS:	1205	PROBABILITY:	0.259E-02	STARTING TIME	4279	I:	28
CLASS:	812	PROBABILITY:	0.345E-03	STARTING TIME	4380	I:	29
CLASS:	1011	PROBABILITY:	0.575E-04	STARTING TIME	4382	I:	30
CLASS:	1111	PROBABILITY:	0.575E-04	STARTING TIME	4383	I:	31
CLASS:	1010	PROBABILITY:	0.575E-03	STARTING TIME	4387	I:	32
CLASS:	701	PROBABILITY:	0.136E+00	STARTING TIME	4557	I:	33
CLASS:	1009	PROBABILITY:	0.172E-03	STARTING TIME	4621	I:	34
CLASS:	707	PROBABILITY:	0.130E-01	STARTING TIME	4652	I:	35
CLASS:	1102	PROBABILITY:	0.529E-02	STARTING TIME	4955	I:	36
CLASS:	1202	PROBABILITY:	0.153E-01	STARTING TIME	4989	I:	37
CLASS:	708	PROBABILITY:	0.632E-03	STARTING TIME	5157	I:	38
CLASS:	1106	PROBABILITY:	0.115E-03	STARTING TIME	5198	I:	39
CLASS:	1201	PROBABILITY:	0.299E-01	STARTING TIME	5221	I:	40
CLASS:	305	PROBABILITY:	0.126E-02	STARTING TIME	5298	I:	41
CLASS:	705	PROBABILITY:	0.109E-02	STARTING TIME	5309	I:	42
CLASS:	807	PROBABILITY:	0.173E-01	STARTING TIME	5483	I:	43

```
CLASS:   103   PROBABILITY:  0.425E-02   STARTING TIME   5516  I:  44
CLASS:   508   PROBABILITY:  0.575E-03   STARTING TIME   5887  I:  45
CLASS:   309   PROBABILITY:  0.230E-03   STARTING TIME   5932  I:  46
CLASS:   908   PROBABILITY:  0.345E-03   STARTING TIME   6196  I:  47
CLASS:   510   PROBABILITY:  0.115E-03   STARTING TIME   6198  I:  48
CLASS:   610   PROBABILITY:  0.345E-03   STARTING TIME   6200  I:  49
CLASS:   904   PROBABILITY:  0.534E-02   STARTING TIME   6582  I:  50
CLASS:   205   PROBABILITY:  0.207E-02   STARTING TIME   6594  I:  51
CLASS:   406   PROBABILITY:  0.517E-03   STARTING TIME   6651  I:  52
CLASS:  1209   PROBABILITY:  0.230E-03   STARTING TIME   6676  I:  53
CLASS:   504   PROBABILITY:  0.126E-02   STARTING TIME   6684  I:  54
CLASS:  1203   PROBABILITY:  0.287E-02   STARTING TIME   6811  I:  55
CLASS:   704   PROBABILITY:  0.348E-01   STARTING TIME   6957  I:  56
CLASS:   211   PROBABILITY:  0.287E-03   STARTING TIME   7091  I:  57
CLASS:  1106   PROBABILITY:  0.115E-03   STARTING TIME   7221  I:  58
CLASS:   602   PROBABILITY:  0.148E-01   STARTING TIME   7267  I:  59
CLASS:   903   PROBABILITY:  0.230E-02   STARTING TIME   7283  I:  60
CLASS:   505   PROBABILITY:  0.178E-02   STARTING TIME   7322  I:  61
CLASS:   502   PROBABILITY:  0.931E-02   STARTING TIME   7533  I:  62
CLASS:  1004   PROBABILITY:  0.109E-02   STARTING TIME   7706  I:  63
CLASS:   512   PROBABILITY:  0.115E-03   STARTING TIME   7725  I:  64
CLASS:   308   PROBABILITY:  0.517E-03   STARTING TIME   7731  I:  65
CLASS:   604   PROBABILITY:  0.379E-02   STARTING TIME   7736  I:  66
CLASS:   906   PROBABILITY:  0.402E-03   STARTING TIME   8127  I:  67
CLASS:   209   PROBABILITY:  0.287E-03   STARTING TIME   8132  I:  68
CLASS:   509   PROBABILITY:  0.115E-03   STARTING TIME   8136  I:  69
CLASS:   709   PROBABILITY:  0.402E-03   STARTING TIME   8139  I:  70
CLASS:   106   PROBABILITY:  0.920E-03   STARTING TIME   8173  I:  71
CLASS:   206   PROBABILITY:  0.103E-02   STARTING TIME   8306  I:  72
CLASS:   606   PROBABILITY:  0.402E-03   STARTING TIME   8410  I:  73
CLASS:   311   PROBABILITY:  0.460E-03   STARTING TIME   8530  I:  74
CLASS:  1207   PROBABILITY:  0.328E-02   STARTING TIME   8653  I:  75
CLASS:   601   PROBABILITY:  0.176E-01   STARTING TIME   9270  I:  76
CLASS:   907   PROBABILITY:  0.420E-02   STARTING TIME   9364  I:  77
CLASS:   805   PROBABILITY:  0.109E-02   STARTING TIME   9819  I:  78
CLASS:   706   PROBABILITY:  0.345E-03   STARTING TIME   9915  I:  79
CLASS:   905   PROBABILITY:  0.690E-03   STARTING TIME   9917  I:  80
CLASS:   811   PROBABILITY:  0.172E-03   STARTING TIME  10336  I:  81
CLASS:   808   PROBABILITY:  0.690E-03   STARTING TIME  10342  I:  82
CLASS:   912   PROBABILITY:  0.575E-04   STARTING TIME  10344  I:  83
CLASS:   909   PROBABILITY:  0.115E-03   STARTING TIME  10345  I:  84
CLASS:   703   PROBABILITY:  0.506E-02   STARTING TIME  10716  I:  85
CLASS:  1006   PROBABILITY:  0.575E-04   STARTING TIME  10745  I:  86
CLASS:  1204   PROBABILITY:  0.368E-02   STARTING TIME  10780  I:  87
CLASS:   112   PROBABILITY:  0.402E-03   STARTING TIME  11188  I:  88
CLASS:  1107   PROBABILITY:  0.747E-03   STARTING TIME  11194  I:  89
CLASS:   507   PROBABILITY:  0.402E-03   STARTING TIME  11325  I:  90
```

```
CLASS:   307   PROBABILITY:  0.632E-03   STARTING TIME  11327  I:  91
CLASS:  1210   PROBABILITY:  0.287E-03   STARTING TIME  11359  I:  92
CLASS:  1012   PROBABILITY:  0.230E-03   STARTING TIME  11380  I:  93
CLASS:   105   PROBABILITY:  0.149E-02   STARTING TIME  11596  I:  94
CLASS:  1104   PROBABILITY:  0.747E-03   STARTING TIME  11706  I:  95
CLASS:  1208   PROBABILITY:  0.402E-03   STARTING TIME  11754  I:  96
CLASS:   405   PROBABILITY:  0.172E-02   STARTING TIME  11878  I:  97
CLASS:  1005   PROBABILITY:  0.345E-03   STARTING TIME  11879  I:  98
CLASS:   612   PROBABILITY:  0.172E-03   STARTING TIME  11958  I:  99
CLASS:   404   PROBABILITY:  0.184E-02   STARTING TIME  12023  I: 100
CLASS:   306   PROBABILITY:  0.690E-03   STARTING TIME  12148  I: 101
CLASS:   608   PROBABILITY:  0.805E-03   STARTING TIME  12176  I: 102
CLASS:   506   PROBABILITY:  0.402E-03   STARTING TIME  12190  I: 103
CLASS:   207   PROBABILITY:  0.862E-03   STARTING TIME  12203  I: 104
CLASS:  1109   PROBABILITY:  0.575E-04   STARTING TIME  12215  I: 105
CLASS:  1108   PROBABILITY:  0.920E-03   STARTING TIME  12216  I: 106
CLASS:   809   PROBABILITY:  0.345E-03   STARTING TIME  12237  I: 107
CLASS:   609   PROBABILITY:  0.287E-03   STARTING TIME  12238  I: 108
CLASS:   712   PROBABILITY:  0.287E-03   STARTING TIME  12418  I: 109
CLASS:   910   PROBABILITY:  0.747E-03   STARTING TIME  12432  I: 110
CLASS:  1008   PROBABILITY:  0.690E-03   STARTING TIME  12440  I: 111
CLASS:  1101   PROBABILITY:  0.420E-02   STARTING TIME  12592  I: 112
CLASS:   102   PROBABILITY:  0.255E-01   STARTING TIME  12612  I: 113
CLASS:   403   PROBABILITY:  0.264E-02   STARTING TIME  12724  I: 114
CLASS:   110   PROBABILITY:  0.287E-03   STARTING TIME  12749  I: 115
CLASS:  1103   PROBABILITY:  0.144E-02   STARTING TIME  12802  I: 116
CLASS:   303   PROBABILITY:  0.287E-02   STARTING TIME  12892  I: 117
CLASS:   804   PROBABILITY:  0.355E-01   STARTING TIME  13343  I: 118
CLASS:  1211   PROBABILITY:  0.460E-03   STARTING TIME  13527  I: 119
CLASS:   409   PROBABILITY:  0.402E-03   STARTING TIME  13750  I: 120
CLASS:  1001   PROBABILITY:  0.833E-02   STARTING TIME  13772  I: 121
CLASS:   801   PROBABILITY:  0.167E+00   STARTING TIME  13786  I: 122
CLASS:  1212   PROBABILITY:  0.287E-03   STARTING TIME  13890  I: 123
CLASS:   312   PROBABILITY:  0.172E-03   STARTING TIME  13894  I: 124
CLASS:   412   PROBABILITY:  0.115E-03   STARTING TIME  13895  I: 125
CLASS:   407   PROBABILITY:  0.230E-03   STARTING TIME  13901  I: 126
CLASS:   210   PROBABILITY:  0.345E-03   STARTING TIME  14325  I: 127
CLASS:   802   PROBABILITY:  0.862E-02   STARTING TIME  14374  I: 128
CLASS:   501   PROBABILITY:  0.460E-02   STARTING TIME  14609  I: 129
CLASS:   111   PROBABILITY:  0.115E-03   STARTING TIME  14648  I: 130
CLASS:   611   PROBABILITY:  0.115E-03   STARTING TIME  15047  I: 131
CLASS:   212   PROBABILITY:  0.172E-03   STARTING TIME  15056  I: 132
CLASS:   911   PROBABILITY:  0.115E-03   STARTING TIME  15057  I: 133
CLASS:   411   PROBABILITY:  0.402E-03   STARTING TIME  15058  I: 134
CLASS:   710   PROBABILITY:  0.155E-02   STARTING TIME  15184  I: 135
CLASS:   208   PROBABILITY:  0.115E-02   STARTING TIME  15328  I: 136
CLASS:   402   PROBABILITY:  0.839E-02   STARTING TIME  15631  I: 137
```

```
CLASS:  1003   PROBABILITY:  0.109E-02   STARTING TIME  15859  I: 138
CLASS:   304   PROBABILITY:  0.132E-02   STARTING TIME  15887  I: 139
CLASS:   806   PROBABILITY:  0.747E-03   STARTING TIME  16009  I: 140
CLASS:  1002   PROBABILITY:  0.483E-02   STARTING TIME  16218  I: 141
CLASS:   202   PROBABILITY:  0.258E-01   STARTING TIME  16730  I: 142
CLASS:   401   PROBABILITY:  0.592E-02   STARTING TIME  17126  I: 143
CLASS:   605   PROBABILITY:  0.213E-02   STARTING TIME  17240  I: 144
NUMBER OF SELECTED WEATHER SEQUENCES:   144

SUM OVER ALL PROBABILITIES        1.0

END OF PROGRAM
```

10. APPENDIX D: I/O STRUCTURE OF MESOS

10.1 General description

To enable a user of the KfK-version of MESOS running the code on a computer a brief user guide is given in this appendix. The subsequent examples of job control language (JCL) refer to the IBM 3090 / Siemens 7890-M computer systems installed at KfK. The original MESOS version has been adapted to these systems by the Abteilung für Angewandte Systemanalyse (AFAS, Department for Applied System Analysis) of KfK.

As already described in Section 2.4, MESOS consists of three modules. The general I/O structure of each of these modules is illustrated in Figure 40.

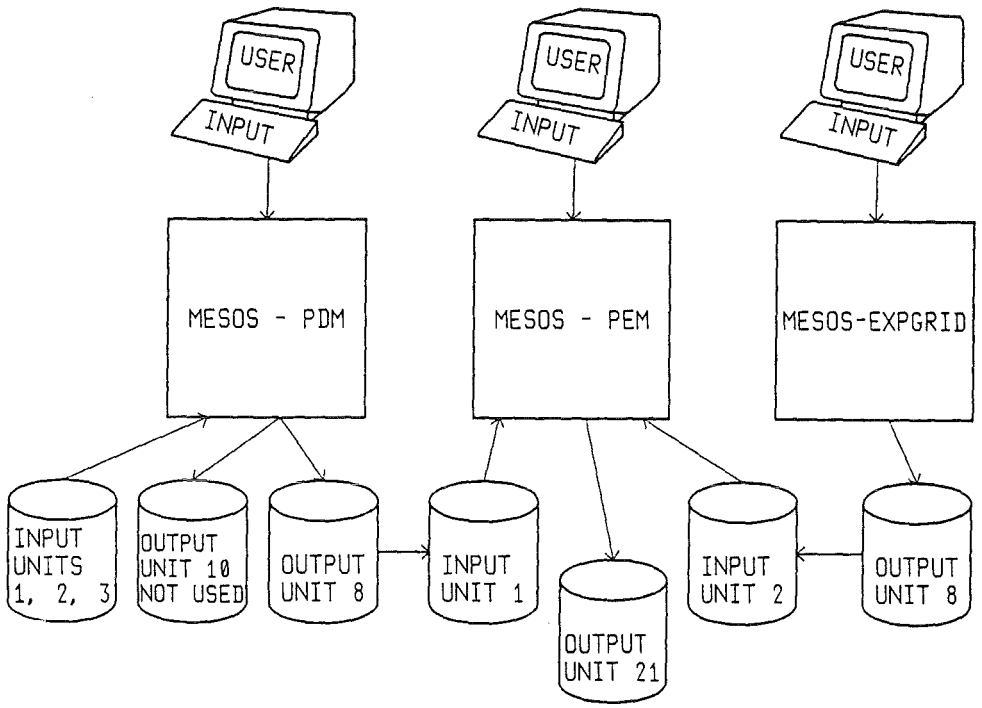

Figure 40. Illustration of I/O structure of MESOS

1. **MESOS-PDM**

   The input for PDM (puff development module) is self-explaining. For calculating the puff histories it requires user defined input data and the following external data sets:

   - Input data sets:

     - Unit 1: pressure data for 1982 and 1983 (first day available: 16.12.1981, last day available: 26.12.1983)

- Unit 2: synoptic data for 1982 and 1983 (see pressure data)

They are the meteorological MESOS data base and are written as formatted data.

- Unit 3: characteristics of the MESOS-area and meteorological data base (geographical coordinates defining the size of the area, period for which meteorological data are available)

- Output data sets:

  - Unit 10: formatted data set; writes some specifications of the meteorological station only for information; not needed for further calculations.

  - Unit 8: it consists of the puff histories; they are written as binary data and are needed for a PEM-run (in PEM read in from unit 1).

For a 2-year-calculation PDM needs about 7 minutes on the computer system mentioned above.

2. **MESOS-EXPGRID**

For transforming the polar concentration grid around the source into geographical coordinates, EXPGRID needs some user defined input data and one external output data set.

- Input data sets: none

- Output data sets:

  - Unit 8: formatted data set with geographical coordinates of the polar grid points; it is input to PEM (read in from unit 2).

3. **MESOS-PEM**

With the grid around the source and the puff histories PEM (population exposure module) calculates the normalized activity concentrations in the air near to the ground and on the ground surface for all nuclides considered. Again user defined input variables and external I/O data sets are required.

- Input data sets:

  - Unit 1: puff histories calculated by PDM (unit 8)

  - Unit 2: radial grid calculated by EXPGRID (unit 8)

- Output data set:

  Unit 21: results of PEM. On this data set only the results for one year should be written; therefore for 2 years 2 separate PEM-runs are required.

It may be advantageous to precalculate the normalized concentrations for every three hours of the two years 1982/1983 and to store them on two data sets. The 1982-file then consists of 365 * 8 = 2920, the 1983-file of 360 * 8 = 2880 concentration patterns (the last 5 days are missing).

10.2 *Examples for Input*

In the following JCL-examples explaining comments are included on occasion; they are embedded in stars (*) and are not part of the actual input.

10.2.1 JCL FOR PDM

The lines marked by numbers embedded in stars are explained subsequently, they are not a part of the input!

```
//INRxxxMB JOB (xxxx,yyy,zzzzz),nnnnnnnnn,NOTIFY=INRxxx,
// REGION=4000K,MSGCLASS=H,TIME=10
// EXEC F7CLG,PARM.C='LANGLVL(77)'
//*MAIN LINES=30
//C.SYSPRINT DD DUMMY
//C.SYSIN DD DSN=INR482.MESOS.FORT(PDM),DISP=SHR
//G.FT05F001 DD *

SOURCE:   LONGITUDE LATITUDE   NAME                                  *******
          10.0000    49.2500   'KARLSRUH'                           *  1  *
_____________________________________________                        *******

STACKHEIGHT/M  PUFFHEIGHT/M  TH.POWER/MW                             *******
10             1             0                                       *  2  *
_____________________________________________                        *******

       FIRST DAY     LAST DAY                                        *******
       01 01 82      31 12 83                                        *  3  *
_____________________________________________                        *******

STANDARD RUN                      MASS  ON SECTORS
WTHOUT/WITH TEST  OUTP. ON FILE   WAY OF TRAJECTORIES   MASS BALANCE

'YES'  'YES'      'YES'           'NO'                  'YES'
_____________________________________  ____________________________________

RUN WITH DEFAULTS (IF "YES" THE REST OF INPUT IS NEGLIGIBLE)

'NO'
_____________________________________________________________________
_____________________________________________________________________
```

```
OUTPUT OF STANDARD RUN ON PRINTER

'YES'
```

```
DIAGNOSTIC OUTPUT
BLAYER  PUFFHR

'NO'    'NO'
```

PUFFS/DAY	NUMBER OF NUCLIDES	DEPOSITING OF IT	TRACKING DAYS
9	4	3	15

IPUFF:	1	2	3	4	PARAMETER	
	1.0	1.0	1.0	1.0	QPUFF	* 5 *
	0.003	0.01	0.0005	0.0	VDEP	* 6 *
	0.00008	0.00008	0.0000008	0.0	WOUT	* 7 *
	0.8	0.6	0.6	1	WEXP	* 8 *
	0	0	0	0	FLAM(DAY)	* 9 *
	0	0	0	0	FLAM(NIGHT)	* 10 *
	1	1	1	1	WMOL	* 11 *

```
/*-------------------------------------------------------*/
/*                input of pressure data                 */
/*-------------------------------------------------------*/
//G.FT01F001 DD DSN=AFS826.DRUCK82.DATA,
//           UNIT=SDG01,VOL=SER=AFS002,DISP=SHR
//           DD DSN=AFS826.DRUCK83.DATA,
//           UNIT=SDG01,VOL=SER=AFS002,DISP=SHR
/*-------------------------------------------------------*/
/*                input of synoptic data                 */
/*-------------------------------------------------------*/
//G.FT02F001 DD DSN=AFS826.SYNOP82.DATA,
//           UNIT=SDG01,VOL=SER=AFS000,DISP=SHR
//           DD DSN=AFS826.SYNOP83.DATA,
//           UNIT=SDG01,VOL=SER=AFS002,DISP=SHR
```

```
/*-------------------------------------------------------*/
/*               definition of MESOS area                */
/*               and period with meteorological data     */
/*-------------------------------------------------------*/
//G.FT03F001 DD DSN=INR482.MESOS.DATA(BASIS82),
//           DISP=OLD,LABEL=(,,,IN)
/*-------------------------------------------------------*/
/*               informative output data set             */
/*               not relevant for subsequent modules     */
/*-------------------------------------------------------*/
//G.FT10F001 DD DSN=INR253.MESOS.DATA,DISP=OLD,LABEL=(,,,OUT)
/*-------------------------------------------------------*/
/*               output data set containing              */
/*               puff histories;                         */
/*               needed as input for PEM                 */
/*-------------------------------------------------------*/
//G.FT08F001 DD DSN=INR253.#####.DATA,DISP=(NEW,KEEP),
//           UNIT=SDG01,VOL=SER=INR006,
//           DCB=(RECFM=VBS,LRECL=13030,BLKSIZE=13030),
//           SPACE=(TRK,(4000,100))
//G.SYSPRINT DD SYSOUT=*
//
```

Description of user defined input variables of PDM:

All user defined input records are read by the FORTRAN statement:

READ(5,*)

The meanings of the variables in the marked lines are:

1

- longitude (deg)
- latitude (deg)
- name (A10) of nuclear site

2

- stack height (m)
- puff height (m)
- thermal power of release (MW)

3

- first day puffs are emitted
- last day puffs are emitted

the options in the following input lines which are not marked were used for different diagnostic tests and can stay unchanged

4

- number of puffs tracked per day;
- number of nuclide groups considered;
- number of depositing nuclides;
- number of days each puff is tracked (do not change this value without controlling the dimensions of arrays in the program)

5

- source strength of the different nuclide groups (for the application in UFOMOD a unit release is assumed)

6

- dry deposition velocity (for 4 nuclide groups)

7

- coefficient in power law which determines the washout coefficient (for 4 nuclide groups)

8

- exponent in power law which determines the washout coefficient (for 4 nuclide groups)

9-11

- parameters necessary for applications considering chemical emissions and the transformation of these elements; for nuclear applications, these parameters are not relevant and should not be changed

  The order of the 4 nuclide groups with different deposition properties is as follows:

1. aerosols
2. elemental iodine
3. organically bound iodine
4. noble gases

10.2.2 JCL FOR EXPGRID

The lines marked by numbers embedded in stars are explained subsequently, they are not a part of the input!

```
//INRxxxEX JOB (xxxx,yyy,zzzzz),nnnnnnnnn,NOTIFY=INRxxx,MSGCLASS=H
//*****************************************************************************
//**    Job-example for MESOS-EXPGRID                                        **
//*****************************************************************************
// EXEC F7CLG
//C.SYSPRINT DD SYSOUT=*
//C.SYSIN DD DSN=INR482.MESOS.FORT(EXPWAA),DISP=SHR
//G.FT05F001 DD * ***
   49.25     10.00                                                    *1*
   64   35  1                                                        *2*
      10.0      20.0      30.0      40.0      50.0                   *3*
      60.0      70.0      80.0      90.0     100.0                   *4*
     125.0     150.0     175.0     200.0     300.0                   *5*
     400.0     500.0     600.0     700.0     800.0                   *6*
     900.0    1000.0    1100.0    1200.0    1300.0                   *7*
    1400.0    1500.0    1600.0    1700.0    1800.0                   *8*
    1900.0    2000.0    2100.0    2200.0    2300.0                   *9*
                                                                     ***
//G.SYSPRINT DD SYSOUT=*
/*-----------------------------------------------------------*/
/*               output data set containing                  */
/*               transformed polar concentration grid        */
/*               needed as input for PEM                     */
/*-----------------------------------------------------------*/
//G.FT08F001 DD DSN=INR482.MESEXP.DATA(KHETOT),DISP=SHR
//
```

Description of the user defined input varables of EXPGRID:

- line *1*: geographic coordinates of the source in degree latitude and longitude
  Input-Format:(1x,2F10.5)

- line *2*: number of azimuthal sectors (max. = 64)
  number of radial distances (max. = 35)
  criteria for the choice of the concentration grid (see Sect. 2.4)
  0 = increasing number of azimuthal sectors with increasing distance
  1 = constant number of azimuthal sectors in each distance
  Input-Format:(1x,I4,I5,I3)

- line *3 - 9* radial distances from the source in km
  Input-Format:(5F10.1)

10.2.3 JCL FOR PEM

The lines marked by numbers embedded in stars are explained subsequently, they are not a part of the input!

```
//INRxxxEE JOB (xxxx,yyy,zzzzz),nnnnnnnnn,REGION=2040K,NOTIFY=INRxxx,
//         MSGCLASS=H,TIME=5
//*****************************************************************************
//**    Job-example for MESOS-PEM                                            **
//*****************************************************************************
// EXEC F7CLG,PARM.C='LANGLVL(77)'
//C.SYSIN DD DSN=INR482.MESOS.FORT(PEMUFO),DISP=SHR
//G.FT05F001 DD *                                                          ***
 10  49.2500 10.0000  17  365  KHE                                        *1*
AEROS AIR   AEROS DRY   AEROS WET   ELMID AIR   ELMID DRY   ELMID WET   *2*
ORGID AIR   ORGID DRY   ORGID WET   NOBLE AIR                            *3*
    1    5    8    2    6    9    3    7   10    4                      *4*
  0.             0.             0.             0.             0.        *5*
  0.             0.             0.             0.             0.        *6*
   1.0   1.0   1.0   1.0   1.0   1.0   1.0   1.0   1.0   1.0            *7*
       1.0   0.33333       1.0       1.0                                *8*
//G.FT06F001 DD SYSOUT=*,DCB=(LRECL=133,BLKSIZE=133,RECFM=FBA)          ***
/*-------------------------------------------------------*/
/*               input data set with puff histories      */
/*               result of PDM                           */
/*-------------------------------------------------------*/
//G.FT01F001 DD DSN=INR482.KH15PH1.DATA,DISP=SHR,
//           UNIT=SDG01,VOL=SER=INR006
/*-------------------------------------------------------*/
/*               input data set transformed coordinates  */
/*               of concentration grid points            */
/*               result of EXPGRID                       */
/*-------------------------------------------------------*/
//G.FT02F001 DD DSN=INR482.MESEXP.DATA(KHETOT),DISP=SHR
/*-------------------------------------------------------*/
/*               output data set with                    */
/*               concentration distributions etc.        */
/*               for one year                            */
/*-------------------------------------------------------*/
//G.FT21F001 DD DSN=INR482.KH1PEM2.DATA,DISP=(OLD,KEEP),
//           UNIT=SDG01,VOL=SER=INR010,
//           DCB=(RECFM=FB,LRECL=13030,BLKSIZE=13030),
//           SPACE=(TRK,(5000,100))
```

Description of user defined input variables of PEM:

- line *1* Input-Format: (I3,1X,2F8.4,2I4)
  - number of different concentration patterens considered, seperated according to different immission modes (air concentration, dry and wet deposition) for 4 different types of nuclides (for noble gases only the air concentrations are taken into account);
  - latitude and longitude of source;
  - first day of in the data base a puff is started (17. day = 1.1.1982); number of days considered
- lines *2-3* Input-Format: (6(3A4))
  - names for identifying the nuclide groups and their immission mode
- line *4* Input-Format: (12I5)
  - index vector characterizing the nuclide groups named in *2-3* for changing the order from (nuc1,nuc2,nuc3,nuc4)air..., ()dry, ()wet to nuc1(air,dry,wet), nuc2(),...;
- lines *5-6* Input-Format: (5E15.8)
  - radioactive half-lifes
    set to 0, because the decay is considered in UFOMOD;
- line *7* Input-Format: (2X,12F6.3)
  - source strength (see input of PDM, line *5*)
- line *8* Input-Format: (4F10.5)
  - correction factors for dry deposition velocities (see also Sect. 2.8)

For one year PEM needs between 20 and 30 minutes of CPU-time on the KfK computer system.

11. REFERENCES

[1] International Atomic Energy Agency
Atmosperic Dispersion in Nuclear Power Plant Siting: A Safety Guide
IAEA, Vienna, 1980, STI/PUB/549

[2] Pasquill, F. and F.B. Smith
Atmospheric Diffusion
3. Edition
Ellis Horwood Ltd., Chichester, U.K., 1983

[3] Rasmussen, N.C.
Reactor Safety Study. An Assessment of Accident Risks in U.S. Commercial Nuclear Power Plants
(NUREG-75/014), WASH-1400. U.S. Nuclear Regulatory Commission, Washington, D.C., October 1975

[4] Ritchie, L.T., J.D. Johnson and R.M. Blond
Calculations of Reactor Consequences, Version 2
Sandia National Laboratories, SAND81-1994, (NUREG/CR-2324), 1981

[5] Ritchie, L.T., D.I. Chanin and J.L. Sprung
MELCOR Accident Consequence Code System (MACCS), Volume II
MACCS Reference Manual
Sandia National Laboratories, SAND86-1562, (NUREG/CR-4691), 1987

[6] Clarke, R.H. and G.N. Kelly
MARC - The NRPB Methodology for Assessing Radiological Consequences of Accidental Releases of Activity
National Radiological Protection Board, UK - Chilton, Didcot NRPB-R127, 1981.

[7] Bayer, A., K. Burkart, J.Ehrhardt, W. Hübschmann, M. Schückler, S.Vogt, W. Jacobi, H.G.Paretzke, K.-R.Trott, E.Hofer and B.Krzykacz
The German Risk Study: Accident Consequence Model and Results of the Study
Nuclear Technology, 59, 20-50, 1982

[8] Sutton, O.G.
Micrometeorology
McGraw-Hill Book Company, New York, 1953, pp. 333

[9] J. Ehrhardt, K. Burkart, I. Hasemann, C. Matzerath, H.-J. Panitz and C. Steinhauer
The Program System UFOMOD for Assessing the Consequences of Nuclear Accidents
KfK - 4330, Kernforschungszentrum Karlsruhe, 1988

[10] Päsler-Sauer, J.
Comparative Calculations and Validation Studies with Atmospheric Dispersion Models
KfK - 4164, Kernforschungszentrum Karlsruhe, 1986

[11] Panitz, H.-J.
Accident Consequence Assessments with Different Atmospheric Dispersion Models - A Benchmark Study
KfK - 4445, Kernforschungszentrum Karlsruhe, 1989

[12] Straka, J., H. Geiss and K.J. Vogt
Diffusion of Waste Air Puffs and Plumes under Changing Weather Conditions
Contr.Atmosph.Physics, 54, 207-221, 1981

[13] Mikkelsen, T., S.E. Larsen and S. Thykier-Nielsen
Description of the RISO Puff Diffusion Model
Nuclear Technology, 67, 56-65, 1984

[14] ApSimon, H.M., A.J.H. Goddard and J. Wrigley
Long-Range Atmospheric Dispersion of Radioisotopes - I. The MESOS model
Atmospheric Environment, 19, 99-111, 1985

[15] ApSimon, H.M., and A.J.H. Goddard
Atmospheric Transport of Radioisotopes and the Assessment of Population Doses on a European Scale. Application of the MESOS Code to the Meteorological Dispersion of Radioactive Discharges from Notional Nuclear Sites in the European Community with Particular Reference to the Mesoscale
Report EUR 9128EN, Commission of the European Communities (CEC), Luxembourg, 1984

[16] Commission of the European Communitues
Methods for Assessing the Off-Site Consequences of Nuclear Accidents
Joint report by the Kernforschungszentrum Karlsruhe GmbH, D-Karlsruhe, and the National Radiological Protection Board, UK-Chilton, Didcot
CEC-Report EUR 10243 EN (1986)

[17] Hübschmann, W. und S. Honcu
ISOLA IV-Ein Fortran 77-Programm zur Berechnung der langfristigen Dosisverteilung in der Umgebung kerntechnischer Anlagen
Report KfK-4146, 1987

[18] Projekt Sicherheitsstudien Entsorgung (PSE)
Abschlußbericht, Fachband 9
Berlin, Januar 1985

[19] Gryning, S.E.
Description of a Recent Nordic Mesoscale Dispersion Experiment over a Land-Water-Land Area (The Oeresund Experiment)
in: Safety of Thermal Water Reactors (Ed.: Skupinski, E., B. Tolley and J. Vilain)
Proceedings of a Seminar on the Results of the European Communities Indirect Action Research Programme on Saftey of Thermal Water Reactors, Brussels, 1-3 October 1984, 427-438
published 1985 by: Graham & Trotman Ltd., Sterling House, 66 Wilton Road, London SW1V 1DE, UK

[20] Thykier-Nielsen, S., S.E. Gryning and T. Mikkelsen
Simulation of the Oeresund-Experiment Tracer Releases with the RISO Mesoscale Puff Diffusion Model
Proceedings from the Workshop II of the Oeresund Experiment, Uppsala, Sweden, October 13-14, 1987, 43-56

[21] Mikkelsen, T., S. Thykier-Nielsen, I. Troen, A.F. de Baas and S.E. Larsen
A Hazard Assessment Model for Complex Terrain
paper presented on the Eight Symposium on Turbulence and Diffusion, April 25-29, 1988, San Diego, Calif.

[22] ApSimon, H.M. and J.J.N. Wilson
Modelling Atmospheric Dispersal of the Chernobyl Release Across Europe
Boundary-Layer-Meteorology, 41, 123-133, 1987

[23] Papadopoulos, D., L.A.König, K.-G. Langguth and S. Fark
Contamination of Precipitation due to Tritium Release into the Atmosphere
Radiation Protection Dosimetry, 16, 95-100, 1986

[24] Panitz, H.-J. and W. Raskob
internal, unpublished KfK report, December 1987

[25] Thykier-Nielsen, S., T. Mikkelsen, H.-J. Panitz and W. Raskob
RIMPUFF: An Atmospheric Dispersion and Deposition Module for the European COSYMA code for Assessing the Consequences After Nuclear Accidents
common report of RISO National Laboratory, Denmark, and Kernforschungszentrum Karlsruhe (KfK), in preparation

[26] Hübschmann, W. and W. Raskob
ISOLA V - A FORTRAN 77 Code for the Calculation of the Long-Term Concentration Distribution in the Environment of Nuclear Installations
KfK - 4604, Kernforschungszentrum Karlsruhe, in preparation

[27] Kao, S.K.
Theories of Atmospheric Transport and Diffusion
in: [28], Chap. 6, 189-239, 1984

[28] Randerson, D. (Editor)
Atmospheric Science and Power Production
DE84005177 (DOE/TIC-27601)
National Technical Information Center, 1984
U.S. Department of Commerce
Springfield, Virginia 22 161

[29] Hanna, S.R.
Turbulent Diffusion: Chimneys and Cooling Towers
Chapter 10 in: Plate, E. (Editor)
Engineering Meteorology
Elsevier Publishing Company, Amsterdam - Oxford - New York, 1982

[30] Thomas, P., H. Dilger, W. Hübschmann, H. Schüttelkopf and S. Vogt
Experimental Determination of the Atmospheric Dispersion Parameters at the Karlsruhe Nuclear Research Center for 60m and 100m Emission Heights
Part 1: Measured Data
KfK - 3090, Kernforschungszentrum Karlsruhe, 1981

[31] Thomas, P., K. Nester
Experimental Determination of the Atmospheric Dispersion Parameters at the Karlsruhe Nuclear Research Center for 60m and 100m Emission Heights
Part 2: Evaluation of Measurements
KfK - 3091, Kernforschungszentrum Karlsruhe, 1981

[32] Geiß, H., K. Nester, P. Thomas und K.J. Vogt
In der Bundesrepublik Deutschland experimentell ermittelte Ausbreitungsparameter für 100 m Emissionshöhe
Jül - 1707, KfK - 3095, Februar 1981
Kernforschungsanlage Jülich in Zusammenarbeit mit dem Kernforschungszentrum Karlsruhe

[33] Bultynck, H. and L.M. Malet
Evaluation of Atmospheric Dilution Factors for Effluents Diffused from an Elevated Continuous Point Source
Tellus, XXIV, 455-472, 1972

[34] Gifford, F.A.
Turbulent Diffusion-Typing Schemes: A Review
Nuclear Safety, 17, 68-86, 1976

[35] Hanna, S.R., G.A. Briggs and R.P. Hosker
Handbook on Atmospheric Diffusion.
Technical Information Center, U.S. Departement of Energy, pp. 102, 1982

[36] Bundesminister für Forschung und Technologie (Hrsg.)
Deutsche Risikostudie Kernkraftwerke - Eine Untersuchung zu dem durch Störfälle in Kernkraftwerken verursachten Risiko
Fachband 8: Unfallfolgenrechnung und Risikoergebnisse.
Verlag TÜV Rheinland GmbH, Köln, 1981

[37] Geiß, H.
Ein Verfahren zur realistischen Ermittlung der Umgebungsbelastung nach kerntechnischen Störfällen unter Einbeziehung von Meßwerten der Umgebungsüberwachung
in: Henning, K. (Redaktion)
Strahlenexposition der Bevölkerung
18. Jahrestagung des Fachverbandes für Strahlenschutz e.V.
6.-10. Oktober 1985 in Lübeck-Travemünde, FS-85-37-T, 339-359

[38] Vogt, K.J., H. Geiß and J. Straka
A New Trajectory Model and its Application for Accident and Risk Assessments paper presented at the 12-th NATO/CCMS International Technical Meeting on Air Pollution Modelling and its Application, Palo Alto, 25./28.08.1981

[39] Geiß, H.
private communication, KFA Jülich, 1985

[40] Möllmann, M.
private communication, KFA Jülich, 1986

[41] Nester, K.
private communication, KfK, 1986

[42] Start, G.E. and L.L. Wendell
Regional Effluent Dispersion Calculations Considering Spatial and Temporal Meteorological Variations
NOAA Technical Memorandum ERL-ARL-44, 1974

[43] Mikkelsen, T., S.E Larsen and I. Troen
Use of a Puff Model to Calculate Dispersion from a Strongly Time Dependent Source
Seminar on Radioactive Releases and their Dispersion in the Atmosphere Following a Hypothetical Reactor Accident, RISO, 22.-25.4.1980, Vol.2, 575-614
Commission of the European Communities, Luxembourg, 1980

[44] Mikkelsen, T., S.E Larsen and H.L. Pesceli
Diffusion of Gaussian Puffs
Quart. J.R. Meteorol. Soc., 113, 81-105, 1987

[45] Smith, F.B.
A Scheme for Estimating the Vertical Dispersion of a Plume from a Source Near Ground Level
3rd Meeting of an Expert Panel on Air Pollution Modelling, Paris, October 1972
Brussels NATO-CCMS Report 14, Chap. XVII, 1-14, 1973

[46] Carson, D.J.
The Development of a Dry Inversion-Capped Convectively Unstable Boundary Layer
Quart. J.R. Meteorol. Soc., 99, 450-467

[47] Doury, A.
Pratiques Françaises en Matière de Prévision Quantitative de la Pollution Atmosphérique Potentielle Liée aux Activités Nucléaires
in: Proceedings of CEC Seminar on Radioactive Releases and their dispersion in the Atmosphere following a Hypothetical Reactor Accident, RISO, 22. - 25. April 1980, 403-448,
Commission of the European Communities, Luxembourg, 1980

[48] Der Bundesminister der Justiz (Hrsg.)
Bekanntmachung der Leitlinien zur Beurteilung der Auslegung von Kernkraftwerken mit Druckwasserreaktoren gegen Störfälle im Sinne des § 28 Abs. 3 der Strahlenschutzverordnung --- Störfall-Leitlinien ---
Bundesanzeiger, Jahrgang 35, Nummer 245a, 1983, Der Bundesminister der Justiz, 5300 Bonn, FRG

[49] Turner, D.B.
Workbook of Atmospheric Dispersion Estimates
U.S. Department of Health, Education and Welfare, Public Health Service, Publ. No. 999-AP-26, 1969

[50] Schwarz, G.
Deposition and Post-Deposition Radionuclide Behaviour in Urban Environments
in: Proceedings of Workshop on Methods for Assessing the Off-Site Radiological Consequences of Nuclear Accidents, 15-19 April 1985, Luxembourg, 533-557
Commission of the European Communities, Report EUR 10397 EN, 1986

[51] Bronstein, I.N and K.A. Semendjajew
Taschenbuch der Mathematik
21. Auflage, Verlag Harri Deutsch, Frankfurt/Main, 1984

[52] Horst, T.W
A Surface Depletion Model for Deposition from a Gaussian Plume
Atmospheric Environment, 11, 41-46, 1977

[53] Horst, T.W
A Review of Gaussian Diffusion-Deposition Models
in:Atmospheric Sulfur Deposition (edited by Shriner, D.S., C.R. Richmond and S.E. Lindberg),pp. 275-283
Ann Arbor Science, Ann Arbor, MI, USA, 1980

[54] Horst, T.W
A Correction to the Gaussian Source Depletion Model
in:Precipitation Scavenging, Dry Deposition and Resuspension (edited by Pruppacher, H.R., R.G. Semonin and W.G.N. Slinn), pp. 1205-1218
Elsevier North Holland, Amsterdam, The Netherlands, 1983

[55] Doran, J.C. and T.W. Horst
An Evaluation of Gaussian Plume-Depletion Models with Dual-Tracer Field Measurements
Atmospheric Environment, 19, 939-951, 1985

[56] Vogt, S., W. Hübschmann und P. Wittek
Niederschlag und Washout im Unfallfolgenmodell der Deutschen Risikostudie - Kernkraftwerke
KfK - 3548, Kernforschungszentrum Karlsruhe, 1983

[57] Briggs, G.A.
Plume Rise Predictions
in: Haugen, D.A. : Lectures on Air Pollution and Environmental Impact Analyses, 59-111.
American Meteorological Society, Boston, Mass., U.S.A., 1976

[58] Gifford, F.
The Rise of Strongly Radioactive Plumes
J. Appl. Met., 6, 644-649, 1967

[59] Kaiser, G.D.
Plume Rise in Nuclear Safety Studies
in: Underwood, B.Y., P.J. Cooper, N.J. Holloway, G.D. Kaiser and W. Nixon : A Review of Specific Effects in Atmospheric Dispersion Calculations, Vol. II, pp. 1-1 - 1-58. Safety and Reliability Directorate, UKAEA.
Final Report of Contract SR011-80 UK(B) between the European Atomic Energy Community and the United Kingdom Atomic Energy Authority, 1983

[60] Vogt, K.J., K. Heinemann, H. Nordsieck, G. Polster, F. Rohloff und L. Angeletti
Jahresbericht Juli 1970 - Juni 1971 über das im Rahmen des Vertrages Nr.SC 24-003-PSTD von der Association EURATOM-C.E.A. geförderte Forschungsvorhaben Ausbreitung und Ablagerung
Bericht Kernforschungsanlage Jülich, Jül-807-ST, 1971

[61] Halitsky, J.
Gas Diffusion near Buildings.
in: Slade, D.H. (Ed.): Meteorology and Atomic Energy 1968.
U.S. Atomic Energy Commission, Division of Technical Information, pp. 221-255, 1968

[62] Cooper, P.J.
Building Effects in Nuclear Safety Studies - A Review.
in: Underwood, B.Y., P.J. Cooper, N.J. Holloway, G.D. Kaiser and W. Nixon : A Review of Specific Effects in Atmospheric Dispersion Calculations, Vol. II, pp. 8-1 - 8-71. Safety and Reliability Directorate, UKAEA.
Final Report of Contract SR011-80 UK(B) between the European Atomic Energy Community and the United Kingdom Atomic Energy Authority, 1983

[63] Prandtl, L., K. Oswatitsch und K. Wieghardt
Führer durch die Strömungslehre, 8. Auflg.
F. Vieweg & Sohn, Braunschweig, pp. 622, 1984

[64] Hunt, J.C.R., C.J. Abell,J.A. Peterka and H. Woo
Kinematical Studies of the Flows Around Free or Surface-Mounted Ostacles; Applying Topology to Flow Visualization.
J. Fluid Mech., 86, Part1, 179-200, 1978

[65] Briggs, G.A.
Lift-Off of Buoyant Gas Initially of the Ground.
ADTL Contribution File No 87. Air Resources Atmospheric Turbulence and Diffusion Laboratory NOAA, Oak Ridge, Tennessee, USA, 1973

[66] Hall, D.J. and R.A. Waters
Further Experiments on a Buoyant Emission from a Building, pp. 44.
Warren Spring Laboratory, Departement of Trade and Industry, Gunnels Wood Road, STEVENAGE, Hertfordshire SG1 2BX, U.K., 1986

[67] Hosker, R.P.
Flow and Diffusion near Obstacles.
in: [28], Chap. 7, pp. 241-326, 1984

[68] Gifford, F.A
Atmospheric Dispersion Calculations Using a Generalised Gaussian Plume Model
Nuclear Safety, 2(2), 56-59, 1960

[69] Ehrhardt, J. and I. Hasemann
UFOMOD: User Guide
KfK - 4331, Kernforschungszentrum Karlsruhe, in preparation

[70] Jacob, P. and H.M. Müller
γ-Exposure from Bi-Gaussian Clouds
GSF-Report, Gesellschaft für Strahlen- und Umweltforschung mbH, München, in preparation

[71] Healy, J.W.
Radioactive Cloud Dose Calculations
in: [28], Chap. 15, 685-745, 1984

[72] Ehrhardt, J. and J.A. Jones
An Outline of COSYMA, a new Program Package for Accident Consequence Assessments
to be published in Nuclear Technology

[73] Jones, J.A.
private communication, NRPB, Chilton/UK, June 1989

[74] Ehrhardt, J., I. Hasemann, H.-J. Panitz and W. Raskob
Example Applications of the Program System UFOMOD in Decision Making
KfK-Report to be published